# Fully automatic analysis of ulnar sided wrist injuries using dynamic CT imaging

**Jesse Wolters – S1808125**

**M3 stage plastische chirurgie**

**Radboud Universitair Medisch Centrum**

**23.01.23 -15.02.24**

Radboud umc

UNIVERSITY OF TWENTE.

# General information

- M3 internship Technical Medicine: Medical imaging and intervention
- Institution: Radboud University Medical Center
- Department: Plastic surgery

## Supervisors:

- Chairman: prof.dr.ir. N.J.J. Verdonschot
- Technical supervisor University of Twente: prof.dr.ir. N.J.J. Verdonschot
- Process supervisor University of Twente: drs. B.J.C.C. Sweep
- Medical supervisor Radboud University Medical Center: dr. E.P.A van der Heijden
- Technical supervisor Radboud University Medical Center: dr. S. Hummelink

# Abstract

**Introduction –** Ulnar sided wrist pain is often called the headache of wrist complaints due to the challenge to find the cause of the pain. Damage to the TFCC or ulna plus cause changes the dynamic kinematics of the DRUJ which, if left untreated, may lead to progressive osteoarthritis. Current diagnosis of TFCC injuries remains difficult, visibility of ligaments on conventional imaging techniques is poor and the golden standard of arthroscopy is invasive. Four-dimensional computed tomography (4DCT) allows for kinematic assessment of wrist motion and may visualise the change in kinematics, improving diagnostics. Thus this thesis aims to investigate the feasibility of using automatic 4DCT analysis to assess the DRUJ and TFCC.

**Methods –** To improve current knowledge about 4DCT, the DRUJ and the TFCC a cadaver, volunteer and patient study was set-up. A previously acquired 4DCT dataset consisting of RUD, FE and CF movement data is used for the development and evaluation of five new and adapted parameters: 3D dynamic ulnar variance, lunate and triquetrum ulnar proximity and a 3D adaptation of the radioulnar line method and the Epicentre method. To enable analysis of these parameters automatic LCS estimation of the ulna was performed and the registration of the ulna was investigated.

**Results –** A cadaver study and a healthy volunteer study were set-up and executed and a patient study consisting focussing on DRUJ instability was METC approved. A method for automatic LCS estimation was proposed and tested and the registration of the ulna was evaluated in which CPD registration performed best and adequate for clinical use. The median 3D ulnar variance increased during ulnar deviation, flexion and clenching of the fist, while it decreased in extension. Ulnar proximity to the lunate and triquetrum was automatically measured. The 3D adaptation of the Radioulnar line method and the Epicentre method were developed and tested on volunteer data and a patient.

**Discussion –** This thesis provides a first stepping stone for the development of automatic 4DCT analysis to assess the DRUJ and TFCC. While not every method has been performed on the clinically most important movement and only one patient was analysed a large volunteer dataset was acquired, and a patient study has been set-up to overcome this gap. Applying the developed methods to this data will further evolve our knowledge of the DRUJ kinematics and may improve the diagnosis of DRUJ instability and ulnar impaction facilitating early treatment and preventing progression.

# List of abbreviations

| | |
|---|---|
| **ΔUV** | Change in ulnar variance during wrist motion |
| **2D** | Two dimensional |
| **3D** | Three dimensional |
| **3DEpi** | 3D adaptation of the epicentre method |
| **3DmRU** | 3D adaptation of the radioulnar line method |
| **4DCT** | Four-dimensional computed tomography |
| **AbAd** | Abduction-adduction |
| **AP** | Anterior posterior |
| **CF** | Clenching of the fist |
| **CPD** | Coherent point drift registration |
| **CR** | Capitate-radial |
| **CT** | Computed tomography |
| **DRUJ** | Distal radioulnar joint |
| **Epi** | Epicentre method |
| **FE** | Flexion-extension |
| **FOV** | Field of view |
| **ICP** | Iterative closest point |
| **LCS** | Local coordinate system |
| **MAPSD** | Median absolute point to surface distance |
| **MCP-1** | First metacarpophalangeal joint |
| **mm** | Millimetre |
| **MRI** | Magnetic resonance imaging |
| **mRU** | Modified radioulnar line method |
| **nnU-net** | no-new U-net |
| **OR** | Opposition-reposition |
| **OSM** | Osteosynthesis material |
| **PA** | Posterior-anterior |
| **POI** | Point of interest |
| **PS** | Pronation-supination |
| **Radboudumc** | Radboud University Medical Centre |
| **ROI** | Region of interest |
| **ROM** | Range of motion |
| **RUD** | Radial-ulnar deviation |
| **TFCC** | Triangular fibrocartilage complex |
| **UKF** | Unscented Kalman filter |
| **VOI** | Volume of interest |
| **WMO** | Medical Research Involving Human Subjects Act |

# Contents

# Chapter 1: General introduction

Distal radioulnar joint (DRUJ) instability is an often underestimated pathology which may entail severe consequences to the wrist if left untreated [1]. The bony structures of the DRUJ only account for about 20% of its stability, the remaining 80% is accounted for by soft tissues of which the triangular fibrocartilage complex (TFCC) is the most important [2]. Damage to this TFCC is one of the most common causes of ulnar-sided wrist pain impinging on everyday activities such as opening a door or shaking hands [3]. Damage to the TFCC cause a change of the dynamics of the bones involved in the DRUJ causing pathologic movements. The lack of stability in the DRUJ leads to subluxation and abutment between the involved bones resulting in progressive ulnocarpal osteoarthritis and DRUJ osteoarthritis.

For patients with a clinical diagnosis of DRUJ instability the first option of choice is conservative treatment consisting of immobilization, rest and hand therapy. After a minimal of 3 months of conservative treatment, up to 43% of patients keeps complaints of pain and loss of function after which surgical treatment consisting of TFCC debridement is opted [4] Due to the progressive nature and the irreversibility of osteoarthritis, early treatment is important and may improve prognosis on the long term. To facilitate early treatment, timely diagnosis is essential, but timely diagnosis of DRUJ instability is still difficult. The current golden standard for diagnosis, of TFCC lesions concerns arthroscopy, which, however, comes with a number of disadvantages including being invasive, expensive and associated with complications. In addition, with arthroscopy the amount of instability cannot be assessed. This renders arthroscopy suboptimal for early diagnosis raising the need for a new diagnostic tool.

## 1.1    The triangular fibrocartilage complex (TFCC)
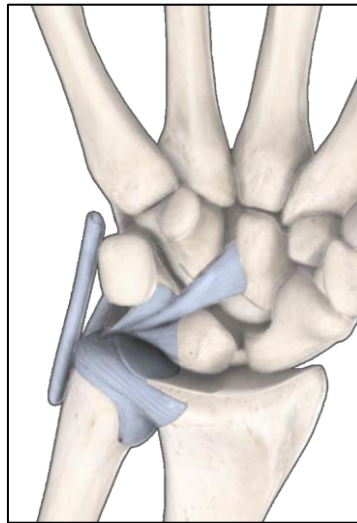


*Figure 1: The wrist with the triangular fibrocartilage complex in blue*

The triangular fibrocartilaginous complex (TFCC), as seen in Figure 1, is the cartilaginous–ligamentous stabilization mechanism of the ulnar sided wrist with the primary function of stabilizing the DRUJ besides acting as a shock absorber across the ulnar-carpal joint *[5] [6]*. The TFCC also enables rotation of the wrist. A surplus of forces may damage the TFCC. TFCC injuries may occur after distal radial fractures in up to 43% of cases, or due to chronic degenerative injury after abnormal loading due to ulnar impaction syndrome *[7] [8]*. TFCC injuries can be classified with the palmer classification as can be seen in Table 1.

When the TFCC is injured, the DRUJ might become unstable, depending on which part of the TFCC is damaged. Lesion of the TFCC origin or insertion or of the dorsal and palmar ligamentous parts of the TFCC might lead to instability of the DRUJ. Due to this pathological movement freedom the ulna may impact with the surrounding carpal bones and radius causing wear and ultimately osteoarthritis. In patients this may present as ulnar sided wrist pain accompanied with clicking or point tenderness between the pisiform and the ulnar head. If left untreated TFCC injuries can lead to pain worsening, functional compromise (such as a decreased grip strength) and ultimately secondary osteoarthritis *[3] [9]*. The osteoarthritis is irreversible so recovery of the TFCC can only prevent further deterioration of the cartilage. Due to this earlier treatment, before there is an onset of osteoarthritis, may lead to better long-term results. In patients with no further underlying pathologies conservative treatment by immobilization and hand therapy or TFCC debridement may be all that is required *[10]*. While for patients with severe osteoarthritis denervation, interposition arthroplasty, hemiarthroplasty, or whole-joint arthroplasty may be needed, which are all more invasive surgical treatment options [5].

Current diagnosis of TFCC injuries remains difficult. On a conventional x-ray no ligaments can be seen, only bones. Therefore, only subluxation or in an even further stadium, osteoarthritis can be found. However, this is only true after the damage has already been done, of course ideally the injury is already diagnosed before this stage. Besides, aetiology cannot be seen, there are many factors that may contribute to osteoarthritis in the wrist. The standard x-ray may show a relatively long ulna, which is a predisposing factor for TFCC damage (see also: 1.4 Ulnar variance and ulnar impaction) but an ulna plus might not be the cause of the complaints. Further imaging can be done using magnetic resonance imaging (MRI) which has better contrast for soft structures and makes it possible to directly visualize ligaments like the TFCC. But, due to the small size of the TFCC compared to the resolution, interpretation of the MRI is difficult resulting in a sensitivity of 0.76 and a specificity of 0.82 for TFCC

diagnosis *[5]*. Computed tomographic arthrography and magnetic resonance arthrography are currently the two most viable imaging techniques with statistically equivalent sensitivity (respectively 0.89 and 0.78) and specificity (respectively 0.89 and 0.85), but these techniques are not widely availabl*e [5]*. The current golden standard is arthroscopy, which is a keyhole surgery which uses a scope to directly look at and interact with the ligaments. While this direct approach may give very conclusive results, it is an invasive technique which is only employed when clinical suspicion is high. Moreover, it is invasive and expensive and the quality of the investigation is highly operator dependent. On top of that it is associated with sick leave and complications and its static character is not able to visualize the kinematics of the DRUJ. The challenge of diagnosing TFCC injuries in addition to the progressive nature of the symptoms when left untreated raises the need for a new imaging technique for early diagnosis of TFCC injuries.

*Table 1: Palmer classification of TFCC injuries [11]*

| Type 1 | Traumatic (occurs secondary to trauma, i.e. fractures of the distal radius) |
|---|---|
| 1A | Central perforation |
| 1B | Ulnar avulsion |
| 1C | Distal avulsion |
| 1D | Radial TFCC disruption |

| Type 2 | Degenerative (Due to ulnar impaction) |
|---|---|
| 2A | TFCC wear |
| 2B | TFCC wear + Lunate and/or ulnar chondromalacia |
| 2C | TFCC perforation + Lunate and/or ulnar chondromalacia |
| 2D | TFCC perforation + Lunate and/or ulnar chondromalacia + Lunotriquetral Ligament perforation |
| 2E | TFCC perforation + Lunate and/or ulnar chondromalacia + Lunotriquetral Ligament perforation + Ulnocarpal osteoarthritis |

## 1.2   4DCT

When assessing dynamic pathologies (such as TFCC lesions) using static imaging techniques, the image is a limited reflection of the pathology. This limitation arises from the fact that the pathology encompasses dimensions beyond the scope of these imaging techniques, leading to either information concealment or compression. Similar to the introduction of the third dimension in computed tomography (CT) improving the reflection of bone structures, the introduction of the temporal dimension may improve the reflection of dynamic structures.

Four-dimensional computed tomography (4DCT) allows for kinematic assessment of active wrist motion. This raises the prospect of non-invasively visualizing small positional changes in bone structures during motion, benefitting from a combination of high spatial and temporal resolutions [9] [12]. The Radboud University Medical Centre (Radboudumc) has access to a Canon Aquilion ONE ViSION CT scanner capable of capturing 4DCT images. At the plastic surgery department at the Radboudumc there is an ongoing study project evaluating the use of 4DCT for the diagnosis of dynamic wrist pathologies. The department has already successfully designed a workflow for automatic analysis of carpal kinematics related to the scapholunate ligament [13].

While 4DCT can theoretically contribute to an improved non-invasive method of diagnosing TFCC injuries, there are limited studies that have explored this application [9]. Therefore, the aim of this master thesis focusses on developing an automatic algorithm for diagnosing TFCC injuries using 4DCT, building upon the automatic algorithm for diagnosing scapholunate injuries as developed by Teule and Haenen [13].

## 1.3   The DRUJ and DRUJ instability

The DRUJ is a complex diarthrodial joint in the wrist located between the sigmoid notch of the distal radius and the ulnar head and allows for forearm pronation and supination [14]. The DRUJ is inherently unstable due to the difference in curvature between the ulnar head (approximately 10mm) and the sigmoid cavity (approximately 15mm) [15]. Thus, the DRUJ requires constant stabilization by soft tissue structures [9]. The structures that provide this stability are the ulnocarpal ligaments, the sheath of the extensor carpi ulnaris and the triangular fibrocartilage. These structures together form the TFCC [15]. When this stabilization factor is injured, the ulnar head has too much freedom of movement resulting in subluxation and abutment with the surrounding bones causing osteoarthritis. This is most likely when pressure is exerted on the DRUJ due to axial loading during grip or during the pronation movement of the wrist.

The diagnosis of a subtle DRUJ instability can be challenging due to subjectivity and lack of validity of clinical tests [16]. Common clinical examination methods such as the piano key method and the DRUJ stress test have limited sensitivity (respectively 66% and 59%) and specificity (respectively 96% and 59%) [17]. CT and MRI can have diagnostic value but subtle DRUJ instability can remain undetected using static imaging modalities (see also: *1.1 The triangular fibrocartilage complex (TFCC)*). Undiagnosed and untreated DRUJ instability can lead to progressive pain worsening, functional compromise and osteoarthritis [9].

Treatment of a TFCC injury has the goal to achieve and maintain anatomic alignment and dynamic stability [9]. Surgical options for repair depend on the location and severity of the TFCC lesion. In some cases, the DRUJ can be stabilized by repairing the TFCC to the fovea. If repair is not feasible the TFCC has to be reconstructed [15]. Reconstruction can be done by an indirect stabilization (i.e. an ulnocarpal sling or tenodesis) or a direct stabilization (i.e. direct radioulnar connection extrinsic to the joint). This stabilisation stops the pathological movement and thus abutment, consequently reducing the aforementioned pain worsening, functional compromise and secondary osteoarthritis.

## 1.4    Ulnar variance and ulnar impaction

Ulnar impaction (also called ulnar abutment, ulnocarpal impaction or loading) is a degenerative wrist condition caused by the ulnar head impacting on the carpal bones. In contrast to the traumatic TFCC lesions which lead to DRUJ instability, ulna impaction might result in an injury of the central part of the TFCC and bone oedema, causing pain. Patients with ulnar impaction have chronic or subacute ulnar-sided wrist pain which may be increased during activity, swelling and limited wrist movement. Movements that increase ulnar variance such as gripping firmly, pronation of the wrist and ulnar deviation of the wrist may also increase symptoms.

Ulnar variance (also called Hulten variance) is the relative difference in length between the ulna and radius measured as the distance between the distal articular surfaces of the ulna and radius in proximal distal direction [18]. TFCC injuries are often associated with increased positive ulnar variance, which is when the articular surface of the ulna is more distal than the articular surface of the radius [8]. Ulnar variance is not a static difference, during pronation the ulna moves relatively distal and dorsal compared to the radius and moves in opposite direction during supination. This results in a relative change in length of the ulna and a change in axial load on the ulna. Normal ulnar variance ranges from a mean of +0.19 mm in supination to a mean of +1.07 mm in pronation [19]. Due to the big differences during wrist motion, a static scan may thus not give the full story. If there is a positive ulnar variance greater than 2.5mm the ulnocarpal load increases from 18% to 42%. Ulnar shortening can increase the stability of the DRUJ by reducing ulnocarpal load and tightening the TFCC ligaments [20].

## 1.5    Outline of the thesis

TFCC injury is a complex injury in which not only the diagnosis is challenging but also the estimation of the clinal consequences. With the help of 4DCT, knowledge of normal and pathologic DRUJ kinematics caused by different type of TFCC lesions might improve both the diagnosis and assessment of clinical implications. This thesis aims to give new insights in the possibility of using 4DCT to automatically assess the TFCC and DRUJ stability. The main research question of this thesis will be: *"What is the feasibility of using automatic 4DCT analysis to assess the DRUJ and TFCC?"*. The goal will be to take the first steps in developing an algorithm that automatically assesses kinematics of the DRUJ and set a basis for future work on TFCC diagnosis using 4DCT. To make this thesis a guidance for future work the focus will be on exploring different aspects of DRUJ kinematics and outlining the ideas and methods used. Therefore, the following sub-questions will be explored:

- How to acquire 4DCT imaging data for the diagnosis of DRUJ instability?
- What is the robustness of an automatically defined ulnar LCS on different segmented ulnar lengths?
- What is the registration quality of the ulna and how can this be optimized?
- How to automatically measure ulnar variance on 4DCT wrist imaging?
- What is the effect of wrist motion on ulnar variance in the healthy population?
- How to create a workflow for measuring and interpreting the proximity between the ulna and the lunate and triquetrum?
- What are the normal proximity values in healthy wrists during motion?
- How can DRUJ stability be assessed automatically using 4DCT data?
- How do the proposed parameters change in the DRUJ instability patient?

This thesis is the first step to ultimately improve the diagnosis of DRUJ instability and TFCC injuries by 4DCT. However, this puzzle cannot be solved before first acquiring all the pieces. The first piece is of course the imaging data. Momentarily imaging data is only available for radioulnar deviation (RUD), flexion- extension (FE) of the wrist and the clenching of the fist (CF). This may be adequate for

determining ulnar proximity but as mentioned, subluxation of the DRUJ is most likely during pronation. Thus a new study has been set up to acquire **acquisitions of the pronation and supination movement of the wrist** (Chapter 2: Acquisition of 4DCT data).

The acquired CT data cannot be analysed directly. Pre-processing of the data is needed to be able to estimate clinical parameters. First the bones need to be segmented. In previous work by the plastic surgery group an AI algorithm was trained to automatically segment the ulna, radius and carpal bones which has been used. The static segmentations are further pre-processed by estimating the local coordinate system (LCS) of the bones easing further calculations. In prior work the LCS of the radius and a number of carpal bones was established but no LCS of the ulna has been available yet. Thus an **ulnar local coordinate system** (Chapter 3: Local coordinate system of the ulna) is defined and evaluated.

While 4DCT adds the big advantage of the temporal dimension directly showing the dynamic kinematics in the wrists, it suffers from increased artifacts and a smaller FOV compared to static CT. To combine the strengths of both imaging techniques the high-resolution static CT bone segmentations are transformed to the locations as perceived in the dynamic scan. To acquire the transformation matrix needed, registration is performed. This has been done before for most carpal bones and the radius by Teule et al. [13] but has not yet been performed for the ulna. To ensure accurate transformation, **registration of the ulna** (Chapter 4: Registration of the ulna) will be evaluated and improved upon.

After the pre-processing is done analysis can be performed. A number of parameters were chosen based on clinical indicator. In current practice positive ulnar variance (measured on plane radiographs) is used as an indirect indicator for ulnar impaction. To gain new insights in the effect of wrist motion on this indicator and to relate our findings to the current clinical practice a method will be produced to automatically measure **ulnar variance** (Chapter 5: Ulnar variance) using 4DCT imaging. To assess the ulnar abutment the distance from the ulna to the surrounding bones will be measured. This **ulnar proximity** (Chapter 6: Ulnocarpal proximity) and the pattern in which the ulna moves in relation to the surrounding bones may give new insights into the damage patterns caused by lesions. **DRUJ stability** (Chapter 7: DRUJ stability) assessment will be done by using previously developed methods for static CT imaging that will be adapted for use on 4DCT.

An important focus of this paper is how to convey the found information to the clinical practitioner and future researchers so this first workflow can be evaluated and improved upon in the future. Functioning as a first building stone in the use of 4DCT for diagnosis in the DRUJ area. To achieve this an outlook on future use and a first (preliminary) insight in the performance of the given parameters in clinical use is given in by comparing a single patient with DRUJ instability with a healthy volunteer (Chapter 8: Automatic analysis of an instable wrist). Finally, a **general discussion**, future perspectives and recommendations are provided in (Chapter 9: General discussion). In the appendix all described protocols and an overview of produced scripts and how they interact is provided. For an overview of the chapters and how they relate to each other see Figure 2: Overview of the chapters and the way chapters are .
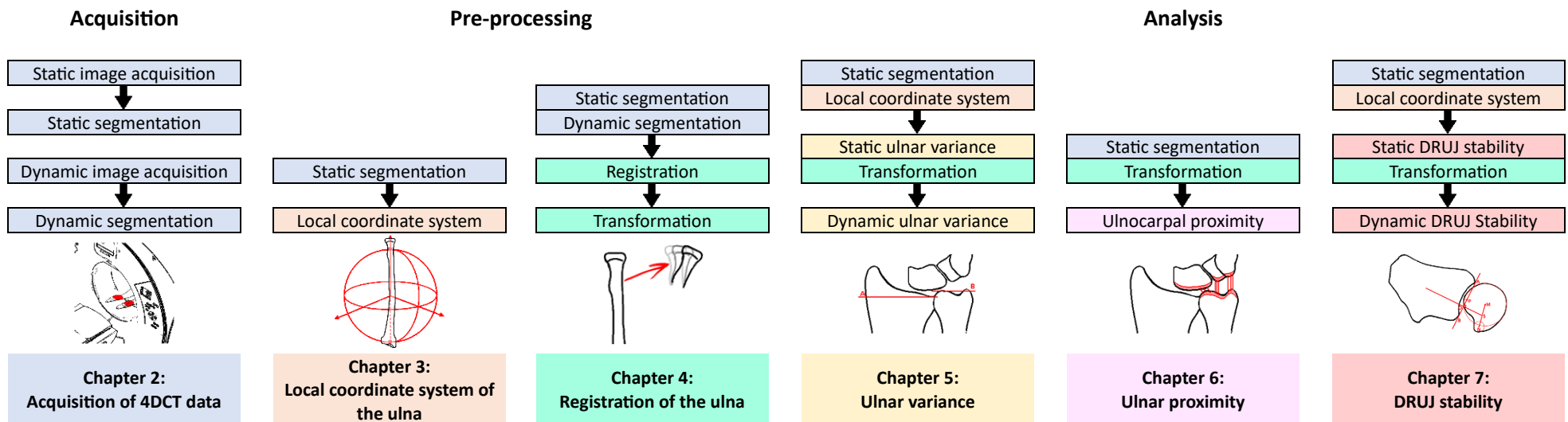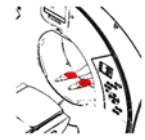
*Figure 2: Overview of the chapters and the way chapters are built upon successive chapters. The blocks matching the colour of the chapters are explored in that chapter. The acquisition and pre-processing are needed for the bigger goal of analysis, where and how they are used is shown above in small vertical flow charts.*

# Chapter 2: Acquisition of 4DCT data

## 2.1 Currently available 4DCT data

The first step in assessing the feasibility of using automatic 4DCT analysis to assess the DRUJ and TFCC is the acquisition of imaging data. While the acquisition of dynamic 4DCT imagery opens the door to visualizing the kinematic dynamics of the wrists it also comes with a number of challenges compared to static imaging.

The first disadvantage is the smaller field of view (FOV) in proximal-distal direction. A conventional CT often consists of a patchwork of images stitched together. When a patient moves through the gantry of the CT scanner several 3D images are taken that are stitched back-to-back creating a bigger 3D volume. In dynamic 4DCT imagery instead of stitching frames back-to-back to enlarge the FOV they are used to visualize movement through time. This limits the FOV in proximal-distal direction to the proper FOV of the CT. Secondly, due to the movement, margins need to be taken into account when selecting the FOV in palmar-dorsal and radial-ulnar direction limiting the resolution in these directions. When acquiring a static scan, the CT laboratory technician draws a tight boundary box around the wrists over which the 512*512 voxels available in the DICOM format are divided. When acquiring data of moving wrist, margins for this movement need to be taken into account and the 512*512 voxels need to be divided over a bigger area reducing the resolution. A last, inherent, disadvantage of 4DCT imagery is the existence of motion artifacts. A projection of a static and dynamic image can be seen in Figure 3.
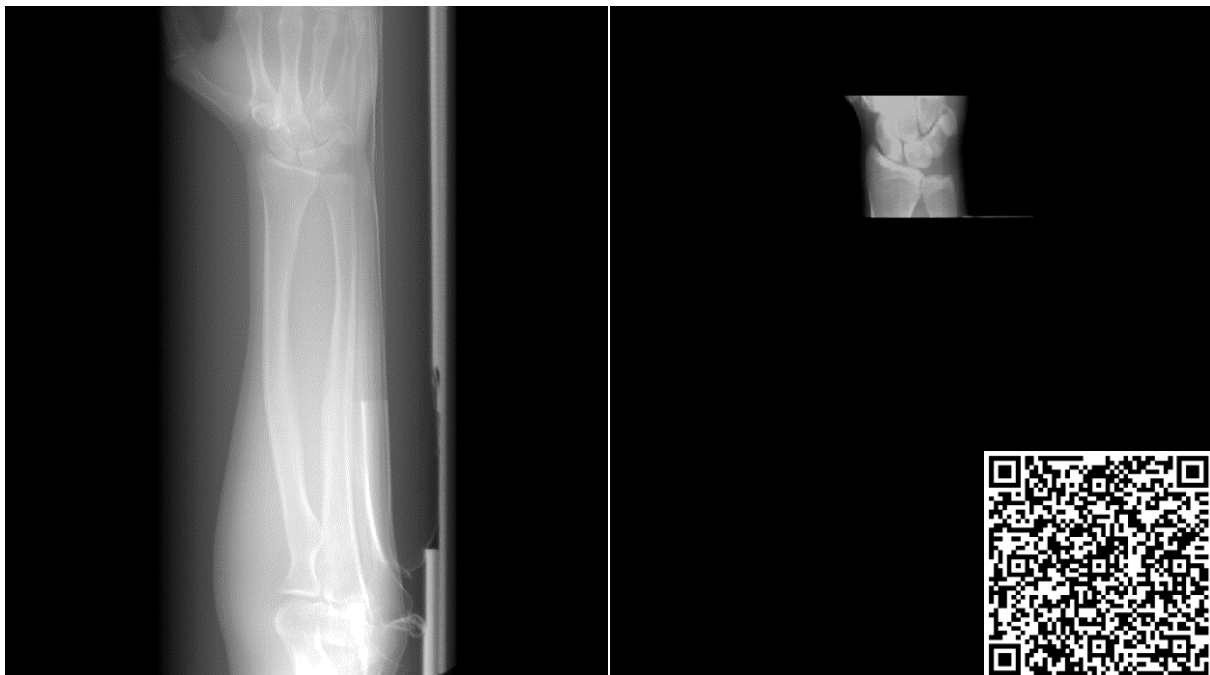


*A: Static acquired image*　　　　　　*B: Dynamic acquired image*
*Figure 3: Projection of both the static scan and the dynamic scan*
*(The QR code can be scanned for a moving version of the dynamic image)*

Thus, while the 4DCT gives a unique source of dynamic kinematic information this comes with the trade-off regarding the static anatomical information. To overcome this problem the anatomical information of the static scan is combined with the kinematic information of the dynamic scan using registration, this is further described in Chapter 4: Registration of the ulna.

Previously, due to a prior study focused on scapholunate ligament injuries, a 4DCT dataset including thirty volunteers was acquired. Since this dataset is focused on assessment of the scapholunate ligament, clinically important movements for these types of injuries are visualised. This includes a

radioulnar deviation (RUD), a flexion and extension (FE) and a clenched fist (CF) movement, distributed over 144 frames with a frequency of ten frames per second. The exact details of the acquisition of this dataset are given in Chapter 3.2.1 Local coordinate system of the ulna: 4DCT dataset. For the complete assessment of the DRUJ and the TFCC, the pronation-supination (PS) movement is clinically most relevant. So, while the currently available dataset can be used for the development of algorithms, new 4DCT data including the PS movement needs to be acquired for a full evaluation of the DRUJ and TFCC. To acquire this new dataset and gain more insight into how different factors influence the proposed 4DCT workflow, two different studies were set-up: a cadaver study and a volunteer and patient study, which will be further described in this chapter.

## 2.2 Cadaver study

### 2.2.1 Study set-up

The expansion of the focus of the project from preoperative scapholunate ligament injuries to other ligamental injuries and postoperative imaging, raises the need for the acquisition of new data. Due to the radiation dose involved with every scan, expanding the current dataset with healthy volunteers and patients is not an easy process, as will be further elaborated on in chapter 2.3 "Volunteer and patient study". As a preparatory step for the volunteer study and to answer a number of research questions, a cadaver study was set up in collaboration with the orthopaedic research lab. For this study static and dynamic CT images of a cadaver arm were acquired during different velocities of the PS movement, in different positions regarding to the gantry and with and without osteosynthesis material. To allow for this a set-up was made that fixated the upper arm in a 90-degree angle from the lower arm and movement was enabled by a stick fixated to digitorum 2-5 with digitorum 1 fixated to the side. The set-up is shown in Figure 4. Further preparation was done by inserting and removing osteosynthesis material in the ulna so easy reinsertion in the CT scanner room would be possible, after which the arm was sutured shut.



| | |
|---|---|
| **A.** The set-up allowing for PS movement of the cadaver arm. (for an offline moving version of the gif follow the QR code) | **B.** Set-up inside the CT scanner |

Figure 4: Set-up of the cadaver arm study

### 2.2.2  Performed experiments.

Below the five experiments performed with the cadaver arm and the thought process behind them are described. The full protocol including a list of all scans can be found in appendix 11.2 Protocol cadaver study.

**Effect of location in the scanner gantry and different reconstruction protocols on image quality**

The current clinically used acquisition workflow is based on what was deemed best at the time of the workflow set-up. To back this up with data an experiment was carried out to acquire data to study and improve on image and segmentation quality. Image quality (in terms of both resolution as well as artefacts) and in continuation the segmentation quality is affected by intrinsic parameters such as the reconstruction and segmentation method as well as extrinsic parameters such as position and velocity of the captured wrist. Fully controlling these extrinsic parameters and the acquisition of a large number of scans of the same arm is not possible in living volunteers and thus warrants the need for a cadaver experiment. This static imaging following both a static as well as a dynamic protocol enables calculation of the steady-state error, the combined error of segmentation and registration in imaging with noise [21].

The signal to noise ratio is predicted to be better in the centre of the gantry than towards the outside of the gantry. With the current protocol (scanning two wrists simultaneously) the wrists are located more towards the outside of the gantry. Imaging the cadaver wrist both at the centre of the gantry as well as in the currently used position will give insight into the difference in signal to noise ratio and aid in making a more well-advised consideration on the trade-off between image quality and radiation.

In the current clinically used acquisition workflow the reconstruction of the analysed data is done by the "BONE" protocol which is supplied standard with the Canon Acquillion ONE ViSION CT scanner. The reconstruction influences many factors including the aforementioned boundary-box and thus resolution in palmar-dorsal and radial-ulnar plane. By acquiring the raw data of the CT acquisition, the reconstruction can be influenced retrospectively and the effect of different reconstruction algorithms on the segmentation quality can be investigated. Potentially the spatial resolution can be doubled by including only one arm and the optimal temporal resolution can be found. Raw data was acquired for all performed experiments. The radiology research group Axti will further investigate the acquired raw data and determine the optimal reconstruction algorithm.

**Estimation of movement velocity on motion artefacts during the PS movement**

Since the start of this internship experiments have been done to include PS movement in the clinical workflow for diagnosing wrist problems. Furthermore, a previous performed study by Dobbe et al. showed an increased error due to motion artifacts when rotation of a phantom is performed in opposite direction to the gantry rotation [21]. Based on both of this data and prior experience with the RUD and FE motion it was decided to perform the PS movement in 10 seconds (as opposed to 7 seconds for both the RUD and the FE motion). When visually analysing the acquired scans with the radiologist it was concluded that these scans are sufficient for visual analysis but would likely pose problems during automatic analysis due to motion artefacts. To determine the optimal speed before the volunteer study described in chapter 2.3.2, a cadaver experiment was set up.

Three different movements were tested: the standard PS movement in 10 seconds; pronation in 7 seconds and pronation in 10 seconds. As described in chapter 1.3 "The DRUJ and DRUJ instability", the pronation movement is clinically the most important. To not further increase the effective dose of the scan it was decided to only capture this movement. After visual inspection this experiment aided in decreasing the speed of the movement to one pronation movement during 10 seconds. Raw data was saved to enable possible future artefact reduction through reconstruction algorithm adaptation.

**Effect of OSM on the segmentation algorithm**

One ultimate goal of the 4DCT project on wrist injuries is to compare pre- and postoperative movement to see if and how intervention changes the kinematics of the wrist. An often used procedure for ulnar impaction is ulnar shortening osteotomy during which the ulna is shortened by removing part of the ulnar shaft. For these interventions OSM in the form of an ulnar shortening plate is used. Due to the high density of the used material these plates are known to cause metal artefacts which will hinder the segmentation algorithm.

To investigate the effect of metal artefacts on the imaging and segmentation performance, the static scan as well as the ten second pronation scan were acquired both with and without the ulnar plate. The insertion of the ulnar plate can be seen in Figure 5. Due to the segmentation workflow not functioning during this internship only visual inspection was possible which showed a relatively clearly distinguishable bone. Quantitative evaluation using segmentation is needed to study the effect on the current workflow. Further investigation should be done by comparing the segmentation with and without the ulnar OSM by visual inspection and for example calculating the mean absolute surface difference. The raw data of the acquired scans was saved to enable future experimentation with the best reconstruction algorithm for the use with OSM.



*Figure 5: The inserted ulnar OSM*

**Test-retest reliability of the segmentation algorithm**

The image and segmentation quality determine the minimal accuracy possible for the whole workflow. When expressing the left-right difference between two wrists it is important to also know what the consecutive difference for the same arm would be. The test-retest reliability for the whole workflow (including movement) will be investigated in the patient study (described in 2.3.4 "DRUJ instability test-retest reliability patient study"). To further differentiate between the effect of patient movement and the steady-state error on the test-retest reliability a cadaver experiment was set-up. Several static and non-moving four second scans (using a dynamic protocol) were acquired of the cadaver arm. Quantitative investigation may be performed when the scans can be segmented.

**Optimal FOV for segmentation and registration**

Although not described in the protocol an extra experiment was performed to make future investigation regarding the optimal FOV possible without exposing volunteers to a higher radiation dose. A scan with a sixteen cm FOV including all carpal bones, the metacarpal bones and part of the ulna and radius was acquired. Using this data, the effect of different FOV locations and size can be

investigated. Due to problems with the segmentation workflow these experiments cannot be performed as of yet but might be interesting in the future.

## 2.3    Volunteer and patient study

### 2.3.1    The set-up of a study with human subjects

For a proper dynamic assessment of the DRUJ and TFCC it is important to analyse all clinically important movements. As described before, only the RUD and FE are not sufficient and thus a new dataset needs to be acquired of both healthy as well as pathological wrists. This new dataset will aid in exploring the differences between normal and pathological wrists; evaluate possible 4DCT-parameters and set-up normal values. Critically important in performing research on human participants is safeguarding the rights, safety and well-being of the subjects. In the Netherlands this is ensured through the Medical research involving human subjects act (WMO). Research that falls under this act needs to be reviewed and approved by a Medical ethical review board (METC) and permission needs to be received from the hospital board. To acquire permission to start the research of both parties the following documents need to reviewed and approved: cover letter; ABR-form; study protocol; Volunteer information letter; informed consent form; recruitment material; liability insurance; WMO insurance; CV main researcher; CV independent researcher; CV other researchers; research statement; radiation ethics form; monitoring plan and data management plan.

During this internship a study was set-up and METC approval was received for 30 left-right volunteer acquisitions during PS, abduction-adduction (AbAd) and opposition-reposition (OR) of the thumb; 30 DRUJ instability patient acquisitions during PS, FE and RUD and test-retest reliability acquisitions of 20 of these patients. A short description of these studies is given below, the full protocol can be found in appendix 11.3 Protocol volunteer and patient study.

### 2.3.2    Healthy volunteer study for DRUJ and MCP-1 normal values estimation

**Method**

To be able to diagnose pathologies in DRUJ instability patients and differentiate those from non-pathological wrists it is essential to study non-pathological wrist kinematics and obtain reference values. To obtain this information for the PS movement I set-up a volunteer study. To enable future further extension of the 4DCT project to the first metacarpophalangeal joint (MCP-1), both clinically important movements for this joint (OR and AbAd) were also performed in this volunteer study. 4DCT scanning was performed bilaterally to allow for comparison between the left and right wrist, which will provide more insight into the extent of non-pathological left-right differences and might increase diagnostic accuracy.

In the volunteer study, thirty healthy participants underwent a bilateral 3D CT scan in neutral wrist position and a bilateral dynamic 4DCT scan while moving the wrist according to the reference protocol as described below. To aid in precise and consistent movement, videos demonstrating correct wrist movement were shown to the participant during image acquisition. A healthy volunteer had to adhere to the following inclusion and exclusion criteria: age between 18-50 years; no medical history of trauma and/or wrist pain and/or surgery, no limited wrist movements; no arthritis as visible on a radioscopic scan and not pregnant. For all healthy volunteers range of motion of all wrist movements were measured manually prior to the scan acquisition.

During the 4DCT scanning, the participants were positioned standing or sitting to the side of the scanner table, with their arms fixed in a neutral position and the radiocarpal joints centred in the scan volume. The healthy participants actively moved their wrists continuously and homogeneously in a pronation movement; an AbAd cycle and an OR cycle. For the pronation movement, volunteers had to move their wrists from a supination position to maximal pronation in 10 seconds. For the AbAd cycle,

the thumb had to be moved from maximal abduction to maximal adduction and back to maximal abduction in 4 seconds. For the OR cycle, the thumb had to be moved from neutral to maximal reposition and back to neutral in 7 seconds. The total exposure to radiation was 21 seconds, and the examination time in the CT room, including volunteer positioning and instruction, was roughly 15 minutes.

**Results**

Five scan sessions were organized during which six volunteers were scanned per session. As of the time of writing all volunteers have been scanned but the data has not been segmented yet which is why this data was used minimally in the rest of this thesis (Chapter 8: "A" compares one of these volunteers to a DRUJ instability patient).

An overview of the included participants and the manually measured range of motion (ROM) is given in Table 2.

*Table 2: Demographics of healthy volunteers*

| Demographics healthy volunteers | n=30 |
|---|---|
| Female | 16 (53%) |
| Age (median (IQR)) | 26,50 (24,25-28.75) |
| Right dominant | 27 (90%) |
| | |
| **Right wrist** | |
| ROM FE (median (IQR)) | 155 (150 – 160) |
| ROM RUD (median (IQR)) | 80 (70 – 85) |
| ROM PS (median (IQR)) | 170 (165 – 180) |
| ROM AbAd (median (IQR)) | 80 (75 – 89) |
| Full opposition reached | 29 |
| | |
| **Left wrist** | |
| ROM FE (median (IQR)) | 155 (150 – 164) |
| ROM RUD (median (IQR)) | 75 (70 – 85) |
| ROM PS (median (IQR)) | 170 (165 – 179) |
| ROM AbAd (median (IQR)) | 80 (76 – 90) |
| Full opposition reached | 29 |

Experience from the volunteer data helped in deciding to shorten the pronation movement in the video to 9 seconds. This to ensure patients have an extra second to finish the movement, preventing the clinically most important part of the motion (extreme pronation) to happen after acquisition.

### 2.3.3    DRUJ instability patient study

**Method**

The goal of the patient study is to determine the diagnostic performance of the 4DCT scan in the diagnosis of DRUJ instability in comparison with arthroscopic findings (gold standard). To accomplish this goal parameter values of DRUJ instable wrists (with an arthroscopy proven TFCC injury) will be compared with non-DRUJ instability wrists. For this both the contralateral wrist as well as healthy reference wrists will be used. This study was set-up and METC approval was achieved but the implementation of this study falls outside the scope of this internship.

In the patient study, 30 DRUJ instability patients will undergo a bilateral 3D CT scan in neutral wrist position and a bilateral dynamic 4DCT scan while moving the wrist according to the reference protocol as described below. These patients have to adhere to the following inclusion and exclusion criteria: clinical suspicion of unilateral DRUJ instability for which both a 3D CT scan and arthroscopy are

indicated; they cannot have a medical history of wrist fractures, known ligament lesion other than the TFCC and/or past wrist surgery nor can they be unable to safely undergo arthroscopy or radiographic imaging. The 4DCT has to take place before the arthroscopy so the normal kinematics are not influenced during the dynamic scanning. Due to waiting times for the arthroscopy this will not cause a delay of care.

The DRUJ protocol is based on clinically important movements for DRUJ instability and ulnar impaction and consists of actively moving the wrists continuously and homogeneously in a pronation movement, a RUD cycle and a clenching fist movement. For the pronation movement, patients have to move the wrist from neutral to maximal pronation in 10 seconds. For the RUD cycle, patients have to move the wrists from neutral to maximal radial deviation, back to neutral and then to maximal ulnar deviation and return to the starting point (neutral position) in 7 seconds. For the clenched fist cycle the patient actively squeezes their wrists and keeps exerting force for a few seconds after which they relax again in 4 seconds. Total exposure to radiation will be 21 seconds and examination time in the CT room, including patient positioning and instruction, will be roughly 15 minutes. The patients will be included in the JBZ in the following months.

Using the acquired data the developed parameters in this thesis and possible future parameters will be evaluated on their clinical usage through distinguishability between arthroscopy proven DRUJ instability wrists and reference wrists and distinguishability between left-right differences in arthroscopy proven DRUJ instability wrists and reference wrists.

### 2.3.4  DRUJ instability test-retest reliability patient study
**Method**
Currently limited knowledge is available about the robustness of the workflow and the resulting parameters. This complicates differentiating with high precision between deviations due to pathologies and deviations due to inaccuracies in the workflow. Knowledge of the reliability of the current workflow is also essential to determine whether the current workflow should be further improved. To test this an intra-patient test-retest reliability study was set-up. This study involves twenty of the patients included in the DRUJ instability study to go through the protocol, as described above, twice. Between both series a 15-minute waiting time is incorporated. In consultation with the METC it was decided on to test this on patients due to their closer approximation to the clinical situation and to keep the burden on volunteers to a minimum.
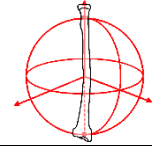
# Chapter 3: Local coordinate system of the ulna

## 3.1 Introduction

Momentarily, there is no good tool for early and objective diagnosis of a TFCC lesion. This is problematic since early treatment of the TFCC lesion may prevent further cartilage deterioration thus preventing pain and the need for more complex surgical interventions like an ulnar head implant. Since a TFCC lesion changes the wrist kinematics, i.e. pronation and supination, 4DCT may be a promising non-invasive tool to gain insight in the state of the TFCC and function of the DRUJ. The 4DCT is capable of recording full three-dimensional (3D) CT scan movies during wrist motion with a frequency of 10 frames per second. The speed with which the 4DCT is able to capture data is both its main advantage as a big disadvantage. The big batch of data may yield a lot of information, but such a big batch of data is also very costly to manually analyse, with respect to money and in hours. On top of that it is very dependent on the skill of the radiologist analysing the data and often only projections of the data are used which may lead to decreased accuracy and reproducibility. This raises the need for automatic analysis to automatically assess bone kinematics. To facilitate automatic analysis a local coordinate system (LCS) of the involved bones is needed. Besides 4DCT has the disadvantage of being hard to interpret due to the moving regions of interest (ROIs) i.e. when investigating ulnar stability, the DRUJ rotates and moves out of the visualised volume. The LCS may be used to stabilize the view on the ulna making this ROI easier to investigate. Depending on the robustness of the LCS method the LCS might be used to help with the registration of the ulna by matching the static and dynamic LCS or be used directly on the dynamic scan.

In a previous study performed at the department of plastic surgery by E.H.S. Teule [22] an LCS is created for the radius based on a method of de Roo et al. [23] In this method, the z-axis is defined as the longest eigenvector of the radius, the x-axis is to be on the plane that passes through both the z-axis and the radial styloid and perpendicular to the z-axis and the origin is defined as the distal intersection of the z-axis and the radial surface. Finally, the y-axis is defined as being perpendicular to the x- and z-axis, the direction of the y-axis is defined by the right-hand rule. Marai et al. [24] have determined the LCS of the ulna in a similar fashion, but instead of using the longest eigenvalue for the z-axis it is defined by the centroids per slice of the ulnar bone and the radial styloid is replaced by the ulnar styloid. At the Radboudumc, LCS calculation of the ulna is not available yet. Since the input data used is a 3D segmentation of the ulna the 2Dfication by the "per slice method" of Marai is not possible. Therefore, in the study of this chapter we aimed to determine an algorithm to automatically define the LCS of the ulna and assess its robustness on different segmented ulnar lengths.

## 3.2 Method

### 3.2.1 4DCT dataset

#### 3.2.1.1 Dataset description

The 4DCT dataset previously acquired to study the function of the scapholunate ligament is used, consisting of thirty-one uninjured dominant wrists of healthy volunteers.

For this dataset the inclusion criteria were as follows:

- Age: 20-40

And the exclusion criteria are as follows:

- Medical history of trauma or surgery of the dominant wrist
- Pain or complaints regarding the dominant wrist
- Pregnancy

- Limited wrist movement of the dominant wrist
- Arthritis visible on CT scan

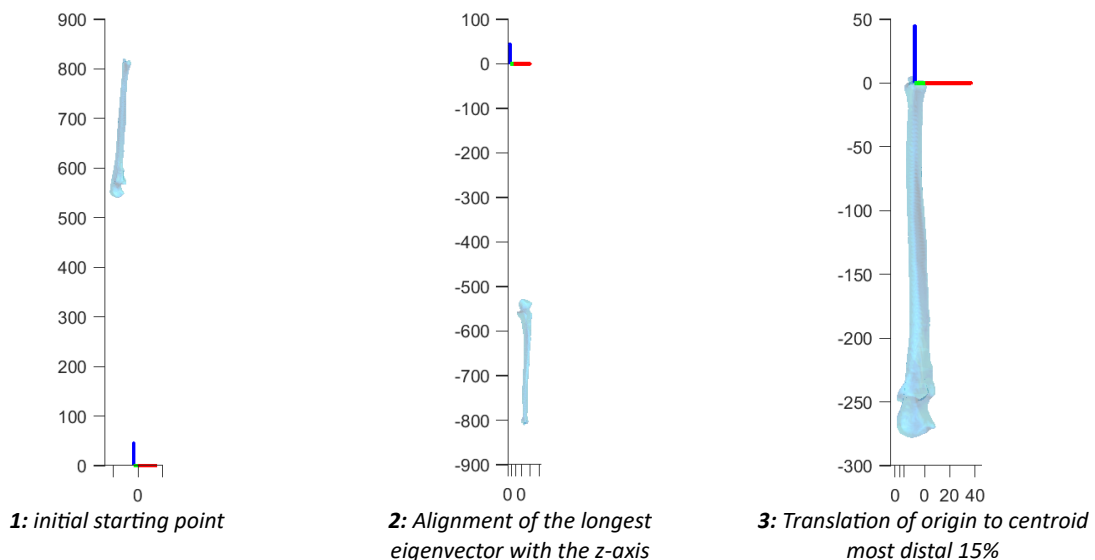### 3.2.1.2    Image acquisition

The same scanning protocol was applied for all volunteers: first a static CT scan including the whole ulna and lunate (and radius and carpal bones but these were not used for acquiring the LCS of the ulna) were obtained whereafter a dynamic CT scan was made including at least the most distal 2 cm of the ulnar head. This dynamic scan consists of two type of movements, each 72 frames at 10 Hz: RUD and FE motion. In order to limit motion artefacts and to get a standardized movement as possible, the dominant forearm is placed in a specialised frame which stabilizes the forearm but allows for wrist movement.

Images are acquired at the Radboudumc, Department of Radiology, using an Aquilion ONE Prism, CT scanner (Canon Medical Systems, Otawara, Japan). The static CT scan has a FOV that covers the full ulna, the full radius and all carpal bones. It is acquired with the following parameters: 80 kV; mA based on dose modulation; CT Dose Index: 0.16 mGy; Dose length product: 8.03 mGy∗cm and voxel dimensions: 0.34 x 0.34 x 0.3. The dynamic 4DCT scan used a smaller FOV of 8 cm including all carpal bones and part of the radius and ulna and consists of 144 frames. The following CT parameters are used: 80 kV; 40 mA, CT Dose Index: 3.4 mGy; Dose length product: 27.5 mGy∗cm; voxel dimensions: 0.63 x 0.63 x 0.5; gantry rotation time: 0.275 s and a scanning time of 7.2 s.

The ulna, radius and carpal bones are segmented in all scans using a 3D no-new U-net (nnU-net) architecture model trained on patches of the image to recognize wrist bones. [25]

## 3.2.2    Ulna LCS estimation

The method for defining the LCS of the ulna, as shown in Figure 6, is adapted from an automatic method for the definition of the LCS of the radius by de Roo et al. [23]



*1: initial starting point*  *2: Alignment of the longest eigenvector with the z-axis*  *3: Translation of origin to centroid most distal 15%*

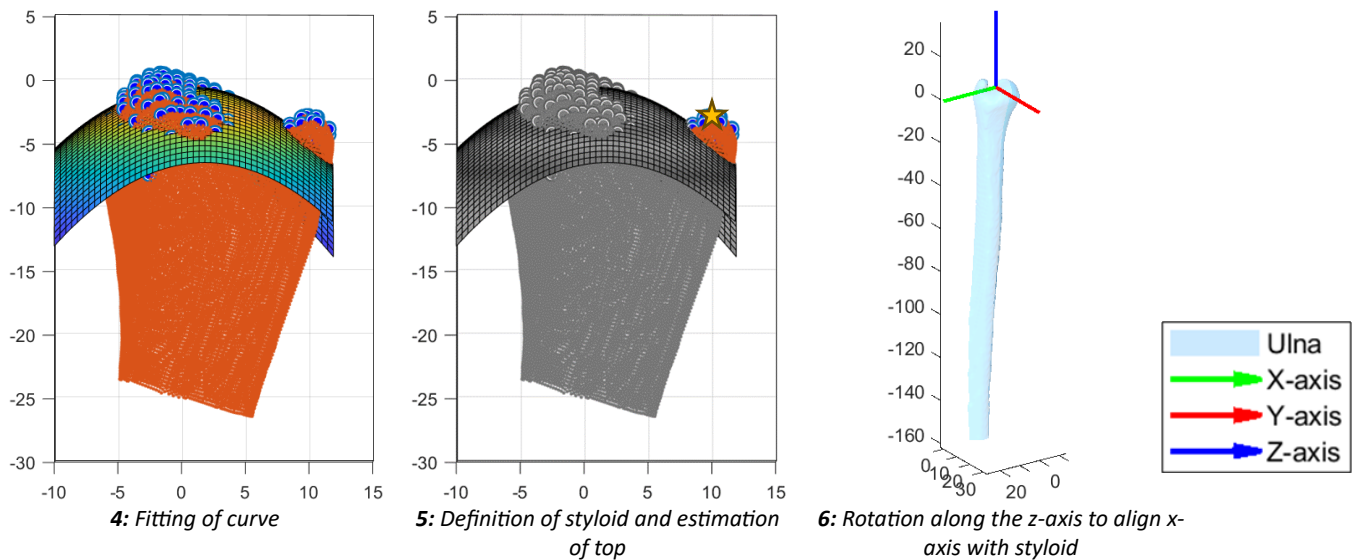| 4: Fitting of curve | 5: Definition of styloid and estimation of top | 6: Rotation along the z-axis to align x-axis with styloid |

Figure 6: Method for defining the LCS of the ulna.

First the inertia tensor is calculated using the vertex coordinates which enables calculation of the eigenvectors and eigenvalues. The vector with the smallest eigenvalue is the longest axis of the bone and is defined as the z-axis. The other eigenvectors are defined as the x- and the y-axis, forming a temporary ulnar coordinate system. A transformation is applied to align this z-axis with the global coordinate system. The z-axis of this temporary ulnar coordinate system is subsequently translated to the centroid of the distal 15% of the ulna. If the resulting part is shorter than 20 mm the most distal 20 mm of the ulna is used.

The length of the ulna is calculated by subtracting the lowest z-value of the ulna from the highest z-value of the ulna. The origin of the temporary ulnar coordinate system is consequently transformed to the distal intersection point of the ulnar surface. The coordinate system is rotated such that the x-axis is on the plane crossing the z-axis and the top of the ulnar styloid. Unlike the radius the styloid is not always the point with the highest z-coordinate.

To identify the styloid the following method is used: first for every square mm the vertex with the highest z-value is identified forming the top layer of the ulna. Afterwards a parabola defined by Equation 1 is fitted to this top layer of the ulna. Consecutively the distances from each point on this top layer to the fitted parabola/curve are calculated. The vertex with the largest distance to this parabola/curve is defined as belonging to the styloid. The vertex with the highest Z-value within 5 mm from this point is defined as the top of the styloid. The x-axis is defined as on the plane crossing both the origin and the top of the styloid and perpendicular the z-axis. The remaining eigenvector is defined as the y-axis in dorsal direction.

*Equation 1: Definition of fitted curve.*

$$a \cdot x^2 + b \cdot y^2$$

### 3.2.3 Evaluation of the ulnar LCS

To evaluate the robustness of the defined LCS on the whole ulna visual inspection is used. When the ulnar LCS is aligned with the global coordinate system, the angle of the ulnar shaft and the location of the ulnar styloid should be relatively similar for all ulnas. The ulnar shaft should be directed in the negative z-direction and the ulnar styloid lays on the x-plane. This is assessed by transforming the LCS of the ulna to the global coordinate system and visually checking these requirements and intra-volunteer similarities.

23

To assess the effect of included percentage of ulna in the segmentation on the LCS definition, the ulna segmentation is shortened in steps of 10% of the total length after which the LCS is redefined and the transformation between the newly defined LCS and the original LCS is calculated. The error of the newly defined LCS is defined as the rotation and absolute translation in respectively the PS, FE and RUD angle and proximal-distal, volar-dorsal and radial-ulnar direction.

## 3.3 Results

### 3.3.1 4DCT dataset

The characteristics of the 4DCT dataset used are described in Table 3. Thirty-one volunteers are included with a median ulnar length of 265.9 mm according to the static CT and a median of 44.3 mm of the distal ulna is included in the FOV during the dynamic CT.

*Table 3: Characteristics of 4DCT dataset of healthy wrists*

| | |
|---|---|
| Number of healthy volunteers | 31 |
| Number of female volunteers | 16 (52%) |
| Number of right wrists | 29 (94%) |
| Median length ulna (mm) | 265.9 |
| Median length segmented part Ulna (mm) | 44.3 |
| Minimum voxel dimensions dynamic scan (mm) | 0.63 x 0.63 x 0.5 |
| Minimum voxel dimensions static scan (mm) | 0.34 x 0.34 x 0.3 |
| Median number of vertices dynamic scan ulna | 8165 |
| Median number of vertices static scan ulna | 197386 |

Figure 7 shows the distribution of the relative ulna length of all dynamic scans to their respective static scan. It can be noticed that in most cases the dynamic scan FOV includes the most distal 10% to 20% of the whole ulna during scanning.
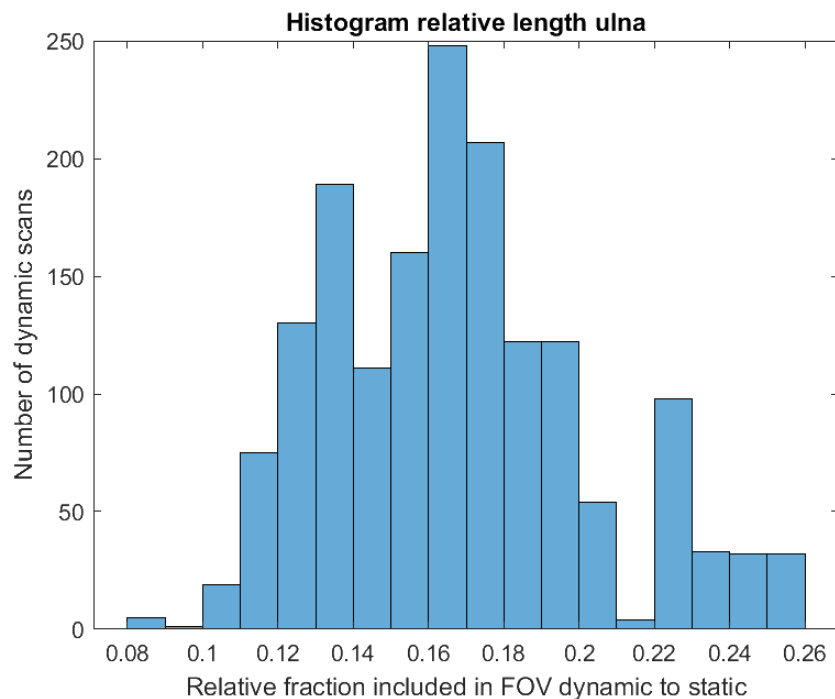


*Figure 7: Histogram showing relative length ulna included in FOV dynamic to static.*

### 3.3.2 Evaluation of the ulnar LCS

Visual examination shows that the used method is able to transform the ulna to their own LCS. Visually all transformed ulnas satisfy the aforementioned criteria in which x-plane crosses the ulnar styloid in all cases and the ulnar shaft lays in the direction of the negative z-axis which shows good robustness for the LCS method on the whole ulna. Figure 8 shows two of the most different ulnar segmentations after transformation of the ulnar LCS to the global coordinate system.
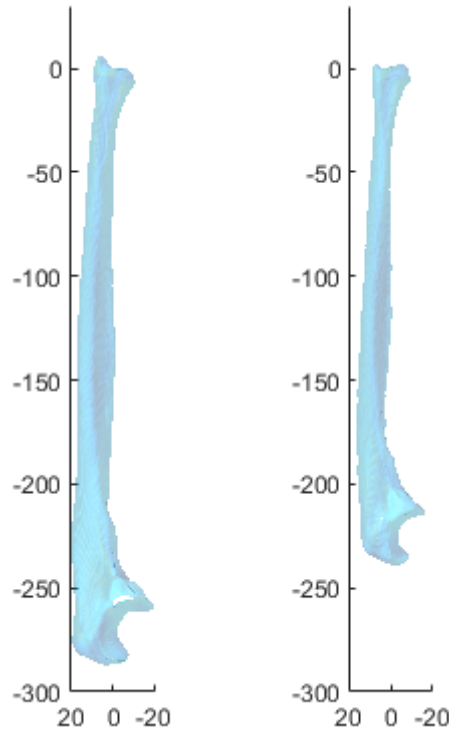


*Figure 8: Visualisation of the longest and shortest ulna in the dataset of thirty-one volunteers aligned with the global coordinate system.*

The biggest median translation error of 2.49mm is in the proximal-distal direction. The other median translation errors stay beneath 2mm. The largest median rotation error of 8.21° is found in the FE angle for 10% of the full ulnar length segmented. The mean rotational error in the pronation-supination angle is -1.72 degrees, in the FE angle 3.1 degrees and in the radial-ulnar deviation angle 0.48 degrees. The total rotation error seems to have a strong relation to the ulnar length in the FOV. Figure 9 shows the translation and rotation error in automatic LCS placement.



*A. The ulnar-radial direction*

*B. The pronation-supination angle*
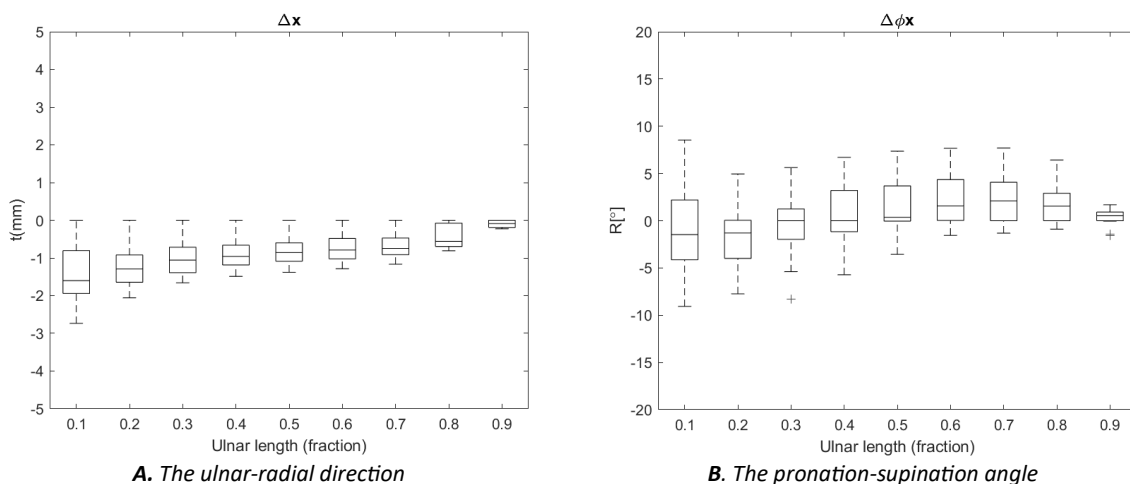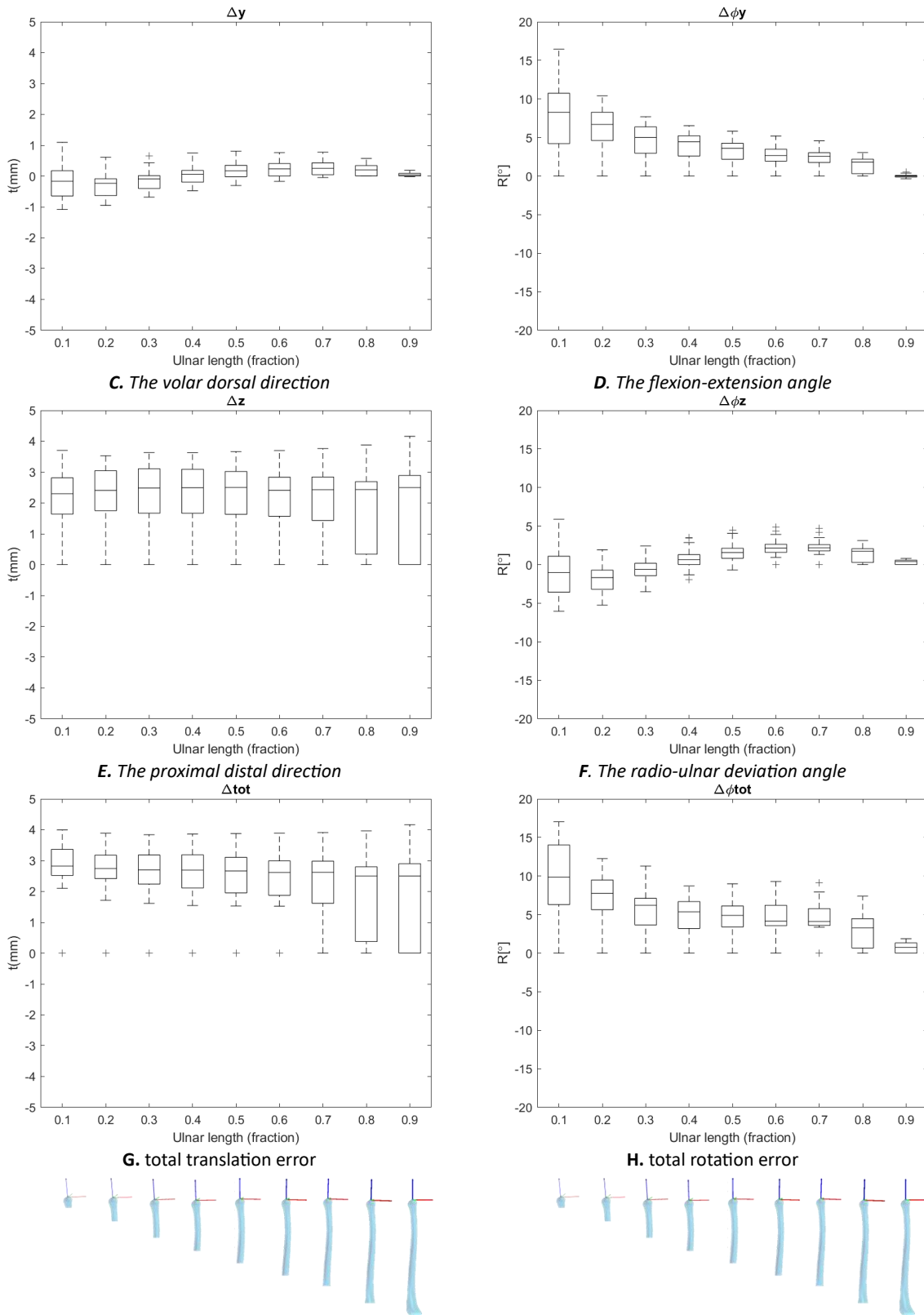
*Figure 9: Effect of fraction of ulna included in segmentation on LCS. The x-axis represents the segmented ulnar length in fraction and the y-axis the error in relative to the LCS of the fully segmented ulna.*

## 3.4   Discussion

In this study we aimed to determine a method to automatically define the LCS of the ulna and assess its robustness on different segmented ulnar lengths. Visual inspection showed that the proposed method robustly defines the LCS of the ulna when using segmentation data of the whole ulna. The expected error on the dynamic scan is between the 5-10$^o$ based on the tests on shorter ulnar fractions. Especially in segmented fractions smaller than 30% of the whole ulna, errors bigger than 5$^o$ in the flexion-extension angle can be seen. This relatively big error -combined with the relatively short relative ulna length as displayed in Figure 7- shows that it is important to first register the whole ulna obtained at the static scan to the dynamic scan before calculating the LCS.

De Roo et al. [23] has evaluated the effect of segmentation of the radius on its local LCS and showed a median error between 0$^o$ and 8$^o$ depending on the angle. In this study the effect of segmentation of the ulna on its local LCS has been studied and we found a bigger error compared to that found by the Roo for the radius which may be caused by the bulk of the volume being proximal for the ulna and distal for the radius. This is considerably larger than in the radius, causing a bigger effect when leaving this part out of the available data for LCS calculation.

Due to the unavailability of a ground truth of the ulnar LCS, the robustness of the LCS of the whole ulna is performed visually. This may create difficulties when using the LCS as a DRUJ stability parameter. Since the accuracy is not known differentiation between inaccuracy and pathological effects is difficult. Haenen et al. calculated the rotational deviation of the proposed method using a statistical shape model (SSM) and measured a median rotational deviation of $1.62°$ $[0.24° - 10.16°]$ [26]. This may be due to the variability in the location of the ulnar styloid but further investigation is needed to define the exact cause. Defining an LCS based on the proximal side of the ulna may be more stable. While the interquartile range of the rotational deviation is quite big the study of Haenen et al. showed that the LCS is most stable in the Z axis which is the only axis used for calculation in this thesis.

## 3.5   Conclusion

To conclude, automatic LCS definition seems visually possible for the static whole segmented ulna but suffers from errors when only using the distal part of the ulna. Therefore, for estimating the LCS of the ulna, first the LCS of the static ulna must be determined and subsequently registering to the dynamic scan must be performed.

# Chapter 4: Registration of the ulna

## 4.1  Introduction

Accurate registration is an essential step in the process of automatic analysis of 4DCT images of the wrist. The 4DCT scans include a new temporal dimension directly showing the dynamic kinematics of the wrists. Information which may be used to improve diagnostics of wrist pathologies such as DRUJ instability and ulnar impaction. But, in contrast to static imaging, dynamic imaging comes with the trade-off of having more artifacts and a smaller FOV (see also Chapter 2: Acquisition of 4DCT data). Registration shows the relation between the static and dynamic data and may be used to create transformation matrices that can form the relation between the two.

A CT scan is acquired by rotating an X-ray source and detector in the form of a gantry around the object that is imaged. After collecting radiographs from a sufficient angular range, a reconstruction algorithm calculates the 3D volume [27]. A faster gantry rotation time allows an increased temporary resolution, but this comes with the trade-off of decreasing the spatial resolution [28]. On top of motion of the imaged object, i.e. the wrist, during acquisition (of the tomographic dataset) creates motion artefacts [27]. The resolution of a static scan is higher, and the bones are not deformed due to motion artefacts. Therefore, it is recommended to register the segmented bones from the static scan on to the bone positions in the dynamic scan. This combines the temporary quality of the dynamic scan with the spatial quality of the static scan. A registration error causes a difference between the perceived location of the registered bone and the actual bone. This registration error is the minimum uncertainty for all motion parameters assessed in later chapters.

Point cloud registration algorithms works by minimizing the potential energy between the two-point clouds defined by the similarity between the two-point clouds. This results in the case of rigid registration in a rotation and a translation [29]. Registration quality is influenced by a number of factors as summarized in Table 4. A low number of data points or a low geometric structure may cause an ill-posed registration problem decreasing registration quality [29]. Influencing variables in this are the shape of the bone, the resolution of the scan, the FOV and number of vertices and faces. Furthermore, close correspondence between the data sets is needed to optimally solve the potential energy minimization problem. Influencing factors in this are the artefacts, quality of segmentation and difference in resolution. Lastly, some registration algorithms tend to fall in local minima hindering correct registration. Influencing factors for this are the type and setting of the registration algorithm and the translation and rotation between the fixed and moving object. Depending on the algorithm used some factors are more important than others.

Table 4: Factors influencing registration.

| Registration algorithm* | |
|---|---|
| Influenced by: | |
| Intrinsic qualities of the ulna: | Differences between static and dynamic scan |
| Geometric structure | Spatial resolution (partial volume effect) |
| | Artefacts (e.g. motion artefacts) * |
| | Fraction of ulna included in FOV scan * |
| | Number of datapoints (faces and vertices) * |
| | Translation and rotation |
| | Errors introduced by segmentation (quality of segmentation and type and setting of registration algorithm) * |

*Factors that can be optimized during this internship*

An algorithm to implement coherent point drift registration (CPD) for the wrist bones has been developed by K.O. Kappe [30] and is further optimized by E.H.S. Teule [22]. The algorithm has been applied to the radius, scaphoid, lunate and capitate. However, the ulna has not been registered yet. This chapter aims to determine the registration quality of the ulna.

## 4.2    Method

### 4.2.1    4DCT dataset
The same dataset is used as described in: 3.2.1 4DCT dataset.

### 4.2.2    Pre-processing of data
Labelled masks of segmented scans are loaded into Matlab (R2020b, The Mathworks Inc, Natick, MA USA). Initial alignment of the segmented bones from the static and dynamic scan is performed based on the mean coordinate of the lunate and ulna. Initial translation is performed to align the mean coordinate of the lunate on both the moving and the fixed volume. Depending on the goal of the experiment the moving volume is always the full static segmentation, and the fixed volume is the dynamic segmentation or a cut version of the static segmentation. Initial rotation of 180 degrees is performed when needed to align the ulna and lunate of both segmentations. To reduce registration time both scans are down sampled to 10% of their original number of faces and vertices with a shape retaining algorithm. Due to the ulna not being completely imaged in the dynamic scans, only the distal part of the static ulna segmentation matching the length of the dynamic segmentation is used for registration.

### 4.2.3    Comparison of registration algorithms

#### 4.2.3.1    Registration algorithms
To find the best registration algorithm for the application of ulna registration a number of registration algorithms are compared: CPD, Iterative Closest point (ICP), normalized ICP, Unscented Kalman Filter-based Registration (UKF) and normalized UKF. For all registration algorithms, experiments are performed to optimize them for the specific application of ulna registration.

*Coherent Point Drift*
Introduced by Myrenko et al. [31] in 2010, CPD treats datapoints as a gaussian distribution centroid. CPD views the registration problem as a probability density estimation function which it solves by using an Expectation-Maximization framework. This is the registration algorithm that has been previously used at the department of plastic surgery of the Radboudumc to register the carpal bones and the

radius. In this study both the version previously used for the other carpal bones as well as the default Matlab function are tested.

*Iterative closest point*
The ICP algorithm [32] uses the closest point operator as defined in Equation 2 to define point correspondences. In this equation C is a point correspondence search function estimating transformation T. The standard ICP registration function of Matlab is used.

*Equation 2: Closest point operator*

$$y_k = C(T(x_i), Y) = \arg\min_{y_k \in Y} \|y_k - T(x_i)\|^2$$

*Unscented Kalman Filter-based registration*
UKF [33] uses a sequential estimator under the filtering network of an UKF as the bases for the registration. The version of the code used for this algorithm is written by Christie et al. [34].

*Normalizing functions*
With the normalized functions we use the 3D direction of the normal vector on top of the 3D coordinate of the vertices. This doubles the amount of data used as input for the registration and elevates from a 3D problem to a 6D problem, decreasing the chance for local extrema.

### 4.2.3.2 Registration
On a randomly selected subset of 500 dynamic scans uniformly distributed over all patients ulnar segmentation was performed after which are subsequently registered to the corresponding dynamic ulnar segmentation using all previously mentioned algorithms. In all cases rigid registration is used. All algorithms resulted in a transformation matrix containing the translation and rotation between the dynamic and the static scan.

### 4.2.3.3 Quantitative analysis
Using the inverse transformation matrix every dynamic ulnar segmentation is registered to their respective static ulnar segmentation. After this both the static and dynamic ulna segmentation are transformed to the LCS of the ulna. Consequently, the registration error is measured as the median absolute point to surface distance (MAPSD) over the distal 2 cm of the ulna, because this always included the region of interest (ROI) of the DRUJ. The MAPSD is calculated using Equation 3 in which $d_{min}(U_s, U_d)$ is the median minimal distance from all vertices in the registered static ulna to the surface of the dynamic ulna and $d_{min}(U_d, U_s)$ is the same calculation the other way. Using this registration error, the different registration algorithms are compared.

*Equation 3: Median absolute point to surface distance*

$$MAPSD = \frac{1}{2}(d_{min}(U_s, U_d) + d_{min}(U_d, U_s))$$

### 4.2.4 Estimation of registration error
Using the registration algorithm that performed best, 3 extra experiments are performed to estimate the registration error of the ulna in a realistic setting and gain insight the size of the role of the factors mentioned in Table 4.

### 4.2.4.1 Static to dynamic registration

In a similar fashion to the comparison of the algorithms, the estimated registration error in a clinical setting is examined by registering the static ulnar segmentation to the respective dynamic ulnar segmentation as shown in *Figure 10*. The registration error is measured over the distal part of the ulna.



**Moving**　　　**Fixed**　　　**Output**

**A:** Static segmentation of the ulna  **B:** Dynamic segmentation of the ulna  **C:** Static segmentation of the ulna registered to dynamic position
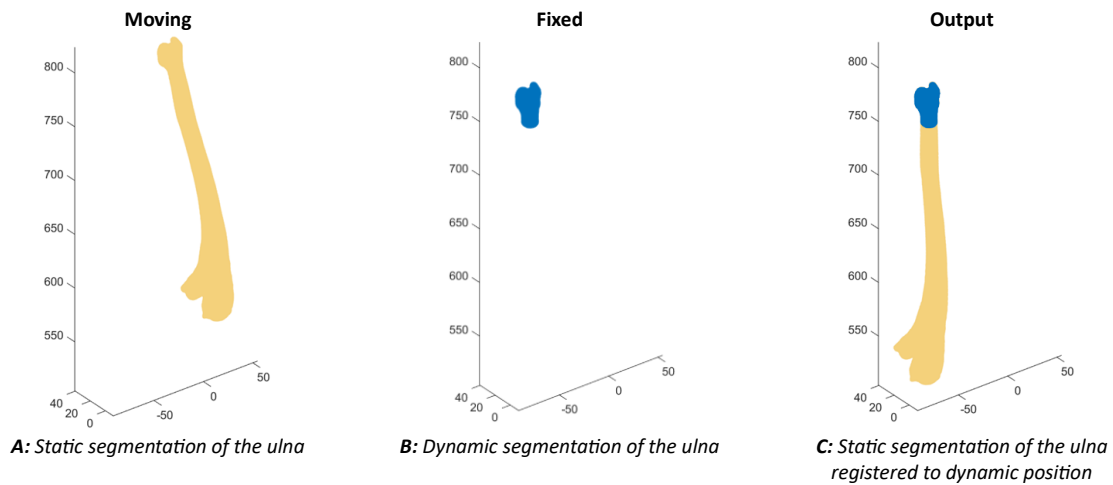
*Figure 10: Static to dynamic registration, the static segmentation including the whole ulna is registered to the dynamic segmentation including only part of the distal ulna.*

### 4.2.4.2 Static to static registration

Consecutively static to static registration is performed to estimate the registration error. This excludes effects from the partial volume difference, possible artefacts, and possible segmentation errors but keeping a realistic difference in translation, rotation and the fraction of ulna included in the FOV. A hypothetical perfect registration algorithm should be able to bring the registration error in this case down to zero making this a good indicator for what optimizing the registration workflow can yield.

For this study the registered static ulna segmentation as obtained in chapter 4.2.4.1 is used as the fixed object. As shown in Figure 11 the registered static ulna is cut to the same length as the corresponding dynamic segmented ulna and down sampled to the same number of faces. Subsequently the non-registered static ulna is registered to the registered cut ulna.



**Moving**　　　**Fixed**　　　**Output**

**A:** Static segmentation of the ulna  **B:** Cut and down sampled static segmentation of the ulna registered to dynamic position  **C:** Static segmentation of the ulna registered to registered static position
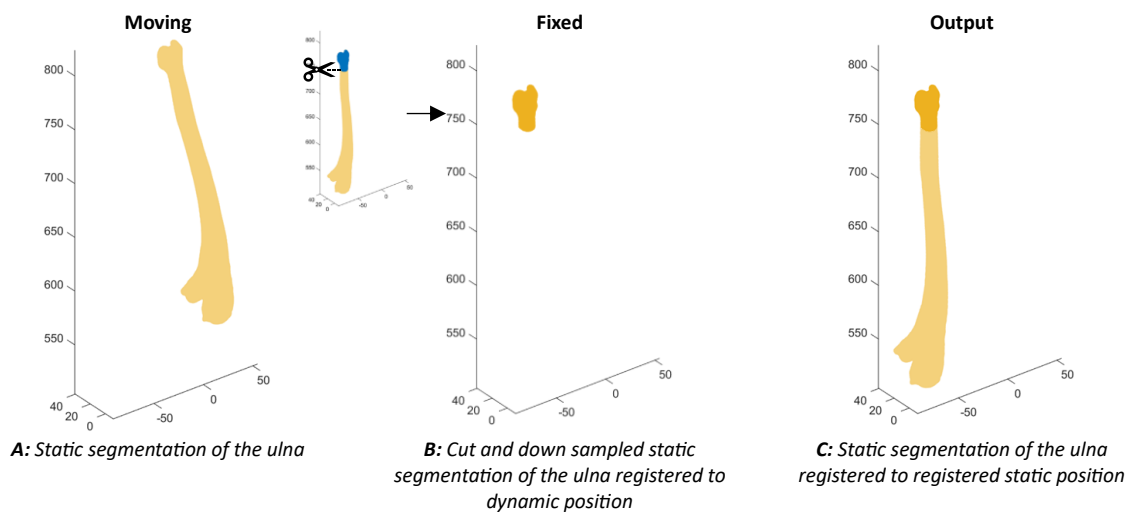
*Figure 11: Static to static segmentation, the static segmentation including the whole ulna is registered to the distal part of the static segmentation previously translated to the dynamic position.*

### 4.2.4.3   *Registration error estimation parameters*

For quantitative assessment of the registration error the MAPSD over the distal 2 cm is calculated. For qualitative assessment visual inspection of the dynamic segmentation, the registered static segmentation and the dynamic scan is performed.

## 4.3   Results

### 4.3.1   Comparison of registration algorithms

A randomly selected subset of 500 dynamic scans uniformly distributed over all patients was analysed. CPD has a smaller MAPSD than the other functions with minimal difference between the version originally used and the version by Matlab.
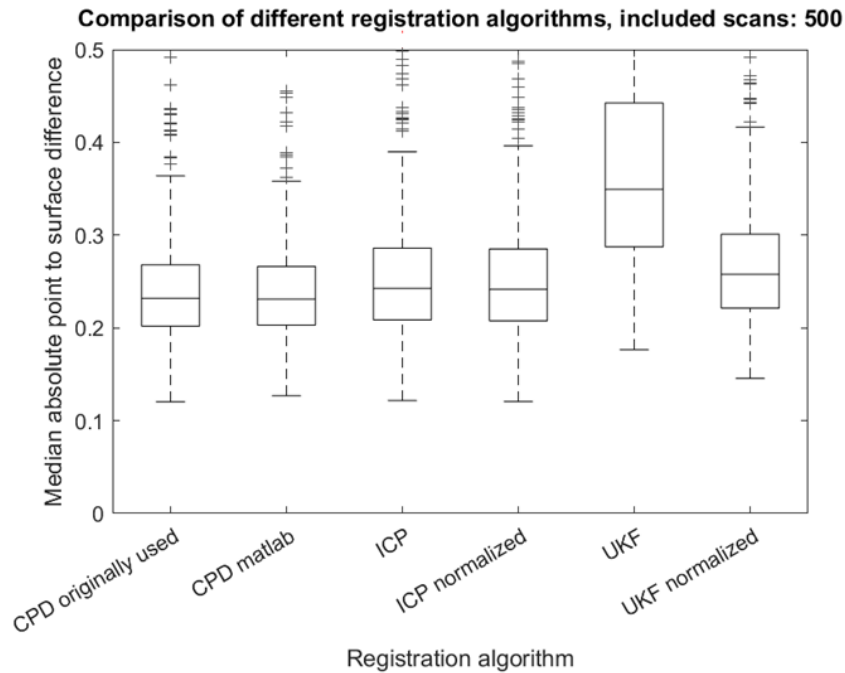


*Figure 12: Comparison of different registration algorithms*

### 4.3.2   Estimation of registration error

Continuing with the original CPD registration algorithm the following results are acquired.

### 4.3.2.1   *Static to dynamic*

Figure 13 shows the MAPSD between the registered static scan and the respective dynamic scan. The median MAPSD is 0.189 mm. The trendline shows that when a relatively longer part of the ulna is scanned the segmentation error is relatively bigger.

*Figure 13: Static to dynamic registration*

Figure 14 shows the registered static segmentation and the dynamic segmentation of a scan with a relatively big error. On the zoomed in picture the registration error can be seen in relation to the voxel size.
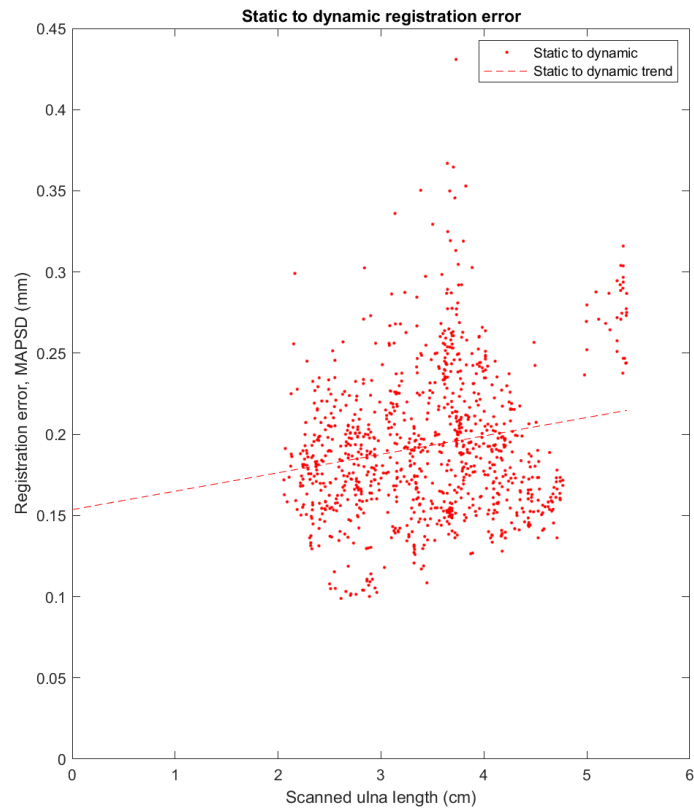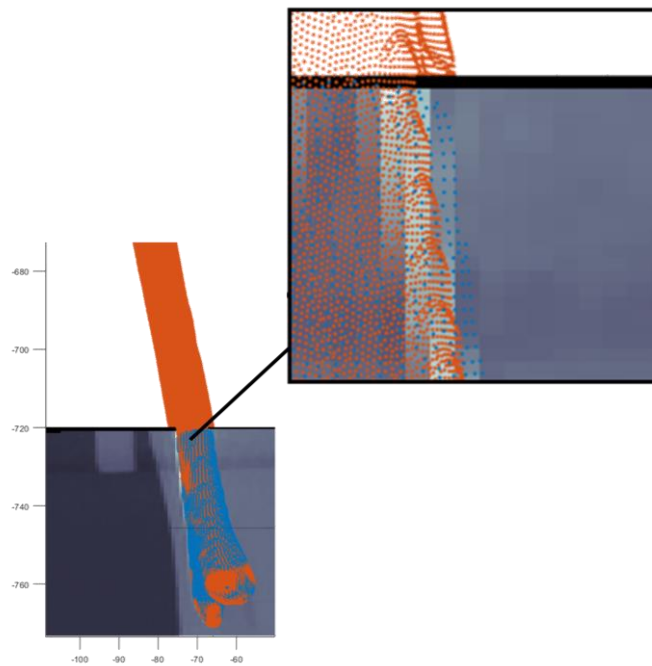


*Figure 14: An example of static to dynamic registration showing the dynamic scan, the dynamic ulna segmentation (blue) and the registered static ulna segmentation (orange)*

33

### 4.3.2.2    Static to static

Figure 15 shows the static-to-static registration error. It can be seen that the registration error is always considerably smaller than the static to dynamic registration error, with a median of 0.0074 mm. A negative trend is shown between the MAPSD and the scanned ulna length which is opposite from what is seen in the static to dynamic.
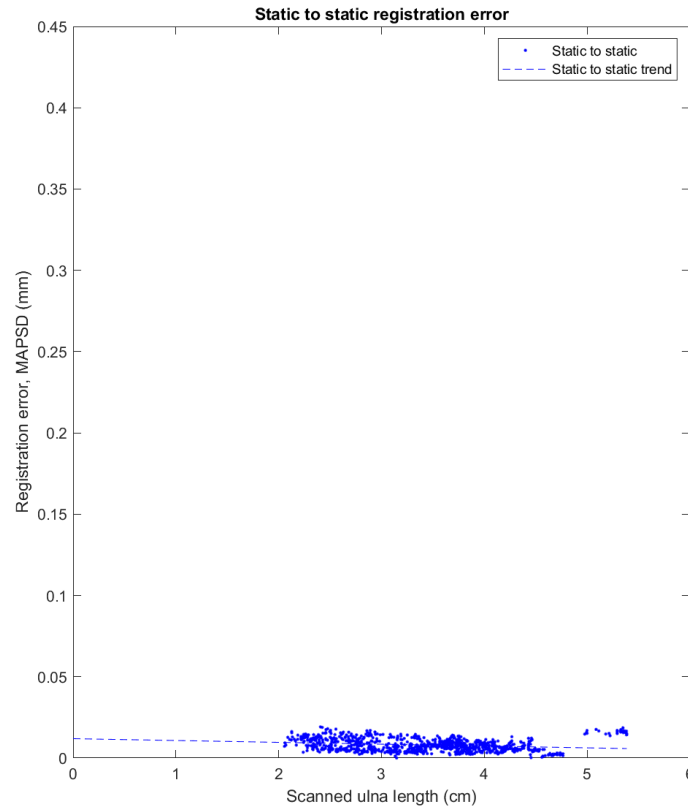


*Figure 15: Static to static segmentation*

## 4.4    Discussion

In this study we aimed to determine the registration quality of the ulna. The CPD registration algorithm already used for the other carpal bones turned out to be the best registration algorithm for the ulna too, this may be affected by noise uncertainty hindering UKF. When estimating the registration error between the static and the dynamic scan a median MAPSD is found of 0.189 mm, this is sufficient, as these values are smaller than the minimum voxel size of the dynamic CT scan (34 x 0.34 x 0.30 mm). When combining the information of the static to dynamic and the static-to-static registrations it can be seen that there is a big difference between the registration error in both experiments. The only factors described in Table 4 that differ between these two experiments are the partial volume distance and motion artifacts. The registration error is thus mostly caused by these factors. Lastly Figure 13 shows that including a bigger part of ulna in the FOV during the dynamic scan will most likely not improve results. Combining this knowledge shows that the registration error is acceptable for parameter estimation. It also shows that improving the factors that can be influenced at the moment is not going to make a huge difference. Therefore, we consider this registration algorithm viable for further estimation of movement parameters.

The segmentation error is previously assessed in a cadaver study [35] where the registration error is assessed by comparing the registered segmentation to a fiducial bead-based determination of bone orientation resulting in a rotation and translation error. This resulted in a translation error of median

0.024mm to a median ~0.8 mm depending on the movement speed which shows similarities with the assessed registration error in this study.

This study gives good insight into registration in the clinical setting. By using data from thirty-one healthy volunteers a realistic assumption can be made of the registration error in a clinical setting. However, it does not give us a definitive insight into how this will affect the investigated parameters since both the dynamic scan as well as the static scan contain errors regarding the bone position. The registration error is measured between the segmented registered static scan and the segmented dynamic scan as the ground truth, in the latter there are potential partial volume effect and motion artefacts present that will increase the MAPSD and affect the registration process making the perfect registration not possible. This error may be further explored in the future by using a different ground truth containing a smaller uncertainty such an artificially controlled ulna of which the exact location is known.

To differentiate between the effect of scan protocol, motion artefacts and segmentation errors a completely non-moving cadaver arm may be used. This fully rules out the effect of motion artefacts and by scanning with different protocols and saving the raw data the effects of the other parameters can be evaluated. Data for this experiment has been obtained (see Chapter 2: Acquisition of 4DCT data) but has not been analysed due to the current lack of a working

## 4.5   Conclusion

In this study, the CPD registration method provided the best registration method for the ulna. The registration error found with this method was relatively small compared to the voxel size of the dynamic scan and acceptably small to use the presented CPD registration method for future research.
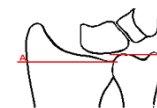
# Chapter 5: Ulnar variance

## 5.1   Introduction

Ulnar variance is defined as the relative difference in length between the radius and ulna. It is used for diagnosing ulnar impaction. A neutral ulnar variance is defined as a situation in which the articular surface of the ulna and radius differ less than 1 mm [36]. When there is a neutral ulnar variance the radius and ulna form a bowl shape of almost continuous height forming a stable base for the carpal bones. With neutral ulnar variance the axial forces are distributed in an 82% to 18% ratio between the radius and ulna, respectively. A deviation in which the ulna exceeds the radius in distal direction is called a positive ulnar variance and deviation in opposite direction is called negative ulnar variance [37]. A correlation between positive ulnar variance and degenerative TFCC lesions has been shown [38]. Ulnar variance differs per person and varies with rotation of the wrist: it increases with pronation and decreases with supination. In addition, it increases with grip. So, ulnar variance has to be determined on the conventional radiograph with the wrist in a neutral position, but it is important to assess also the length of the ulna in a pronated, supinated and fist position to evaluate if there might be a dynamic ulna positive variance. A positive ulnar variance is associated with an increased axial load crossing the ulna, increasing the risk ulna impaction causing TFCC and cartilage degeneration; a positive ulnar variance of 2.5 mm increases the force transferred across the ulna from 18% to 42% of the total load exerted on the wrist [39]. Depending on the amount of the ulnar variance and associated ulnar impaction, damage of ligaments and cartilage occur which might progress to wrist arthritis if left untreated [40] [41].

Previous studies determined ulnar variance on static conventional radiographs or CT images using different methods. Both Roner et al. and Suojärvi et al., define the articular surface of the ulna as the most distal point of the ulna excluding the styloid [42] [43]. However, the radial articular surface is differently defined by both. The study of Roner has defined this surface as the most distal point of the sigmoid notch edge of the radius while the study of Suojärvi defined it as a midpoint between the volar and dorsal ulnar corners of the radius, which has been previously defined by Medoff et al. as the central reference point [44]. The study of Roner uses manual landmarks while the study of Suojärvi uses registered landmarks using a previously developed mathematical model of the wrist. However, this model is only available on original CT images and thus not on the segmented dataset used in this study. Currently there is no method for defining ulnar variance automatically. The change of ulnar variance during wrist motion has only been studied on static radiographs in different static positions like full pronation and supination. Measuring ulnar variance continuously during wrist rotation using dynamic CT's may provide more insight into the effect of wrist position on ulnar variance. These findings may provide new insights about the use of ulnar variance as a predictive value for ulnar impaction. In the study of this chapter, we aimed to determine how to automatically measure ulnar variance on 4DCT and to quantify the effect of wrist motion on ulnar variance.

## 5.2   Method

### 5.2.1   4DCT dataset

The same 4DCT dataset as described in 3.2.1 4DCT dataset was used. For the calculation of ulnar variance segmented meshes of the ulna and radius were used. Static segmentations were used for calculation of the top of the articular surface of the radius and ulna. Dynamic segmentations during a full range of motion of RUD, FE and CF were used for acquiring dynamic data of ulnar variance.

### 5.2.2   Automatic assessment of ulnar variance on the static segmentation

In this study ulnar variance is calculated as the distance in the direction of the radial axis between the most distal point of the ulnar articular surface and the most distal point of radial sigmoid notch (see also Figure 16). Teule et al. have developed a method for the definition of the radial axis. To determine the ulnar variance the distal point of the ulnar articular surface and the most distal point of radial sigmoid notch have to be determined *[13]*. Both these areas of interests (AOI's) are shown in Figure 16.



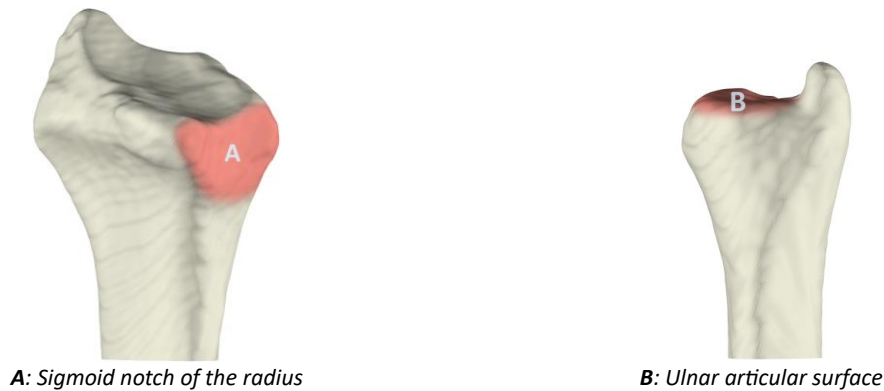*A*: Sigmoid notch of the radius                        *B*: Ulnar articular surface

*Figure 16: Areas of interest for calculation of the ulnar variance*

To extract the most distal point of the ulnar articular surface, the distal surface of the ulna excluding the styloid is extracted. To ease the calculation, the ulnar segmentation is transformed to its own LCS by the method described in Chapter 3: Local coordinate system of the ulna.

First, to save on computing power a rough estimation of the ulnar head is extracted by deleting all vertices but those within 3 cm of the most distal z-value (of the ulna in its own LCS). Afterwards, to exclude the styloid every vertex belonging to the styloid is determined. From the ulnar head the vertex with the highest z-value is defined as the styloid top and the vertex with the lowest mean curvature is defined as the styloid bottom. Subsequently a cylinder is constructed parallel to the z-axis of the ulna using the x-and y-value of the styloid top as the coordinates of the centre axis, and the distance between the styloid top and bottom for both the height and radius of the styloid, *Figure 17.A* shows this cylinder . The biggest group of connected vertices is defined as the styloid. Subsequently, the vertex of the ulnar head excluding the styloid with the highest z-value is determined to be the top of the articular surface of the ulna. This is shown in Figure 17.B.

**A:** *Definition of the ulnar styloid. Defined by the biggest group of connected vertices within the cylinder (A) determined by styloid top (B) and the styloid bottom (C).*

**B:** *Top of the articular surface of the ulna defined as the vertex with the highest z-value in the direction of the longitudinal ulnar axis after excluding the styloid (D).*
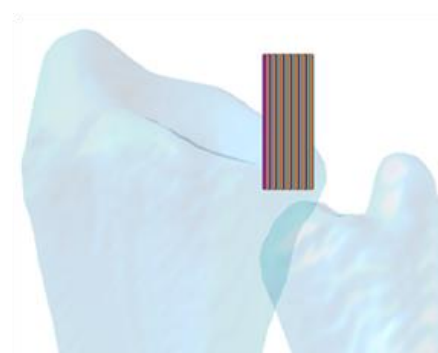
*Figure 17: Method for determining top ulnar articular surface.*

To find the top of the radial sigmoid notch first the volar and dorsal ulnar corners are defined, since the distal boundary of the sigmoid notch runs between these corners (Figure 18). The radius is transformed according to its own LCS using the method developed by Teule et al. [13]. Subsequently the radius is rotated around its z-axis, so the median of the ulnar head is on the xz-plane in positive y direction. The xy-plane splits the radius in a volar side in negative y direction of the xz-plane and the dorsal side in positive y-direction. As a result, the volar ulnar corner can be extracted as the radius vertex with the x-value with y < 0 and the dorsal ulnar corner as the vertex with the highest y-value and y > 0.

A grid following the contours of the radius is used to find the distal edge of the sigmoid notch. The ulnar corners are used as the boundaries of this grid with 1mm spacing in the yz-plane. To ensure that the whole distal edge is included. A margin is used of 1 cm volar of the volar ulnar corner, 1 cm dorsal of the dorsal ulnar corner, 2 cm distal of the most distal of the two corners and 0.5 cm proximal of the most proximal of the corners, to ensure it surrounds the distal edge of the sigmoid notch. This grid is fitted to the radial head as can be seen in Figure 18. After that, for every point on the fitted grid the mean curvature is calculated and the most distal point having a curvature of more than 0.1 is defined as the top of the sigmoid notch. Any outliers, defined as deranging more than 0.5 cm from the expected line, are filtered out after which the most distal point is said to be the top of the sigmoid notch.
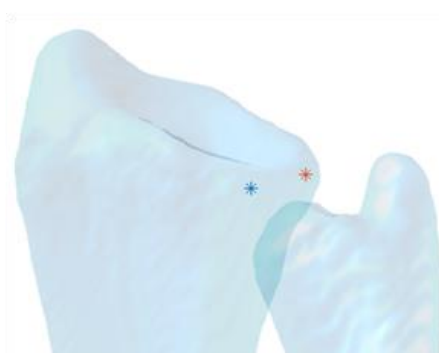


*A. Rotate radius so the ulna is on the x-axis and determine volar and dorsal ulnar corner*

*B. Create grid surrounding first estimation*

*C. Fit grid to radius*

*D. Estimate mean curvature in z direction*

*E. Estimate most distal point with more than 0.1 curvature for every row and filter*
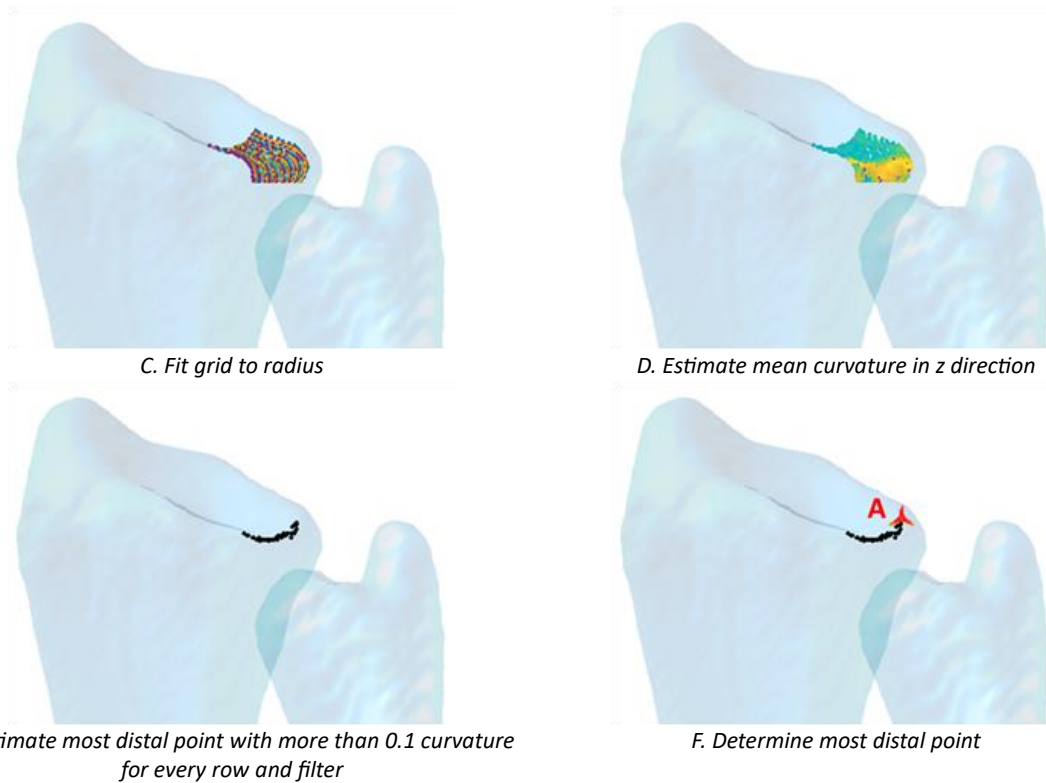
*F. Determine most distal point*

*Figure 18: Method for determining top radial sigmoid notch.*

Thereafter, the ulnar variance can be calculated by measuring the relative difference in z-value between the top of the sigmoid notch of the radius and the top of the articular surface of the ulna along the axis of the radius. This can be performed directly on the static scan, but all three parameters can also be transformed to the positions of the dynamic scan to calculate the ulnar variance during motion.

### 5.2.3   Dynamic analysis of ulnar variance

To evaluate the ulnar variance during wrist motion transformation of the three parameters (the radial axis; the top of the radial sigmoid notch and the top of the ulnar articular surface) from the static to dynamic position is performed. This is done by using previously acquired transformation matrices of the radius and ulna (see also Chapter 4: Registration of the ulna). After transformation the vector between the two transformed points is measured along the transformed radial axis. The obtained ulnar variance values are interpolated and expressed for every wrist motion and plotted against the capitate-radial (CR) angle in the coronal plane for  RUD motion and the CR angle in sagittal plane for the  FE motion. This CR angle is defined as the angle between the radial axis and the capitate axis both previously defined by the plastic surgery group at the Radboudumc. The CF motion cannot be expressed against the angle and is thus only visualised from the beginning till the end of the movement expressed per frame. To visualize change in ulnar variance during wrist motion (ΔUV) the data is also plotted as the ΔUV from neutral position for the RUD and FE and as difference from the start of the motion for CF.

### 5.3   Results

### 5.3.1   Automatic assessment of ulnar variance

Visual inspection of the ulnar variance shows the radial length line corresponding with the top of the sigmoid notch and the ulnar length line corresponding with the top of the articular surface of the ulna. An example of the ulnar variance measurement can be seen in Figure 19.
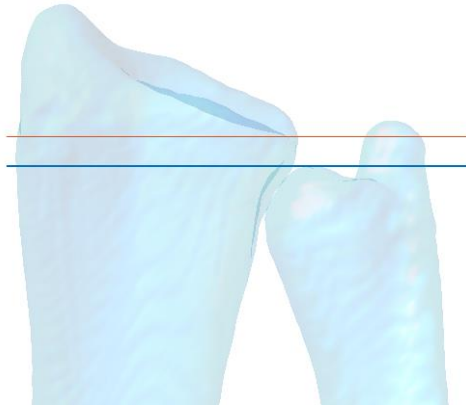
*Figure 19: Visual example of the ulnar variance parameters in a volunteer with a severe 'ulnar minus' with the blue line depicting the measurement of the articular surface of the ulna and the red line depicting the measurement of the articular surface of the radius*

### 5.3.2    Dynamic analysis of ulnar variance

In the group of included volunteers without wrist complaints the median ulnar variance is within -0.21 mm [-1.11 mm – 0.42 mm] of neutral for all movements. The ΔUV fluctuates the most during FE motion with a median range of 0.67 mm [0.55 mm – 0.81 mm] and fluctuates the least during CF motion with a median range of 0.35 mm [0.19 mm – 0.53 mm]. An overview of all characteristics is provided in Table 5.

*Table 5: Overview of the ulnar variance characteristics of the volunteers without wrist complaints*
*Range is defined as: range = maximal ulnar variance – minimal ulnar variance*

|  | **Neutral** (mm) | **RUD** (mm) | **FE** (mm) | **CF** (mm) |
|---|---|---|---|---|
| **Median ulnar variance** (IQR) | -0.21 (-1.11 – 0.42) | -0.17 (-1.09 – 0.39) | -0.14 (-1.08 – 0.46) | -0.18 (-1.21 – 0.45) |
| **Minimal ulnar variance** | -4.96 | -5.11 | -5.12 | -4.65 |
| **Maximal ulnar variance** | 2.54 | 2.79 | 2.53 | 2.02 |
| **Median range** (IQR) | - | 0.45 (0.37 – 0.58) | 0.67 (0.55 – 0.81) | 0.35 (0.19 – 0.53) |

**Ulnar variance during  RUD motion of the wrist**



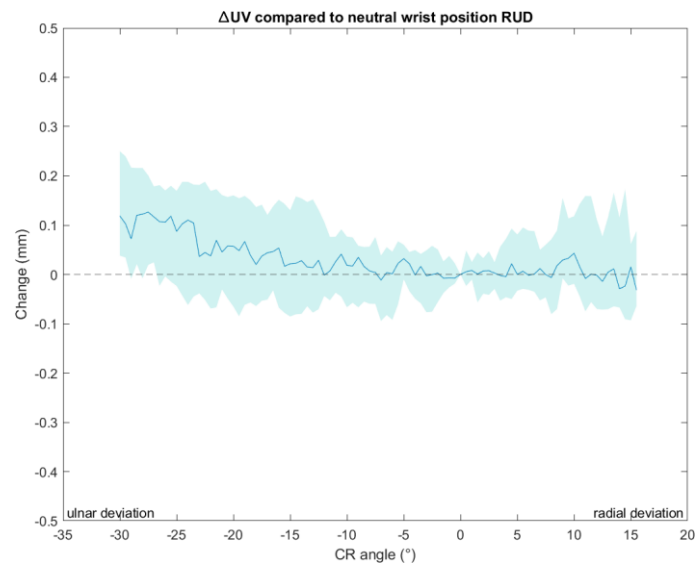*Figure 20: Plot depicting the median ΔUV during the RUD motion expressed against the coronal CR angle for all angles reached by at least fifteen volunteers.*

During the  RUD motion it can be seen that the range between the different volunteers is a lot bigger than the effect of motion on the ulnar variance. The actual ΔUV during motion and in which stage of the motion the fluctuation happens seems to differ per volunteer. Median the ulnar variance increases with ulnar deviation starting around a -10 degrees CR angle, there is a minimal decrease in ulnar variance during radial deviation. This can also be seen in Figure 20.

**Ulnar variance during FE motion of the wrist**
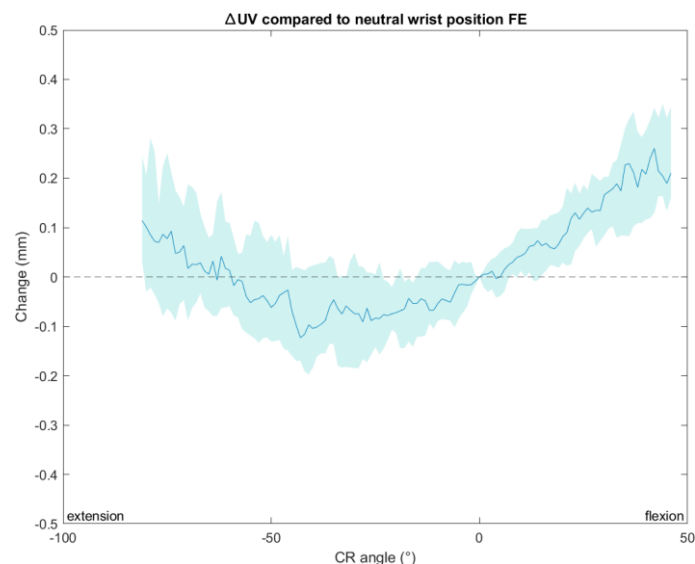


*Figure 21: Plot depicting the median Δ ulnar variance during the FE motion expressed against the sagittal CR angle for all angles reached by at least fifteen volunteers.*

Visually the range of ulnar variance is comparable between FE and RUD while the course of the ulnar variance seems to increase slightly at the outer edges of motion during FE. When looking only at the variation (relative to neutral position) during motion a clearer relationship between the  FE motion and the measured ulnar variance can be seen. In the outer ends of motion, the ulnar variance is most

41

positive, especially in flexion movement. The most negative ulnar variance is reached at a sagittal CR angle of between -40 degrees and -20 degrees (Figure 21).

**Ulnar variance during CF motion**



*Figure 22: Plot depicting the change in ulnar variance during the CF motion for all thirty-one volunteers.*

Because the CF motion cannot be quantified against the CR angle, the ulnar variance is expressed against the start of the motion till th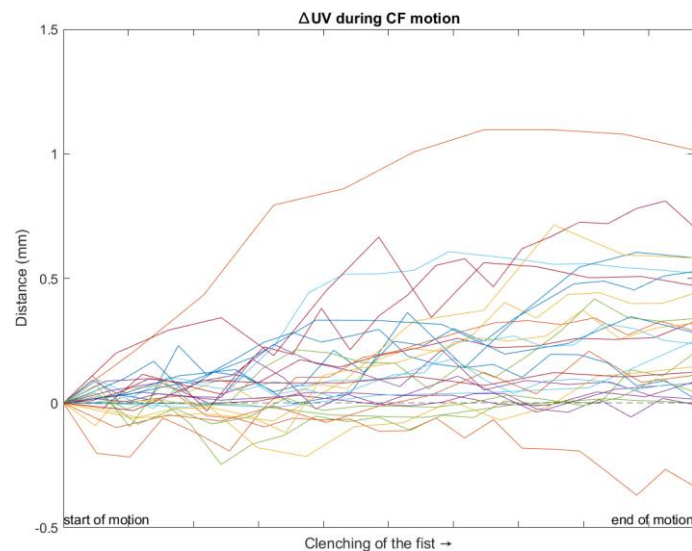e end of the motion. It can be seen that ulnar variance differs less during the CF motion than the RUD and FE motion which may be due to the shorter nature of the motion (4 seconds). When looking only at the ΔUV during the CF motion it can be seen that there is a big difference in the course of the ΔUV between the different volunteers. Overall, an increase of ulnar variance during the CF motion can be seen (Figure 22).

## 5.4    Discussion

In this chapter we aimed to determine how ulnar variance can be automatically measured on 4DCT and what the effect of wrist motion is on ulnar variance. A method was developed to automatically find the points of interest on the static CT segmentations and transform these to their respective dynamic locations to automatically assess ulnar variance on dynamic 4DCT data. With visual inspection these transformed points seem to concur with the expected locations. The median ulnar variance found in neutral wrist position was -0.21 mm and this corresponds with literature on ulnar variance measured on a standard radiograph. In a study by Freedman et al. the average ulnar variance was found to be -0.13 ± 1.5 mm on the left and -0.29 ± 1.6 mm on the right wrist [45]. In another study in adolescents by Goldfarb et al. the mean ulnar variance found was –0.7 mm for men and –0.4 mm for women [46]; in a third study by Schuurman et al. the neutral ulnar variance found was -0.07(1.60) mm for the left arm and -0.30(1.86) mm for the right arm [47] and in a fourth study by Jung et al. 0.74 ± 1.46 mm [48]. This difference in literature may be explained due to the conventional x-ray being influenced by the incidence angle of the x-ray; due to the challenge to place the hand in perfect neutral position and the difference in measuring techniques and skills. Due to the automatic measuring of CR angle not having the hand in perfect neutral position is less of an issue since normal values for every CR angle may be obtained. In case of a not perfectly neutral position it would be possible to compare with normal values in a similar position instead of normal values in neutral position. The difference in measured ulnar variance between an anterior-posterior (AP) and posterior-anterior (PA) radiographs was found to be up to 1.77mm [47]. Since with CT, images are not influenced by x-ray and wrist position, the presented method enables a more valid and reproducible objective ulnar variance calculation. Due to the added

radiation, it is however not advised for daily clinical practice. This also shows that objective measurement using x-ray is not feasible making it difficult to test the method against the golden standard.

Since the different CF measurements have been executed in differing positions, speed and force it is hard to define strict conclusions to this data. While one volunteer has an increase of more than 1 mm there are even volunteers that have a decrease in ulnar variance. This may be due to the power of the clenching fist and the lack of perfectly neutral position of the wrist for all volunteers. Repeating the experiment but with a force measurement may make it possible to combine the data better and express the ΔUV relative to the exerted force.

The analysis of ulnar variance with 4DCT data gives new insights in the ΔUV during motion. In all movements a ΔUV in ulnar variance can be seen. This ΔUV was minimal for RUD and bigger for FE and CF. The ΔUV was most extreme at the outer edges of the motion but this may be due fewer people reaching these CR angles. In prior literature most notably forearm pronation and grip have been known to create a dynamic increase in ulnar variance [49] [50]. Since we do not have processed data on PS movement yet, we could not assess this. In prior literature static measurements have shown the ulnar variance to increase by 0.02 mm in ulnar deviation and 0.24 mm in radial deviation. The current 4DCT data shows almost no ΔUV during radial deviation and 0.1 mm ΔUV during ulnar deviation. The ΔUV during FE is larger with an increase of 0.59 mm in extension. The used method shows that ulnar variance in neutral position gives an underestimation compared to the ulnar variance during FE motion indicating the need of measuring ulnar variance also during flexion and extension to decrease the chance of missing pathological positive ulnar variance values that may explain the complaints of the patients.

## 5.5   Conclusion

To conclude, a method to automatically assess ulnar variance on both static as well as dynamic CT data has been developed. The method overcomes a number of problems that come with measuring ulnar variance on conventional radiographs such as subjectivity, effect of direction of x-ray projection and difficulty of placement of the hand in neutral position. Ulnar variance was shown to change during movement This may mean that positive ulnar variance as the cause for ulnar sided wrist complaints is missed or that the cause of ulnar sided wrist complaints during certain movements cannot be seen on the conventional ulnar variance measurements while they can be seen on dynamic measurements.

# Chapter 6: Ulnocarpal proximity

## 6.1    Introduction

Ulnar sided wrist pain is often called the headache of wrist complaints since it challenging to find the cause of the pain. Despite the long-standing awareness of the relationship between ulnar plus variance and ulnar wrist pain (called ulna impaction syndrome), currently no objective diagnostic tool exists in which the axial load on the ulnocarpal side of the wrist can be visualized and quantified. Currently, the diagnosis of ulna impaction is based on ulnar variance measured on a plain radiograph. However, ulnar impaction has been shown to occur even in wrists with neutral or negative ulnar variance [51]. Furthermore, as has been shown in: *Chapter 5: Ulnar variance,* ulnar variance fluctuates throughout wrist motion further complicating the use of ulnar variance as a predictive value for ulnar impaction. Ulnar impaction has been investigated on MRI, but this only shows bone signal changes after further deterioration and thus is not useable for early diagnosis of impaction [52]. According to a study by Imaeda et al. using MRI imaging to investigate ulnar impaction bone signal changes were found in 90% of the cases at the ulnar side of the lunate, in 40% of the cases at the radial site of the triquetrum and in 10% of the cases at the distal ulna [52].

In addition, TFCC lesions can lead to ulnar sided wrist pain. Palmer's classification describes that TFCC injuries can arise from either traumatic incidents or degenerative processes [11]. Ulnar impaction syndrome is related with degenerative injuries in the centre of the TFCC due to increased ulnar loading [51]. In contrast, traumatic TFCC injuries occur mainly at the periphery of the TFCC complex leading to DRUJ instability and -if left untreated- to progressive arthritic changes on the lunate, ulna and triquetrum [53]. Till now, only with wrist arthroscopy, the type and severity of the TFCC lesion can be analysed but still it is not possible to analyse the effect of the TFCC on the DRUJ kinematics. To adequately diagnose and treat ulnar sided wrist pain there is a need for a more objective tool to analyse the axial load across the ulnar sided wrist and the stability of the DRU joint during wrist motion.

4DCT makes it possible to investigate ulnar impaction directly by quantifying the distance between the ulna and the surrounding bones. Moreover, analysis of the ulnocarpal kinematics may give new insights into the motion patterns and interrelationships between the wrist bones and may be used for injury localisation. To give insight in the possible pathological bone kinematics of ulnar impaction the closest distance between the ulna and lunate and triquetrum is calculated, and the corresponding closest proximity points are decided for every bone. The lunate, triquetrum and ulna were chosen because these bones are most frequently affected by ulnar impaction. [52].

In this chapter we aim to create a workflow for measuring and interpreting the proximity between the ulna, lunate and triquetrum and investigate the normal proximity values in healthy wrists.

## 6.2    Method

### 6.2.1    4DCT dataset

The same dataset as described in: 3.2.1 4DCT dataset was used: two cycles of movements (FE and  RUD motion) of 31 volunteers. For the calculation of ulnar proximity both static as well as dynamic segmentations were needed of the ulna, lunate and triquetrum.

### 6.2.2    Pre-processing of data

The 4DCT scans have been automatically segmented with the use of an AI algorithm based on nnU-net resulting in labelled meshes of the ulna, triquetrum and lunate using the method as developed by Teule et al. [22]. Subsequently, the static to dynamic transformation matrices for the ulna, lunate and triquetrum were calculated using the method described in Chapter 4: Registration of the ulna.

### 6.2.3   Assessment of ulnar proximity on CT data

To compute the minimal distance between the ulna and the two carpal bones, point to surface distance calculations were used. To save on computing time and resources, an initial volume of interest (VOI) was created containing the proximal ulnar part of the lunate, the proximal radial part of the triquetrum and the head of the ulna. To extract these VOIs first a transformation of the three bones to the ulnar LCS was performed to easily identify the spatial position of the bones. The VOIs were identified as follows: The ulnar head was defined as all ulnar vertices with a z-value within 1 cm of the lowest z-value of the triquetrum and lunate. The radial proximal part of the triquetrum was defined as all vertices with a z-value within 1 cm of the highest z-value of ulna and all vertices with an x-value within 1 cm of the highest x-value of the ulna. Similarly, the ulnar proximal part of the lunate was defined as all vertices with a z-value within 1 cm of the highest z-value of the ulna and all vertices with an x-value within 1 cm of the lowest x-value of the ulna. Consequently, the distances between all vertices within these VOIs was calculated. Using this, vertices closest to another bone were identified and the distance between these vertices was computed resulting in the ulnar-carpal proximity.

### 6.2.4   4DCT ulnar proximity assessment on healthy volunteers

To compute the ulnar proximity for the full range of motion the ulnar, lunate and triquetrum meshes obtained from the static scan were transformed to the dynamic position using the prior obtained static to dynamic transformation matrices. Per wrist the ulnar carpal proximity was calculated for the three motions performed: RUD, FE and CF. The carpal proximity was expressed to wrist position measured in CR angles as explained in Chapter 5: Ulnar variance. To visualize the data the relation between the ulnocarpal proximity was plotted for both the triquetrum and the lunate and the related vertices were expressed on an heightmap. The data was combined for all healthy wrists for the CR angle reached by at least fifteen volunteers.

### 6.2.5   Relation between ulnar variance and ulnar proximity

To evaluate the use of ulnar variance as a predictive value for ulnar proximity the median ulnar variance as found in Chapter 5: Ulnar variance was used to express the minimal ulnar proximity for both the lunate as the triquetrum. Since the styloid length may compensate for the shorter ulnar variance, this data is also included.

## 6.3 Results

### 6.3.1 4DCT ulnar proximity assessment on healthy volunteers

**Ulnar proximity in neutral position**

In neutral position there is quite a big variance between the healthy volunteers for both the triquetrum as well as the lunate the minimal distance from the ulna to the triquetrum is 3.88 mm and the maximal distance is 9.83 mm, for the ulna to the lunate this is respectively 1.65 to 6.72 mm. An overview of ulnar proximity in neutral position is given in Table 6.

*Table 6: Overview of ulnar proximity in neutral position of the wrist*

|  | **Triquetrum** (mm) | **Lunate** (mm) |
|---|---|---|
| **Median dorsal 3DmRU** (IQR) | 7.22 (6.22 – 8.54) | 2.71 (2.42 – 3.58) |
| **Minimal dorsal 3DmRU** | 3.88 | 1.65 |
| **Maximal dorsal 3DmRU** | 9.83 | 6.72 |

**RUD motion of the wrist**
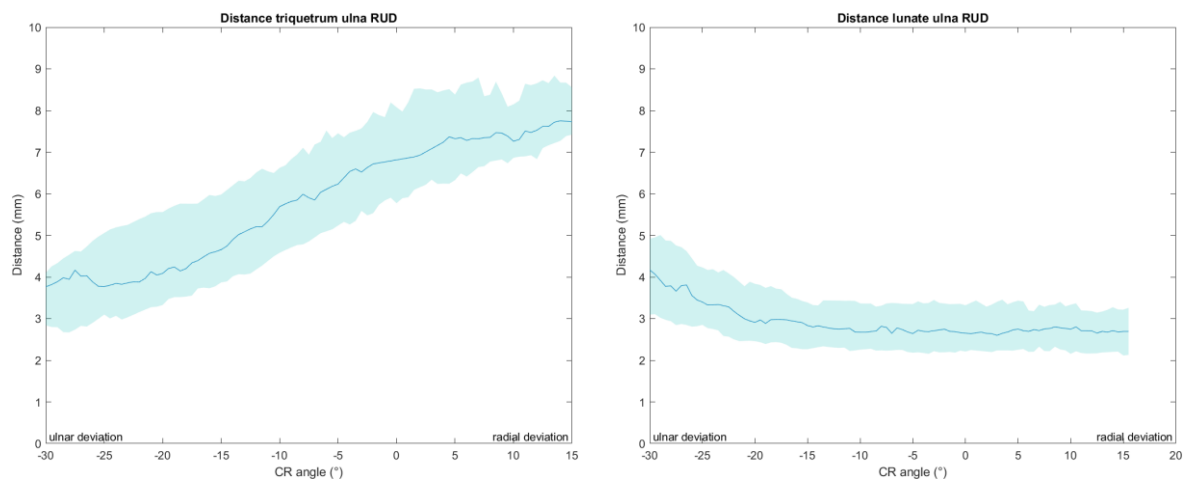


*A. Distance between the triquetrum and ulna when moving the wrist from ulnar to radial deviation expressed against the coronal CR angle*

*B. Distance between the lunate and ulna when moving the wrist from ulnar to radial deviation expressed against the coronal CR angle.*

*Figure 23: Ulnar proximity during RUD motion*

The interpolated data of the distance between the triquetrum and ulna shows an approximate linear relation between the radial carpal angle and the distance between the ulna and triquetrum. This ranges from a median distance of 3.67 mm in ulnar deviation to a median of 8.48 mm in radial deviation. The distance between the lunate and the ulna stays relatively constant during radial deviation due to the round shape of the distal lunate. In more extreme ulnar deviation, the distance increases as the lunate moves away from the ulna (Figure 23). An overview of the ulnar proximity during RUD motion can be found in Table 7.

|  | **Triquetrum** (mm) | **Lunate** (mm) |
|---|---|---|
| **Median dorsal 3DmRU** (IQR) | 6.49 (5.72 – 7.21) | 2.71 (2.25 – 3.45) |
| **Minimal dorsal 3DmRU** | 1.00 | 1.57 |
| **Maximal dorsal 3DmRU** | 9.99 | 7.63 |
| **Median range** (IQR) | 5.12 (4.21 – 6.28) | 1.42 (0.84 – 3.00) |

**FE motion of the wrist**



**A.** *Distance between the triquetrum and ulna when moving the wrist from extension to flexion expressed against the sagittal CR angle*

**B.** *Distance between the lunate and ulna when moving the wrist from extension to flexion expressed against the sagittal CR angle.*
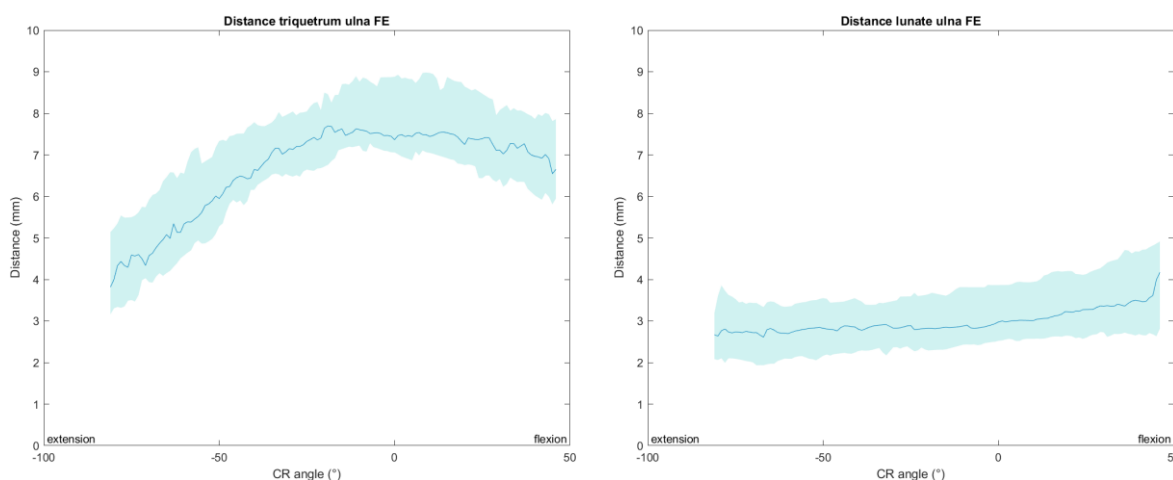
*Figure 24: Ulnar proximity during FE motion*

The interpolated data during  FE motion of the wrist shows the triquetrum being the closest to the ulna during extreme flexion with a median of 3.81 mm at a CR angle of -81°. The triquetrum is moving further away from the ulna when moving from extension to flexion to a maximum of 7.83 mm at a -9° CR angle. After this the distance between the triquetrum and ulna slowly decreases again during further flexion. Figure 24A shows this relation. The distance between the lunate and the ulna changes minimally from extension to flexion of the wrist slowly increasing from a median of 2.63 mm in extension to 3.47 mm in extension. The ulna lunate distance quickly increases in the more extreme flexion movement when the median distance rises to 4.17 mm. This can also be seen in Figure 24B. The ulnar proximity to the lunate reaches within 0.82 mm for a healthy volunteer, an overview of ulnar proximity during  FE motion can be found in Table 8.

|  | Triquetrum (mm) | Lunate (mm) |
|---|---|---|
| **Median dorsal 3DmRU** (IQR) | 6.44 (5.78 – 7.35) | 2.82 (2.35 – 3.81) |
| **Minimal dorsal 3DmRU** | 2.32 | 0.82 |
| **Maximal dorsal 3DmRU** | 9.99 | 7.52 |
| **Median range** (IQR) | 4.49 (3.27 – 5.13) | 1.30 (0.94 – 1.59) |

**CF motion**



*A. Distance between the triquetrum and ulna when clenching the fist*

*B. Distance between the lunate and ulna when clenching the fist.*
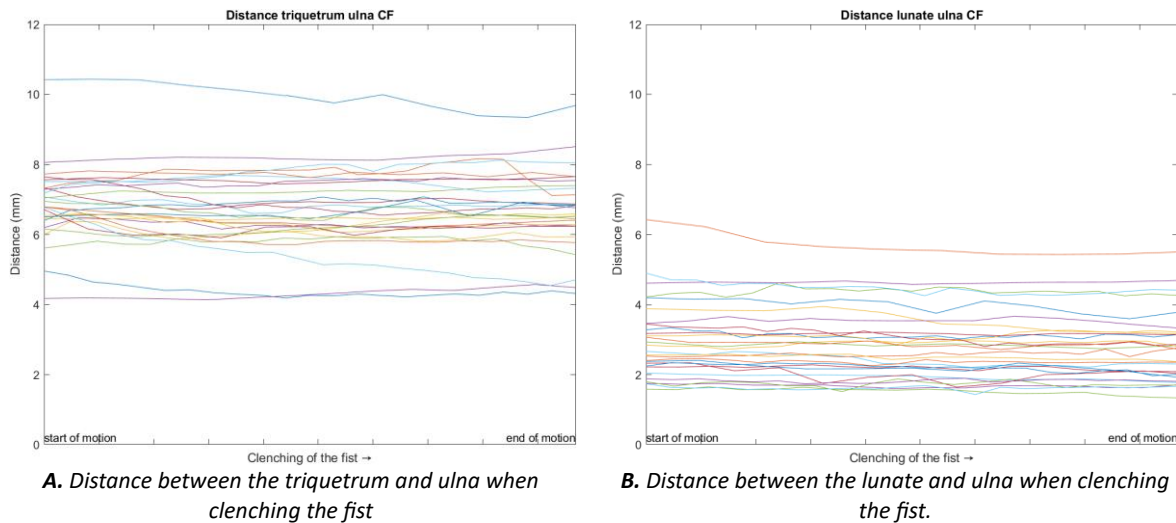
*Figure 25: Ulnar proximity during CF motion*

During CF the change in ulna triquetrum distance is highly dependent on the volunteer. In the most extreme cases there is a decrease of 2.24 mm during the CF but also an increase of almost 1 mm was measured. All volunteers stayed above 4 mm during the whole CF motion as can be seen in Figure 25A. The distance between the lunate and ulna overall decreases during CF with almost 1 mm in the most extreme case. The closest interpolated distance measured between the ulna and lunate was 1.33 mm during full clench. An overview for all volunteers is given in Figure 25B. An overview of ulnar proximity during CF motion can be found in Table 9.

*Table 9: Overview of ulnar proximity during CF motion*
*Range is defined as: range = maximal ulnar proximity – minimal ulnar proximity*

|  | Triquetrum (mm) | Lunate (mm) |
|---|---|---|
| **Median dorsal 3DmRU** (IQR) | 6.56 (6.17 – 7.44) | 2.69 (2.11 – 3.35) |
| **Minimal dorsal 3DmRU** | 4.13 | 1.33 |
| **Maximal dorsal 3DmRU** | 9.99 | 6.42 |
| **Median range** (IQR) | 0.52 (0.33 – 0.76) | 0.32 (0.20 – 0.47) |

### 6.3.2 Relation between ulnar variance and ulnar proximity

As ulnar variance is often used as a predicting factor for ulnar impaction the relationship between ulnar variance and ulnar proximity was investigated. A clear relationship between ulnar variance and lunate proximity was seen in cases with a negative ulnar variance while this relationship was less clear in the cases with a more positive ulnar variance. No clear relation was seen between the styloid length and lunate proximity and adding the styloid length to the ulnar variance decreases the correlation. These relationships are plotted in Figure 26.

**Relation between distance to the lunate, ulnar variance and styloid length**
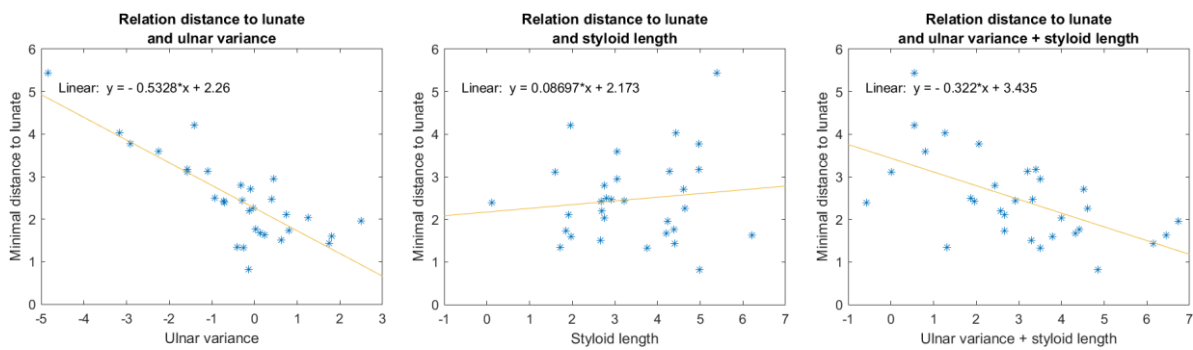


*Figure 26: Relation between distance to the lunate, ulnar variance and styloid length*

The relationship between the ulnar triquetrum proximity and ulnar variance is less strong. A relationship can be seen though. Again, adding the styloid length decreases the correlation as can be seen in Figure 27.

**Relation between distance to the triquetrum, ulnar variance and styloid length**
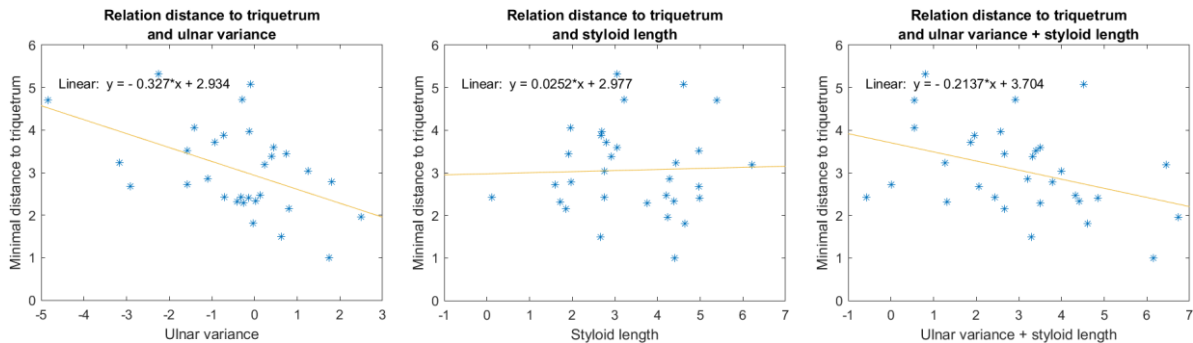


*Figure 27: Relation between distance to the triquetrum, ulnar variance and styloid length*

### 6.3.3 Ulnar impaction in the volunteer population without wrist complaints

To visualize the relation between the quantification and dynamic movement of the wrist, GIFs were created. Figure 28 shows the kinematics during FE motion for a random volunteer.
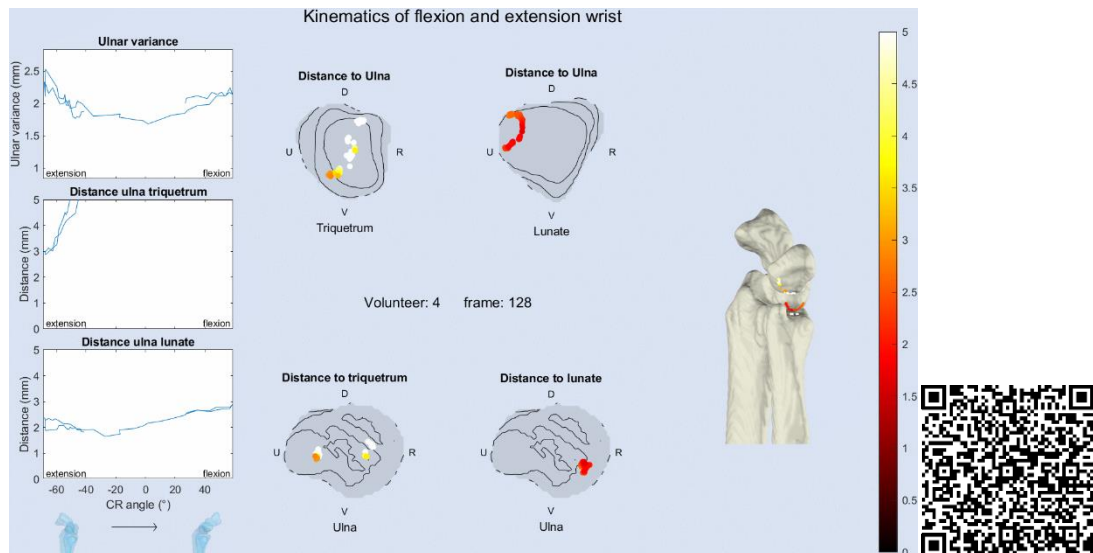
*Figure 28: Example of kinematics during FE for a random volunteer*
*(for an offline moving version of the gif follow the QR code)*

There were two volunteers for whom the ulnar proximity reached within 1 mm. In one case this was true for the lunate and in one case this was true for the triquetrum. In these cases, it may be possible that there is impaction between the cartilage of the ulna, the TFCC and cartilage of the triquetrum or ulna. In the case of ulnar proximity to the triquetrum this occurred during  RUD motion and may be caused by the kinematics of the wrist as can be seen in Figure 29. In the case of ulnar proximity to the lunate this occurred during  FE motion but this may be caused due to a registration/segmentation error caused by motion artefacts due to a sudden proximal movement as can be seen in Figure 30.



*Figure 29: Possible ulnar impaction with the triquetrum during  RUD motion*
*(for an offline moving version of the gif follow the QR code)*

**A.** Possible ulnar impaction with the lunate during FE motion

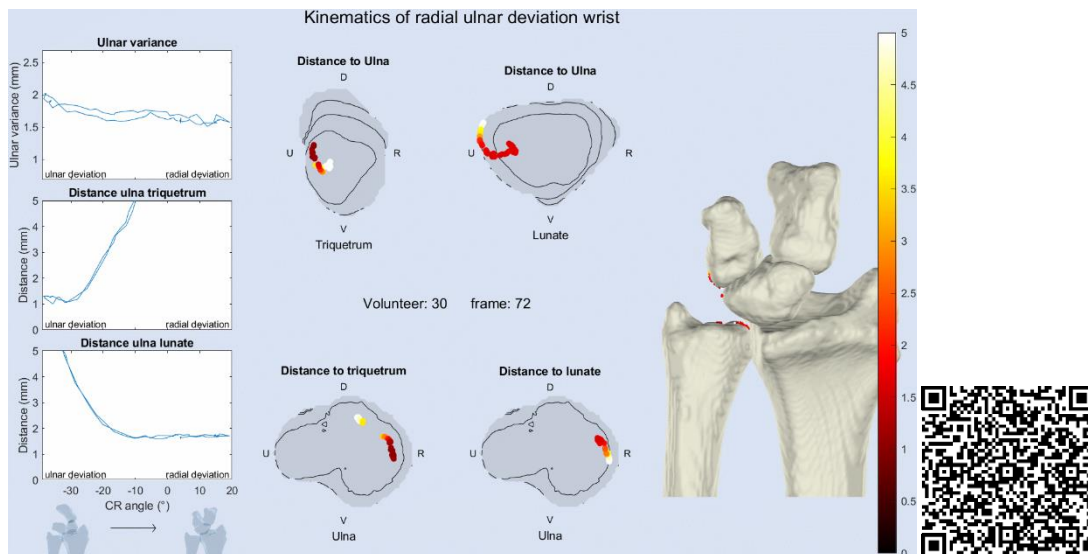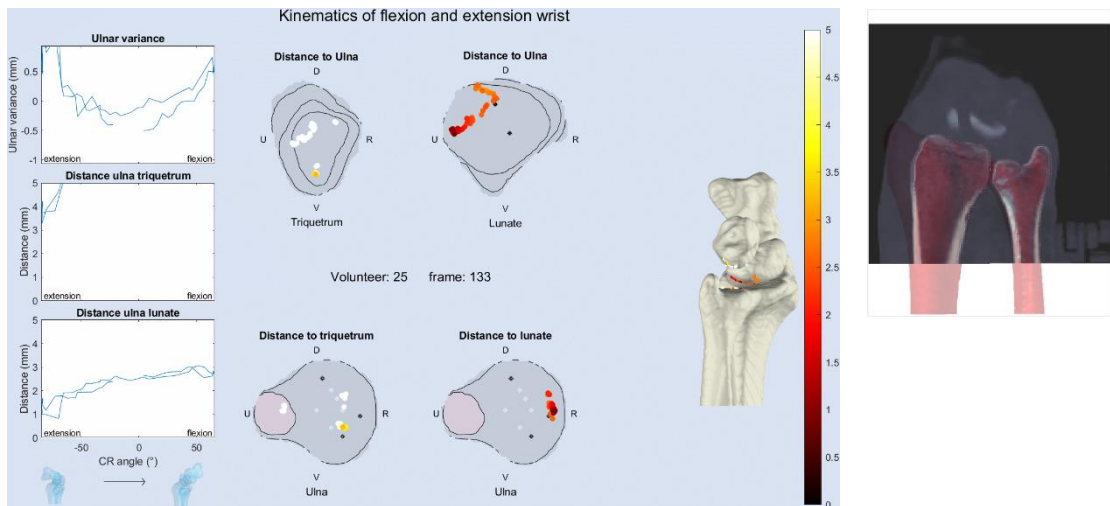**B.** The segmented ulna and radius on the CT projection showing motion artefacts due to a sudden proximal movement of the wrist.

*Figure 30: Possible ulnar impaction with the lunate during FE motion (for an offline moving version of the gif follow the QR code)*

## 6.4 Discussion

In this study we aimed to create a workflow for measuring and interpreting the proximity between the ulna and the lunate and triquetrum and investigate the relations between them in wrists of healthy volunteers. A method was established to measure the minimal distance between the ulna and the triquetrum and lunate using mesh to mesh distance calculation. An algorithm was developed to perform the measurements automatically, both in the static CT images as in the dynamic obtained CT images. During RUD the lunate rotates around its axis, barely getting closer to the ulna, while the triquetrum moves towards the ulna, thereby decreasing the distance between the two. Similar to the RUD motion, the lunate is not getting closer to the ulna during FE whereas the triquetrum moves towards the ulna during both flexion as well as extension of the wrist. Figure 27 shows that in extreme flexion the lunate suddenly gets farther away from the ulna.

For some volunteers it can be seen that the line of radial deviation diverges from the line of ulnar deviation while in other cases both movements are almost exactly reflections of each other. When visually reviewing the individual volunteers, it can be seen that several volunteers tend to pronate their wrist during the RUD and FE which may explain this. A motion guiding device may be used to improve the consistency of wrist motion and to ease comparison between different individuals making the identification of outliers easier.

In the group of thirty-one volunteers with no wrist complaints there where two wrists which might lead to symptomatic ulnar impaction in the future. Ulnar impaction can exist without complaints for many years depending on the amount of impact and loading (use) of the wrist. The 4DCT actually showing and making it possible to dynamically quantify this impaction may aid the certainty of the diagnosis behind the complaints.

The change in ulnar variance is believed to be most strongly present during the PS movement and the gripping of the fist. Due to segmentation problems, we have not analysed these movements as of this moment in time. Due to this it is not possible to draw hard conclusions from our data yet. What we can

do though is describing the data available. A strong negative correlation between ulnar variance and ulnar proximity can be seen during negative ulnar variance. However, this correlation is only moderate in positive ulnar variance. This means that there are other factors that contribute to ulnar impaction that are not known yet. This data does suggest that it is not beneficial to add the styloid length to the ulnar variance in predicting ulnar impaction, but investigation of more patients with ulnar impaction may shed another light on this. This is even more true for impaction with the triquetrum since there is even less of a clear relationship with ulnar variance. The proposed technique can be a tool to further investigate what happens during ulnar impaction and why some people with positive ulnar variance do not have complaints while others have.

Patients mostly complain about pain during a pronated and forceful grip [54]. At the moment these wrist movements are assessed separately to make analysis per motion type possible. It may be viable to increase sensitivity and lower radiation dose by combining the pronated and forceful grip movement, which may lead to a higher likelihood of capturing the ulnar impaction. This motion may also be the most viable place to start investigating while some people with a positive ulnar variance have complaints while others have not.

Since the algorithm has only been performed on volunteers without complaints, no definitive insight can be given on the diagnostic power of the chosen method (proximity). However, the proposed method has given new insight on kinematics of the wrist and the normal proximity values of the wrist which might aid practitioners into investigating the cause of ulnar wrist pain.

## 6.5   Conclusion

To conclude, an algorithm was proposed to automatically measure and visualize the proximity between the ulna and the triquetrum and lunate. This method may be used to gain more direct insight into the kinematics of the ulnar sided wrist and the ulnar impaction. The wrist in healthy participants behaved like expected, opening the path to investigate the kinematics of pathological wrists compared to healthy wrists.
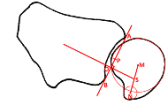
# Chapter 7:  DRUJ stability

## 7.1    Introduction

Due to the difference in circumference between the ulnar head (10 mm) and the sigmoid cavity (15 mm) the DRUJ is an inherently unstable joint and requires constant stabilization by the TFCC [15] [9]. When this stabilization factor is damaged, the DRUJ becomes unstable which may result in ulnar head subluxation during exerted pressure or pronation. DRUJ instability is a pathological excessive translational movement of the ulnar head in relation to the sigmoid notch, specifically in the volar-dorsal direction. It is a progressive condition and can lead to progressive pain worsening, functional compromise and ultimately secondary osteoarthritis if left untreated [9]. To prevent this, surgical reconstruction (either indirect by an ulnocarpal sling or tenodesis or direct by a radioulnar tether extrinsic to the joint) can be performed to stabilize the DRUJ and prevent further deterioration [15].

The diagnosis of a subtle DRUJ instability can be a challenge due to the clinical examination suffering from subjectivity and lack of validity [16]. All methods have as an end goal to quantify the degree of relative translation between the ulnar head and the radius defining the DRUJ as instable when there is excessive translation and/or a big left-right difference. The Common clinical examination methods such as the piano key sign test and the DRUJ stress test have limited sensitivity (respectively 66% and 59%) and specificity (respectively 96% and 59%) [17]. Static imaging techniques such as CT and MRI can have diagnostic value in more extreme cases with constant subluxation or clear TFCC damage, but more subtle DRUJ instability may remain undetected using static imaging modalities. Investigating the kinematics of the DRUJ during motion with 4DCT may provide more insight into DRUJ stability, possibly improving diagnosis. A study by Carr et al. analysed 4DCT scans visually and their results showed that assessment of the 4DCT scan changed diagnosis in 4 cases in which DRUJ instability was determined to be the cause of the experienced symptoms [55].

To quantify relative translation of the DRUJ and give insight on the stability of the DRUJ on static CT scans and provide an objective analysis, several parameters have been developed. These parameters include the radioulnar line method or Mino method; the modified radioulnar line method (mRU); the subluxation ratio; the epicentre method (Epi); the radioulnar method and the congruent method [17] [56] [57]. For a full description of all parameters see appendix 11.1. While differing in their exact method, all methods use a series of anatomical landmarks or arbitrary points. These points are manually selected on the axial slice with either the widest part of the sigmoid notch or perpendicular to the distal radial/ulnar meta diaphysis [9] [58] and result in a ratio describing the DRUJ stability.

A number of studies have applied these parameters to 4DCT imaging. A study by Shakoor et al. evaluating the dorsal-volar parameters: mRU and Epi on 4DCT data in 10 asymptomatic wrists by 2 observers perceived that the mRU detected changes in the volar and dorsal positions of the ulnar head in relation to the sigmoid notch where the Epi did not [9]. In contrast, a study by Wijffels et al. used conventional CT data of both normal and posttraumatic wrists and concluded that there is a large normal variation for all investigated parameters and the use of the Epi is advised [16]. A third study by Swartman et al. using 4DCT data confirms this, perceiving large normal ranges causing a high percentage of false positives during clinical trials [58].

All mentioned studies have performed parameter evaluation based on a single axial slice, thereby limiting their analysis to 2D. Full 3D evaluation may increase the uniformity of the results. Furthermore, all studies have analysed up to eleven frames resulting in a relatively low temporal resolution unable to show dynamic changes and thus describing median values and trends. As DRUJ stability may only lead to subtle changes in the dynamic kinematics of the wrist, it is probable that these studies may have missed DRUJ instability. Increasing the temporal resolution and further standardizing these

measurements by expressing the measurements against the wrist position could make it possible to compare wrist kinematics during the full range of motion. Subsequently exploring the change of the parameters during motion may aid in the assessment of more subtle differences in DRUJ stability.

To overcome these challenges two methods will be proposed to analyse the DRUJ stability. A 3D adaptation of the radioulnar line method (3DmRU) and a 3D adaptation of the Epicentre method (3DEpi) should be performed during wrist motion at a high temporal resolution. Manual analysis on high temporal resolution data is very time and labour intensive raising the need for automatic analysis.

Therefore, the aim of this chapter is to develop an automatic workflow to assess DRUJ stability by measuring the dorsal-volar translation during wrist motion using 4DCT and to investigate normal values in healthy wrists during RUD and FE.

## 7.2    Method

### 7.2.1    4DCT dataset

The same dataset as described in: 3.2.1 4DCT dataset was used: two cycles of movements (FE and  RUD motion) of thirty-one volunteers. For both the 3DmRU and the 3DEpi static as well as dynamic segmentations of the ulna and the radius were used.

### 7.2.2    Automatic point mapping with the use of a statistical shape model

Both the 3DmRU as well as the 3DEpi make use of a number of radial anatomical landmarks. These landmarks are: the volar margin of the sigmoid notch, the dorsal margin of the sigmoid notch, the volar radial corner of the radius and the dorsal radial corner of the radius. For automatic definition of the anatomical landmarks a SSM of the radius was developed using a previously established method by Haenen et al.. A SSM is a mathematical representation of the variation in shape within a population. By using a number of thirty-one different radial bones as input, the SSM calculates a mean shape and provides a statistical framework that accounts for variability in anatomy. This allows for alteration of the mean shape to match the observed shape of the radius for different anatomical variations with a root mean squared error of 0.73 mm. By selecting the preferred anatomical landmarks on the mean shape and altering the shape to match the shape of a target bone, the corresponding locations can be estimated by closest point approximation. Since the specific SSM method used does not allow for changes in bone length, the target bone is first registered to the mean shape using CPD registration with scaling. Sequentially the mean shape is fitted to the scaled bone. After the mean shape has approximated the shape of the scaled bone, the corresponding anatomical landmarks are estimated by closest point approximation. The mapping of these found anatomical landmarks will be visually evaluated.

### 7.2.3 Automatic assessment using a 3D adaptation of the radioulnar line method
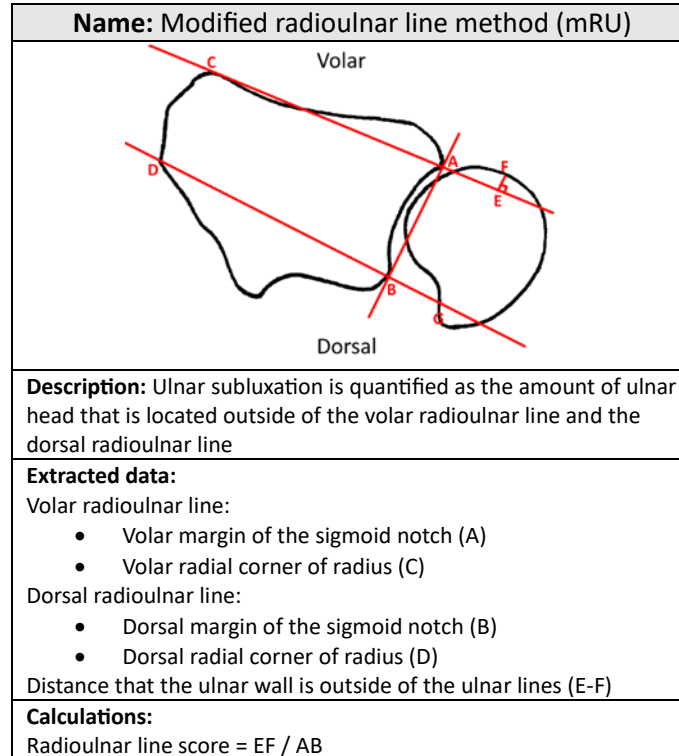
| **Name:** Modified radioulnar line method (mRU) |
|---|
|  |
| **Description:** Ulnar subluxation is quantified as the amount of ulnar head that is located outside of the volar radioulnar line and the dorsal radioulnar line |
| **Extracted data:**<br>Volar radioulnar line:<br>    • Volar margin of the sigmoid notch (A)<br>    • Volar radial corner of radius (C)<br>Dorsal radioulnar line:<br>    • Dorsal margin of the sigmoid notch (B)<br>    • Dorsal radial corner of radius (D)<br>Distance that the ulnar wall is outside of the ulnar lines (E-F) |
| **Calculations:**<br>Radioulnar line score = EF / AB |

*Figure 31: Modified radioulnar line method*

The mRU quantifies subluxation by the width of the ulnar head being located outside of the volar radioulnar line as shown in Figure 31. For the 3DmRU the four points (A,B,C,D) are identified on the mesh of the static radius with automatic landmark mapping of the SSM as described above. After all points of interest (POI) are identified on the static radial mesh, they are transformed to their respective dynamic position using the previously acquired transformation matrices. Subsequently all data is transformed to the LCS of the radius after which rotation around the Z-axis of the radius takes place to align the volar radioulnar line with the y-axis (Figure 32). Following this the volar-most point of the ulnar head (defined as the most distal 3 cm of the ulna) is determined as the vertex with the smallest y-value (point F in Figure 32). The distance from this point to the volar ulnar line (E-F) is divided by the length of the sigmoid notch of the radius (A-B in Figure 35), which provides the 3D mRU score. The regular mRU typically measures the distance of the ulnar head relative to the volar radioulnar line. Since subluxation towards the dorsal side is more common and to reduce the chance of dorsal subluxation to be missed the method was extended towards the dorsal side [59]. The same method but in opposite direction is used for the dorsal radioulnar line. The volar 3DmRU and the dorsal 3DmRU will be expressed separately. To express the 3DmRU during motion the score is calculated for every position during FE and RUD motion and the median, maximum, minimum values and range are calculated for every motion. The Δ3DmRU is calculated for every position during FE and RUD motion and expressed against the CR angle.
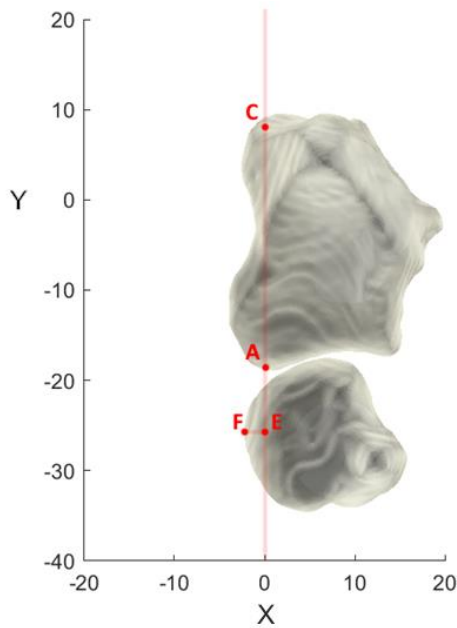
*Figure 32: 3D adaptation of the volar mRU*

## 7.2.4 Automatic assessment using a 3D adaptation of the epicentre method

| **Name:** Epicentre method |
|---|
|  |
| **Description:** Ulnar subluxation is quantified as the distance between the middle of the sigmoid notch (P) and the intersection point (O) of the line from the centre of rotation of the DRUJ (S) perpendicular to the line connecting the volar and dorsal margins of the sigmoid notch (AB). |
| **Extracted data:**<br>Intersection point (O) of:<br> • The line connecting:<br>   ○ Volar margin of the sigmoid notch (A)<br>   ○ Dorsal margin of the sigmoid notch (B)<br> • And a perpendicular line crossing the centre of rotation of the DRUJ (S) defined as the midpoint between<br>   ○ Centre of the ulnar styloid (N)<br>   ○ Centre of the ulnar head (M)<br>Middle of the sigmoid notch (P) which is the midpoint between:<br> • Volar margin of the sigmoid notch (A)<br> • Dorsal margin of the sigmoid notch (B) |
| **Calculations:**<br>Epicentre method score = OP / AB |

*Figure 33: Epicentre method*

The 3D adaptation of the Epi follows a similar method as the 3D adaptation of the mRU. The required POI's on the radius are selected with the same method using the SSM after which the same transformations are performed. Instead of aligning the radioulnar line with the y-axis of the radius, the line connecting the volar and dorsal margin of the ulnar notch are aligned with the x-axis of the radius. The centre of the ulnar head (S) is defined as the origin of the ulnar LCS (Chapter 3: Local coordinate system of the ulna). The Epi score is defined as the difference in x-value between A and S divided by the difference in x-value between S and B. To express the 3DEpi during motion the score is calculated for every position during FE and RUD motion and the median, maximum, minimum values and range are calculated for every wrist position. The Δ3DEpi is calculated for every position during FE and RUD motion and expressed against the CR angle.
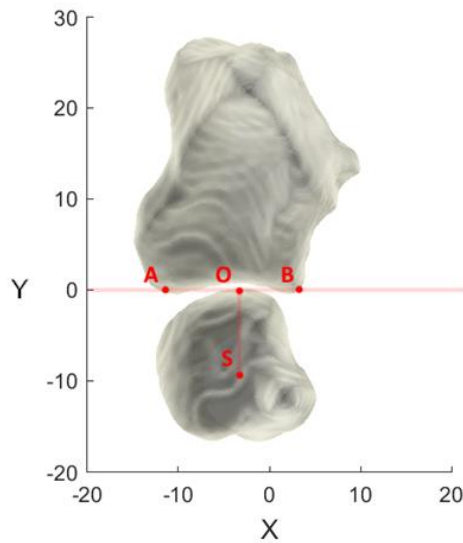


*Figure 34: 3D adaptation of the Epi*

## 7.3    Results

### 7.3.1    Automatic point mapping with the use of a statistical shape model

The shape of the fitted SSM visually corresponds with that of the target bone as can be seen in the example given in Figure 35.A. While the fitted SSM closely assumes the shape of the target bone the POI's do not always seem to perfectly match their respective locations as can be seen in Figure 35 B&C.
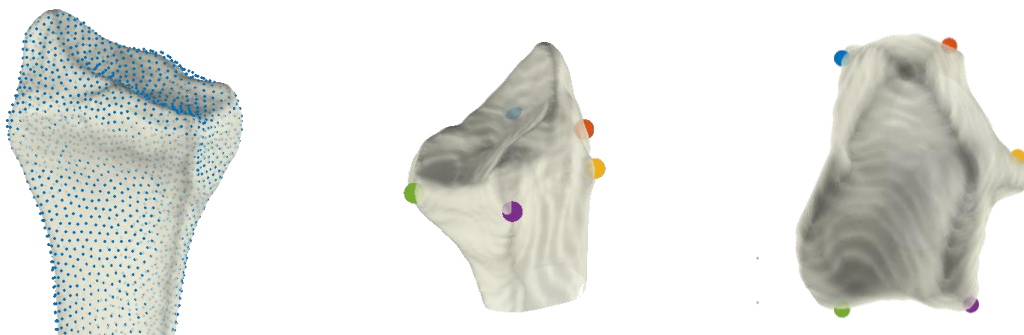


*A. Example of the SSM fitted (blue dots) to a target bone (white bone)*   *B. Example of the POI's as defined by the fitted SSM on the target bone*   *C. Top view of the POI's as defined by the fitted SSM on the target bone*

*Figure 35: Example of the fitted SSM and point mapping.*

### 7.3.2 Automatic assessment using a 3D adaptation of the radioulnar line method

The 3DmRU was estimated in thirty-one healthy volunteers during RUD and FE motion. For all motions the volar edge of the ulnar head was median located close to the volar radioulnar line with a volar 3DmRU ranging from -0.01 [-0.09 – 0.07] to 0.00 [-0.06 – 0.09] (in which positive values are volar of the radioulnar line and negative values are dorsal of the radioulnar line). The volar 3DmRU ranged from a maximum (furthest volar of the volar radioulnar line) of 0.37 during RUD to a minimum (furthest dorsal from the volar radioulnar line) of -0.23 during FE. An overview of the volar 3DmRU given in Table 10.

*Table 10: Overview of the volar 3DmRU characteristics of the volunteers without wrist complaints*
*Range is defined as: range = maximal 3DmRU – minimal 3DmRU*

|  | **Neutral** | **RUD** | **FE** |
|---|---|---|---|
| **Median volar 3DmRU** (IQR) | -0.01 (-0.09 – 0.07) | -0.01 (-0.09 – 0.09) | 0.00 (-0.06 – 0.09) |
| **Minimal volar 3DmRU** | -0.19 | -0.19 | -0.23 |
| **Maximal volar 3DmRU** | 0.30 | 0.37 | 0.34 |
| **Median range** (IQR) | - | 0.10 (0.08 – 0.15) | 0.08 (0.05 – 0.10) |

The median estimation of the Δ3DmRU for CR angles reached by a minimum of 15 volunteers shows that the ulnar head moves volar relative to the volar radioulnar line during both ulnar deviation as well as radial deviation while not exceeding 0.05 (Figure 36). During FE the Δ3DmRU remains smaller, just exceeding 0.02. The Δ3DmRU for both motions is shown in Figure 36.
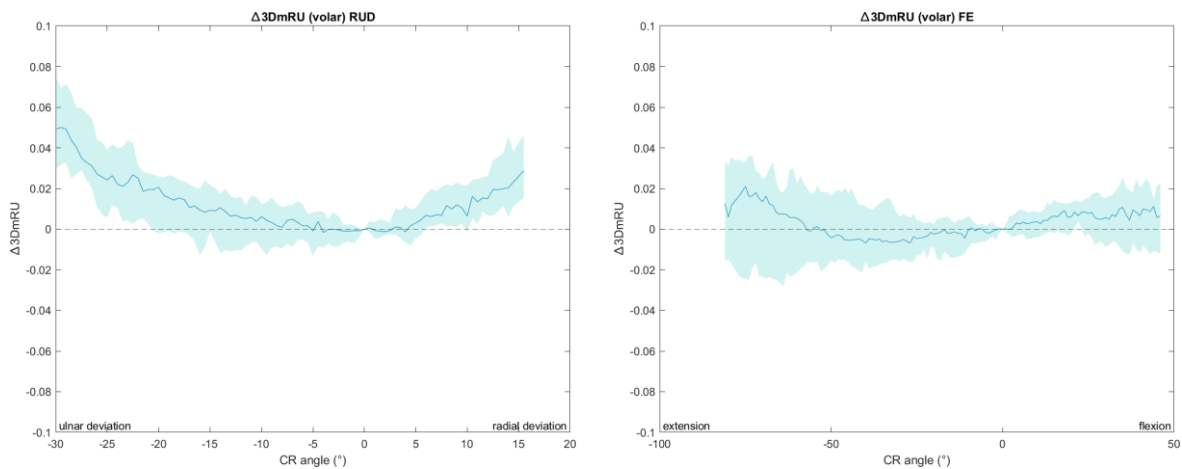


**A.** *The volar Δ3DmRU from ulnar deviation to radial deviation expressed against the CR angle*

**B.** *The volar Δ3DmRU from extension to flexion expressed against the CR angle.*

*Figure 36: The volar Δ3DmRU during motion as reached by at least fifteen volunteers.*

During both RUD and FE, the dorsal 3DmRU ranges between -0.28 to 0.25 with a median value of 0.00 for both movements. The overview of the dorsal 3DmRU during motion is given in Table 11.

|  | Neutral | RUD | FE |
|---|---|---|---|
| **Median dorsal 3DmRU** (IQR) | 0.00 (-0.09 – 0.09) | 0.00 (-0.10 – 0.08) | 0.00 (-0.07 – 0.09) |
| **Minimal dorsal 3DmRU** | -0.19 | -0.28 | -0.25 |
| **Maximal dorsal 3DmRU** | 0.26 | 0.25 | 0.24 |
| **Median range** (IQR) | - | 0.09 (0.07 – 0.13) | 0.08 (0.06 – 0.11) |

The dorsal Δ3DmRU for CR angles reached by a minimum of fifteen volunteers shows that the outer dorsal edge of the ulnar head moves relatively volar during ulnar deviation, radial deviation and extension while moving relatively dorsal during flexion. The median dorsal Δ3DmRU has an absolute maximum of 0.04 during RUD and 0.03 for FE.



**A.** The dorsal Δ3DmRU from ulnar deviation to radial deviation expressed against the CR angle

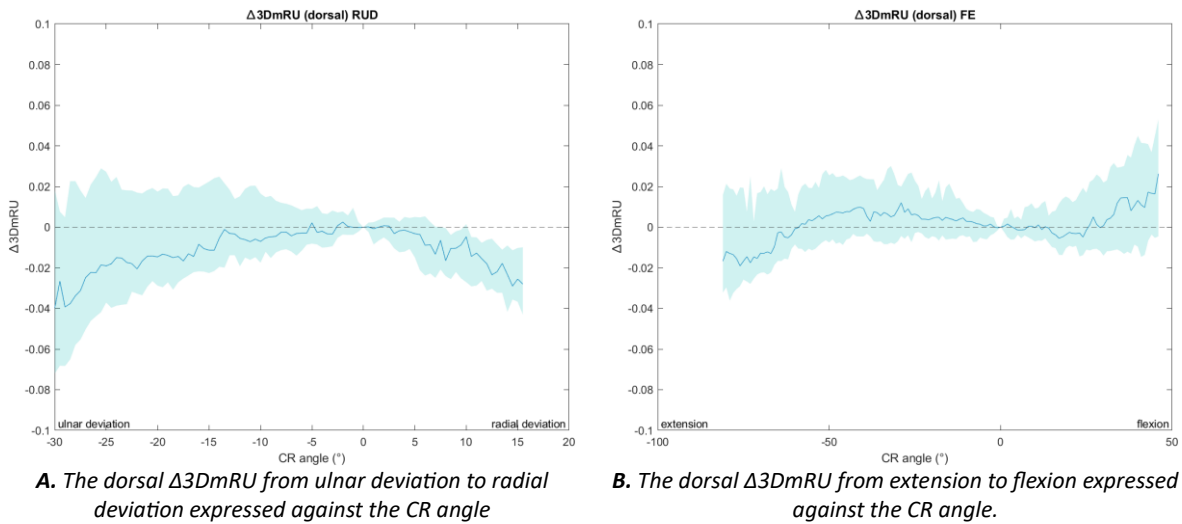**B.** The dorsal Δ3DmRU from extension to flexion expressed against the CR angle.

Figure 37: The dorsal Δ3DmRU during motion as reached by at least fifteen volunteers.

### 7.3.3 Automatic assessment using a 3D adaptation of the epicentre method

During RUD the 3DEpi ranges from -0.21 to 0.29 with a median value of -0.03 [-0.10 – 0.03]. During FE this range is smaller from -0.21 to 0.26; with a median value of -0.04 [-0.11 – 0.02]. An overview of 3DEpi during motion is given in Table 12.

Table 12: Overview of the 3DEpi characteristics of the volunteers without wrist complaints
Range is defined as: range = maximal 3DEpi – minimal 3DEpi

|  | Neutral | RUD | FE |
|---|---|---|---|
| **Median 3DEpi** (IQR) | -0.04 (-0.11 – 0.26) | -0.03 (-0.10 – 0.03) | -0.04 (-0.11 – 0.02) |
| **Minimal 3DEpi** | -0.20 | -0.21 | -0.21 |
| **Maximal 3DEpi** | 0.22 | 0.29 | 0.26 |
| **Median range** (IQR) | - | 0.10 (0.07 – 0.13) | 0.08 (0.05 – 0.09) |

The Δ3DEpi shows that the origin of the ulna moves volar relative to the sigmoid notch during ulnar deviation, radial deviation and extension while moving dorsal during flexion. The median Δ3DEpi has an absolute maximum of 0.04 during RUD and 0.02 for FE.



**A.** *The Δ3DEpi from ulnar deviation to radial deviation expressed against the CR angle*

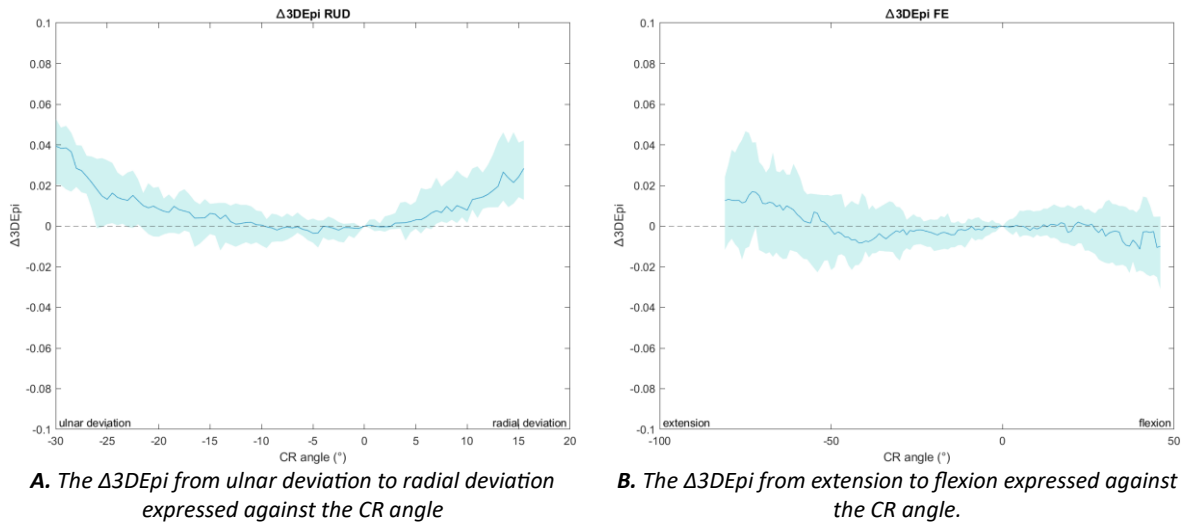**B.** *The Δ3DEpi from extension to flexion expressed against the CR angle.*

*Figure 38: The 3DEpi during motion as reached by at least fifteen volunteers.*

## 7.4   Discussion

A method was developed for DRUJ stability assessment using a fully automatic workflow for the measurement of ulnar head translation in relation to the sigmoid notch during full range of motion using a 3D adaptation of both the mRU and the Epi. The method was performed on 4DCT images of RUD and FE motions of thirty-one healthy volunteers resulting in normal values for both methods. For both methods there is a relatively big range of normal values, reaching at least a ratio range of 0,5 between all volunteers. This may be explainable due to the large interpatient variability but may also complicate its use for differentiating healthy from pathological wrists, the Δ of both methods shows a relatively narrow range for both the volar 3DmRU and the 3DEpi. With the use of continuous 4DCT analysis, the ΔmRU and Δ3DEpi may be used to investigate the difference in laxity between both wrists and has the potential to be a useful parameter in DRUJ stability analysis.

While this study shows a prove of concept for the workflow of both methods during FE and RUD, DRUJ subluxation usually occurs during pronation. Both RUD as well as FE wrist motion primarily takes place in the radiocarpal and midcarpal joints, and to a lesser extent in the DRUJ due to the ulnocarpal ligaments and extensor carpi ulnaris sheath, both components of the TFCC which are connected to the carpus. During PS the rotation warrants the need of the external stabilizing of the TFCC and thus the laxity of the DRUJ is more pronounced during these motions. Since the pronation movement is clinically most important, a good evaluation of the proposed method using FE and RUD data is difficult. On top of that, Wijffels et al. recommended the use of bilateral scanning for estimation of DRUJ stability due to the big variation in the healthy population [16]. Bilateral PS data was acquired during acquisition of a new group of volunteers (see Chapter 2: Acquisition of 4DCT data) but due to segmentation difficulties and time constraints this data has not been evaluated yet. Applying the proposed method to this new dataset and investigating normal ranges would give further inside into its use as a clinical tool.

Most previously performed studies based on the mRU and Epi also analysed the PS movement. In a study by Swartmann et al., investigating reference ranges during PS movement on cadavers, the volar mRU ranged from -0.32 to 0.87 and the Epi ranged from -0.40 to 0.23 [58]. In a second study by Shakoor

et al., investigating asymptomatic contralateral wrists of ten patients during PS movement, the volar mRU ranged from -0.12 to 0.11 and the Epi ranged from 0.03 to 0.10 [9]. The bigger ranges of the study of Swartmann et al. can be explained by the expected bigger range of motion of the ulnar head relative to the sigmoid notch during pronation in relation to RUD and FE. The smaller range found by Shakoor might be affected by the range of wrist motion, which is not defined in the study. The differences in normal ranges between both studies does show the need for a more reproducible method though.

While this is the first time DRUJ translation movements were measured continuously during a full range of motion there are some limitations to the study. The current method for mapping the POI's on the radius was done with the use of an SSM. The SSM was not developed for this purpose and while the mapped POI's visually correspond closely with their respective anatomical landmarks on the target bone, it is not perfect. An improved method for atlas-based mapping of the POIs might improve consistency and thus accuracy of the method. Objective evaluation using manual mapping is needed to determine if the accuracy of the current method suffices. Due to contralateral similarities bilateral scanning might make increase accuracy with the current method. The planned reliability study (see also Chapter 2: Acquisition of 4DCT data) will help to further explore the consistency of the anatomical mapping. The current study is strengthened by the big dataset of thirty-one volunteers and the fully automatic character of the workflow.

## 7.5   Conclusion

To conclude, a workflow was developed to estimate DRUJ stability using the 3DmRU and the 3DEpi measuring the ulnar head translation relative to the sigmoid notch during a full range of motion for the first time. The workflow was performed on both FE as well as  RUD motions of thirty-one healthy wrists and normal values were estimated. The visually analysed results of this study were promising, although the developed method should be applied to the 4DCT bilateral pronation data to determine the potential of the 3DmRU and the 3DEpi as a clinical tool for DRUJ stability assessment.

# Chapter 8: Automatic analysis of an instable wrist

*A case report*

## 8.1   Introduction

In the previous chapters a workflow has been set up for automatic analysis of the ulnar sided wrist. The final goal of this project is to use this workflow to distinguish pathological wrists from non-pathological wrists. As a means of improving diagnostics and thus preventing progression of ulnar sided wrist pain and/or preventing arthroscopies in non-pathological wrists. However, up till now this has only been a theoretical goal and all tests have been performed on healthy wrists. Full analysis of pathological wrists is not possible since inclusion for the patient study as described in Chapter 2: Acquisition of 4DCT data has not yet started. However, bilateral 4DCT data of one patient diagnosed with unilateral DRUJ instability based on dynamic 4DCT data was acquired in a previous study focused on the scapholunate joint. This case report will present the results of a fully automatic analysis of DRUJ stability during PS motion of the wrist and discuss the ability of this workflow to differentiate between the healthy and pathological wrist. To achieve this three different wrists will be analysed using the method presented in chapter 7: one healthy wrist from the DRUJ-volunteer study (Chapter 2: Acquisition of 4DCT data), and both wrists of this patient.

## 8.2   Case description

A 50-year old male patient (from here on called P001) was referred from an outpatient clinic: the Jeroen Bosch hospital. P001 reported ulnar sided wrist pain in the right wrist and limited movement of the wrist. P001 experienced trauma two years prior due to a forced motion of the wrist. During physical examination the following was found in the right wrist: Watson's shift test and Reagon's ballet test were negative but the clinical practitioner noted localized pressure pain at the lunate and axial compression pain on the ulnar side during PS movement. Furthermore the DRUJ was deemed stable but crepitations were felt in this area. Based on the clinical examination P001 was deemed suspect for a scapholunate ligament lesion or ulnar impaction syndrome. P001 was referred to the RadboudUMC for a bilateral static and 4DCT scan during FE, RUD, CF and PS movements. Based on the static scan the radiologist reported normal proportions of the scapholunate joint on both sides and no signs of ulna plus but bilateral severe arthrosis of the DRUJ. Moreover, during dynamic imaging of the wrist abnormal movement of the DRUJ was reported in the left wrist while no signs of abnormal movement of the DRUJ were reported for the right wrist. An increased distance in the scapholunate joint was observed in the right wrist, however this was within the normal margins. Based on these findings the following conclusion was drawn: Severe DRUJ (Distal Radioulnar Joint) arthrosis on both sides with abnormal mobility on the left, differential diagnosis DRUJ instability. So while there were complaints of ulnar sided wrist pain in the right wrist, abnormal movement was seen in the left wrist. During further investigation of the right wrist an MRI was made from which the following was concluded: Degenerative changes in the DRUJ  and secondary degenerative changes in the distal ulna and rupture of the volar insertion of the TFCC. Since normal values during PS movement are not available yet the results will be compared with those of one of the healthy volunteers included in the DRUJ volunteer study (see Chapter 2: Acquisition of 4DCT data). Summarized the following three wrists will be compared: a pathological wrist with ulnar sided wrist pain showing no signs of abnormal movement visible in the DRUJ but showing DRUJ arthrosis and a rupture of the TFCC; the contralateral wrist showing severe showing DRUJ arthrosis and abnormal movement visible in the DRUJ and a healthy wrist.

## 8.3   Automatic 4DCT analysis

The stability of the DRUJ was analysed using the method as presented in Chapter 7: DRUJ stability. As described before, the clinically important movement for analysing the stability of the DRUJ is the PS

movement. The volunteer followed the PS protocol as described in Chapter 2: Acquisition of 4DCT data. Since P001 was scanned in the march 2023, P001 still followed the old protocol in which a full pronation and supination movement was performed in 10 seconds (instead of only a pronation movement in 10 seconds). The 3DEpi score; the volar 3DmRu and the dorsal 3DmRu were calculated and compared between the three wrists and all wrists were visually compared to each other.

The PS movement has not been analysed before, therefore no method of expressing the angle of motion has been presented yet. Thus for the purpose of this case report the PS angle was defined as the angle in the transversal plane between the x-axis of the radius and the line crossing the styloid of the ulna and the origin of the ulnar LCS, for a visual representation of the CS angle see Figure 39.
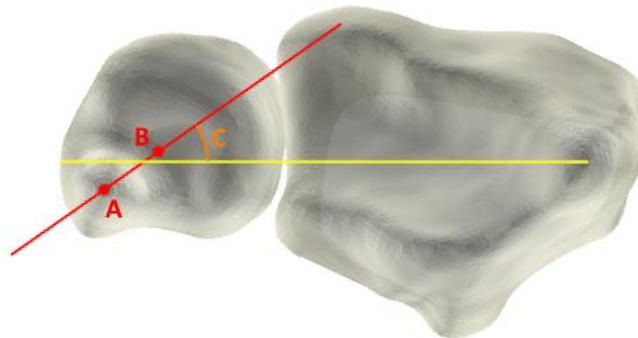


*Figure 39: Calculation of the PS angle (C), defined as the angle in the transversal plane between the x-axis of the radius (yellow line) and the and the line crossing the styloid of the ulna (A) and the origin of the ulnar LCS (B)*

## 8.4   Results

In the healthy volunteer the origin of the ulnar LCS is located almost perfectly in the middle of the sigmoid notch during maximal supination, defined by a 3DEpi score of 0.00 (Figure 40.A). The 3DEpi decreases from 24° of supination to 60° of pronation, after which it increases again. The 3DEpi of both wrists of P001 are similar to each other, both showing a more negative 3DEpi score than the healthy volunteer. This indicates that the origin of the ulnar LCS is located more dorsal relative to the radius. Thus the ulnar head is located relatively dorsal compared to the sigmoid notch. From the Δ3DEpi it can be observed that the 3DEpi changes more in supination for P001 while it changes more in pronation for the healthy volunteer (Figure 40.B). The volar 3DmRu is overall lower for the wrists of P001 compared to the healthy volunteer. For all three wrists the volar 3DmRu decreases from supination to pronation till a PS angle of about 20° after which it increases for both wrists of P001 and stays relatively constant for the healthy volunteer (Figure 40.C&D). Sharp peaks can be observed in the 3DmRu score of both wrists of P001. The dorsal 3DmRu score is more similar between both wrists of P001 and the healthy volunteer than the volar 3DmRu (Figure 40.E&F).

A visual representation of the three moving wrists and the corresponding findings is shown in Figure 41.
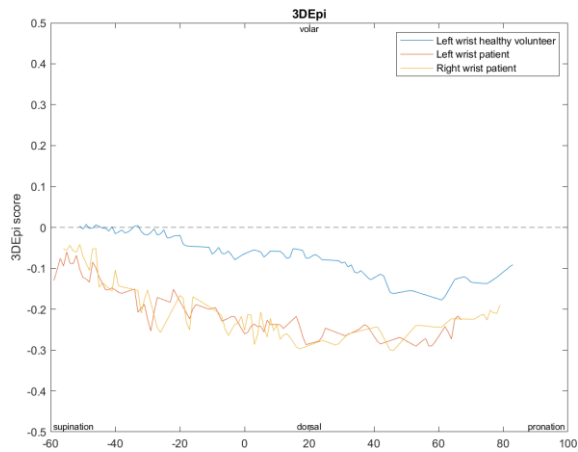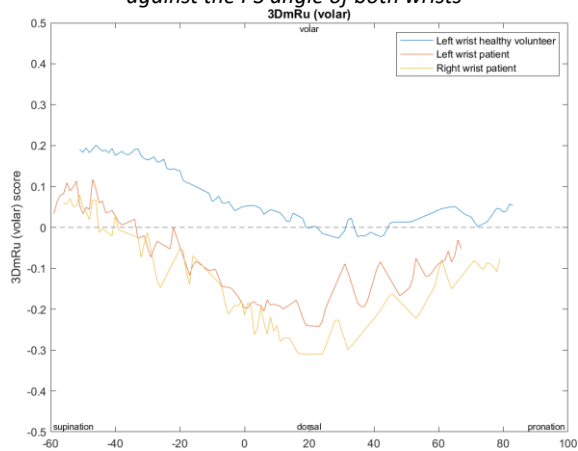
**A.** The 3DEpi from pronation to supination expressed against the PS angle of both wrists

**B.** The Δ3DEpi from pronation to supination expressed against the PS angle of both wrists

**C.** The volar 3DmRu from pronation to supination expressed against the PS angle of both wrists

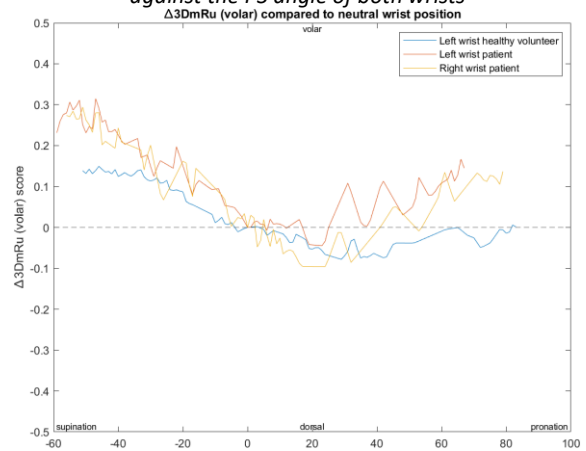**D.** The volar Δ3DmRu from pronation to supination expressed against the PS angle of both wrists
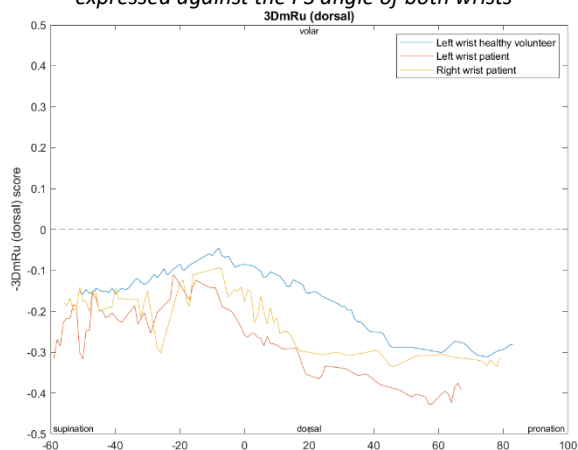
**E.** The negative dorsal 3DmRu from pronation to supination expressed against the PS angle of both wrists
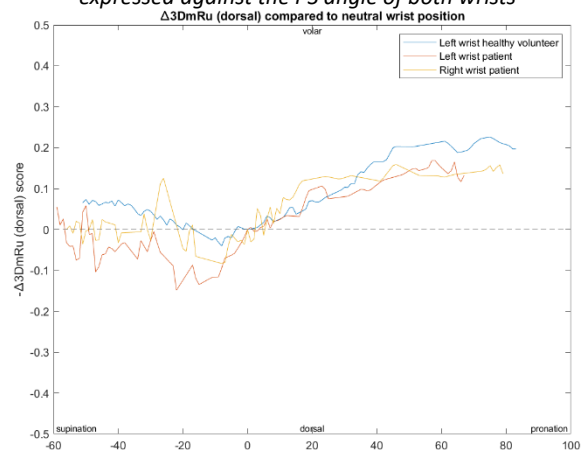
**F.** The negative dorsal Δ3DmRu from pronation to supination expressed against the PS angle of both wrists

*Figure 40: The DRUJ stability of both wrists of P001 compared to a healthy volunteer*
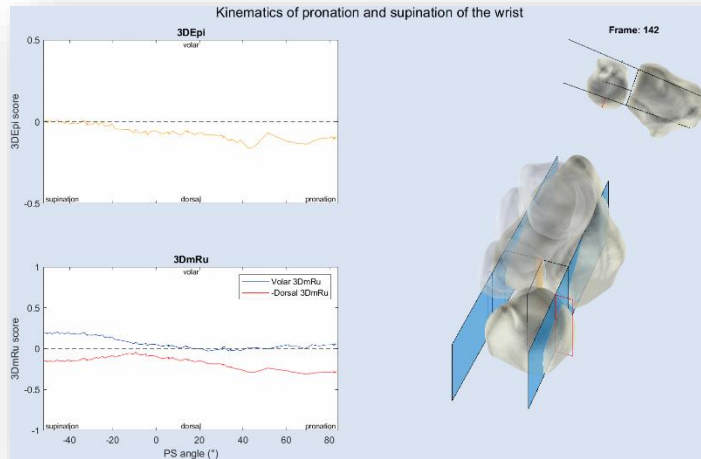
*A. Visualisation of DRUJ stability in a healthy volunteer*
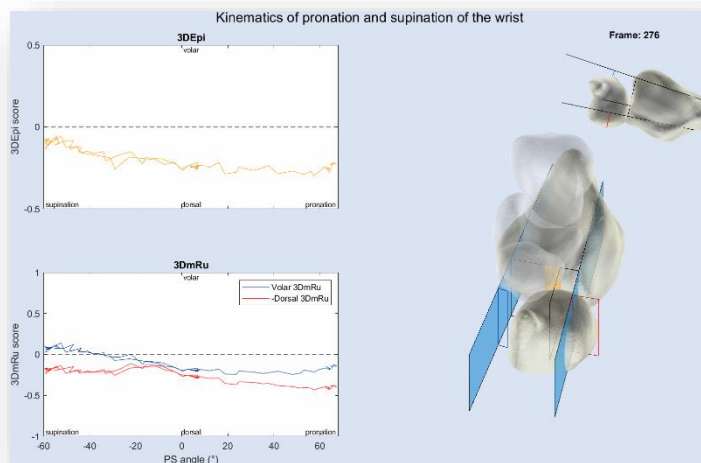


*B. Visualisation of DRUJ stability in the left wrist of P001*
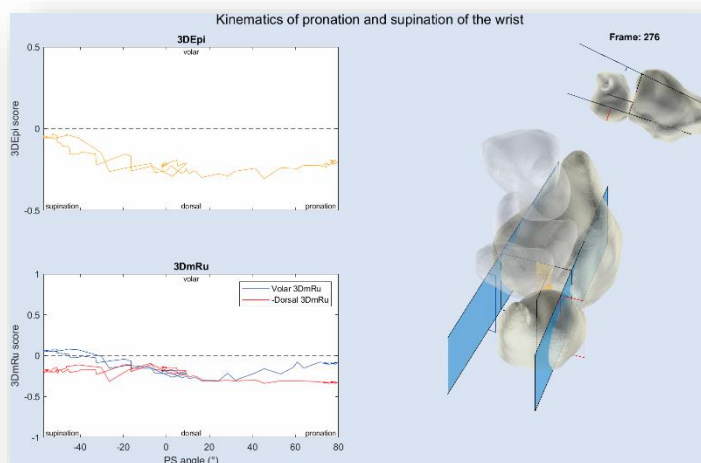


*C. Visualisation of DRUJ stability in the right wrist of P001*

*Figure 41: Visual representation of the 3DEpi and 3DmRu of both wrists of P001 and a healthy wrist*

## 8.5   Discussion

In this chapter the developed method for assessing DRUJ stability was applied to a patient diagnosed with DRUJ instability and for the first time in this thesis a comparison between healthy and pathological data was made. To achieve this the proposed workflow was modified to PS data and successfully applied to patient data. The results of this study show a perceivable difference between the wrist of the healthy volunteer and both wrists of P001. However, differing from the radiology rapport, no clear differentiation was observed between both wrists of P001. Since only one patient and one volunteer was included in the analysis, caution is needed in drawing general conclusions.

For both the 3DEpi as well as the volar 3DmRu a clear difference can be seen between both wrists of P001 and the wrist of the healthy volunteer. With the conventional Epi the DRUJ is considered normal when the centre of the ulnar head is located within the middle half of the sigmoid notch [17]. This corresponds with a 3DEpi score between -0.25 and 0.25. Both the left as well as the right wrist of P001 exceed this with respective minimal 3DEpi scores of -0.29 and -0.30 whereas the healthy stays within this range with a minimal 3DEpi score of -0.17. This relatively dorsal position of the ulnar head suggests laxity in the volar part of the TFCC. DRUJ subluxation was not observed. It is interesting to notice that there is especially more volar to dorsal translation in the injured wrists when moving from supination to neutral in comparison to in pronation. This could be caused by the laxity of the volar component of the DRUJ. The difference between the P001 and the healthy volunteer is less pronounced in the dorsal 3DmRu, which is expected since the conventional mRu only measures the volar protrusion and the dorsal 3DmRu may only be valuable to indicate dorsal subluxation which is not seen in this patient. Visually P001 seems to show smoother data which may be due to increased registration errors caused by motion artefacts. Possibly showing a beneficial effect of only visualising pronation instead of a full PS cycle in 10 seconds.

In the performed analysis both wrists of P001 returned similar DRUJ stability parameter scores for both wrists This differs from the radiology report, in which abnormal movement of the DRUJ was only reported in the left wrist Severe arthrosis of the DRUJ was however reported in both wrists. A possible explanation for this is that the measured DRUJ stability parameters measure a bilateral laxity of the DRUJ during volar dorsal translation, which could be  a different kind of movement than the perceived abnormal movement of the DRUJ described by the radiologist. Another explanation is that DRUJ laxity and due to this abnormal motion, is present in both wrists but was only perceived in one wrist by the radiologist. This may correlate with the bilateral severe DRUJ arthrosis and the rupture of the volar insertion of the TFCC in the right wrist. As mentioned before the challenge of manual interpretation of 4DCT data is one of the reasons automatic analysis and quantification of 4DCT data is important.

To conclude both the 3DEpi and the volar 3DmRu show a clear differentiation between the wrists of P001 and the wrist of the healthy volunteer. This may indicate potential in the use of 4DCT to visualise laxity of the TFCC. However, these findings do not correspond with the dynamic findings of the radiologist which may indicate that the measured parameter did not cover the abnormal motion observed by the radiologist but can also show the added benefit of automatic analysis and quantification in 4DCT. Further investigation including more wrists is needed to draw further conclusions.
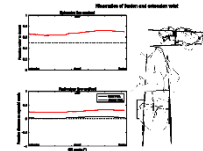
# Chapter 9: General discussion

The main aim of this thesis was to explore the feasibility of using automatic 4DCT analysis to assess the function of the DRUJ and TFCC. To achieve this: a workflow was set-up, several aspects of this workflow were explored and evaluated and new data was gathered. These are only the first steps and clinical use is still several steps away, but they are essential steps in broadening the scope of 4DCT research. The upcoming patient study is needed to evaluate the clinical use of the proposed workflow and will give further inside in the future steps. This chapter will first revisit the ultimate goal of the project and subsequently evaluate the research questions that were set up in chapter 1.5 and after which recommendations on the next steps for the project will be provided. A quick visual summary of the thesis can be found in Figure 43.

The ultimate end goal of the 4DCT DRUJ and TFCC project will be to combine a number of automatic parameters into an easily interpretable score evaluating ulnar impaction; the state of the TFCC and DRUJ stability with high precision. Improved diagnostics of the DRUJ using objective, reproducible and quantitative parameters may improve long term treatment outcomes and prevent progression of osteoarthritis. After the treatment the same parameters can be used to evaluate the effect of this treatment aiding in data-driven decision making and possibly further improving TFCC lesion care. Ideally this final version may be integrated in the standard CT interface. While this is not possible yet, a visual overview of the parameters explored in this thesis already gives insight into the kinematics of the DRUJ. An important part of introducing 4DCT in the clinical workflow is giving the clinical practitioner insight into how the parameters are measured. The clinical practitioner is ultimately responsible for the diagnosis and thus needs to be able to interpret and trust the measured parameters to be able to make a well-considered judgement. I think clear visualisation such as shown in Figure 42 is essential in this and where possible black boxes need to be avoided.
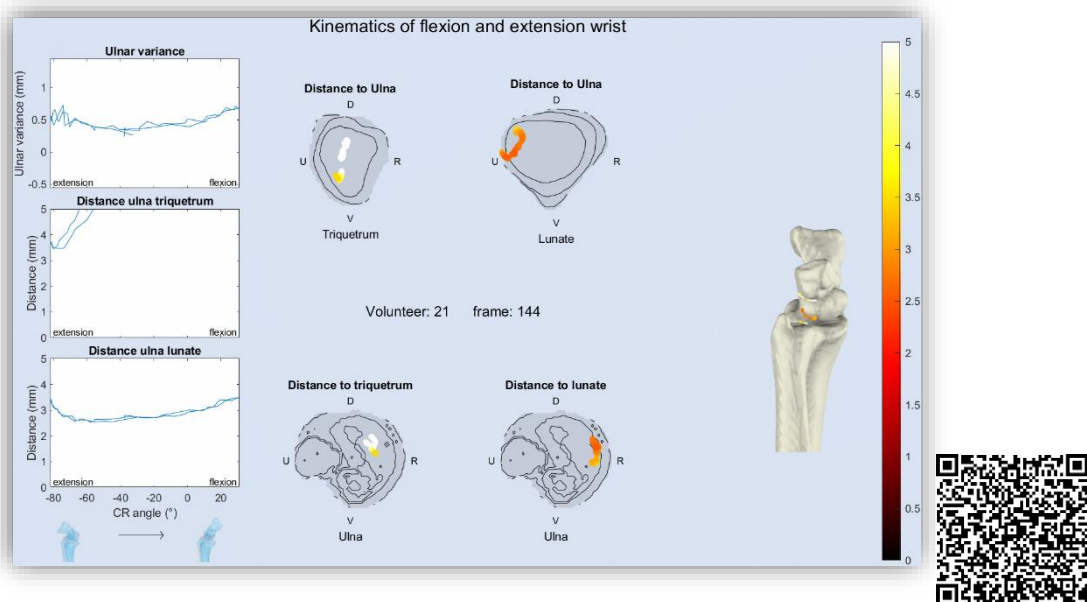


*A. Visual representation of ulnar variance and ulnar proximity evaluation*
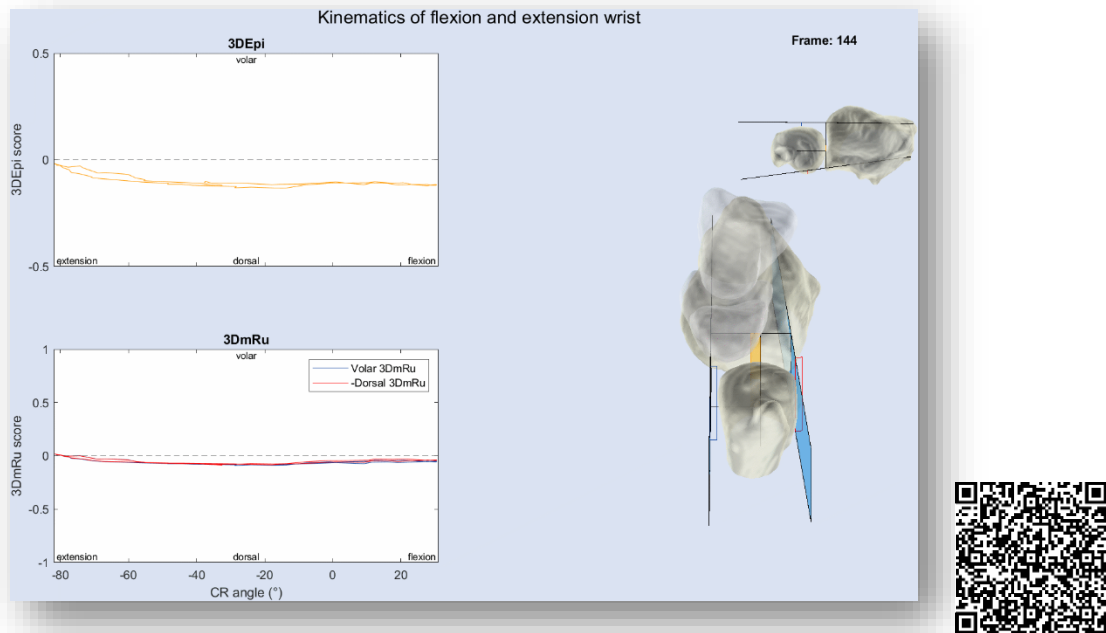
**B.** *Visual representation of ulnar stability evaluation*
*Figure 42: Visual representation of evaluated parameters.*

Chapter 2: "Acquisition of 4DCT data" describes the cadaver, volunteer and patient study that have been set-up to acquire relevant data to explore the use of 4DCT to assess the DRUJ and TFCC. Acquiring this data is essential for data-driven considerations in the workflow, establishing reference values and evaluating the performance of parameters. Both cadaver and volunteer data were gathered and are available for analysis in the near future. Currently the cadaver study already gave insights into the pronation speed for the volunteer study and the volunteer study further aided in adapting the protocol for the patient study hopefully improving visualisation. The PS data acquired in the volunteer study can be used to analyse the DRUJ parameters in their clinically most relevant motion and establish reference values as was demonstrated in Chapter 8: Automatic analysis of an instable wrist. In the upcoming year ulnar impaction and DRUJ instability patients will be included to acquire insight in the pathological wrist and the test-retest reliability of the workflow. Analysis of this data and comparison of this data to the established reference values will prove the clinical value of the established parameters.

Chapter 3: "Local coordinate system of the ulna" proposes and evaluates the robustness of an automatic method for determining the LCS of the ulna. The method showed to be feasible when performed on the whole ulna but suffers from errors when only performed on the distal ulna. Thus, estimation of the LCS on the static ulna and consecutive registration to the dynamic position is advised. In a different study using a SSM this LCS was shown to be stable along the Z-axis but showed a median rotational deviation of 1.62° [0.24° – 10.16°] in the x-y plane. Due to the Z-axis being the only axis used for calculations in this thesis, this is hypothesized to not negatively influence the presented parameters. Due to this, improvement of the proposed LCS defining method is not a high priority using the presented parameters but may be needed for the estimation of future parameters.

Chapter 4: "Registration of the ulna" analyses the registration quality of the ulna. Five different registration methods were evaluated of which CPD registration performed the best. Further evaluation of the CPD method showed that the registration error found with this method was relatively small compared to the voxel size of the dynamic scan with a median MAPSD of 0.189 mm and acceptably small for clinical use. While this is not a priority, in the future the registration might be improved by

using the same resolution for both the static and dynamic scan achieved by using similar reconstruction methods for both the static as dynamic data.

Chapter 5: "Ulnar variance" proposes a method for automatic measurement of a 3D adaptation of the ulnar variance parameter during continuous motion of the wrist. Using this method the effect of wrist motion on ulnar variance is evaluated in healthy volunteers during FE, RUD and CF and normal values are established. The proposed 3D method overcomes a number of problems that come with measuring ulnar variance on conventional radiographs, such as subjectivity, effect of direction and angle of x-ray projection and overprojection. The 3D ulnar variance was found to increase during ulnar deviation, flexion and CF, while it decreased in the first 40 degrees of extension, after which an increase was observed. This shows the significance of the effect of wrist position on ulnar variance. This chapter was written before the automatic mapping of anatomical landmarks using SSM was developed. The workflow may become more efficient by using anatomical mapping for estimation of the sigmoid notch. Further analysis of the acquired bilateral PS volunteer data and future patient data is needed to gain more insight into the left right symmetry of continuous ulnar variance measurements and the difference between healthy and pathological ulnar variance during movement.

Chapter 6: "Ulnocarpal proximity" proposes a workflow for automatic analysis of the ulnar proximity to the lunate and triquetrum and establishes reference values for these parameters during continuous RUD, FE and CF motion in the healthy wrist. Videos were created to evaluate ulnar kinematics of healthy wrists visualising the movement of the carpal bones in relation to the ulna. The proposed method was used to measure the normal distance between the ulna and the carpal bones and is hypothesised to directly visualise impact between these bones during ulnar impaction. Ultimately aiding in earlier diagnosis of impaction possibly preventing (further) osteoarthritis. While the current method may be used on every motion of the wrist, application to the acquired PS volunteer data is needed to evaluate and establish normal values on the full range of motion of the wrist. It is assumed that there is a left-right symmetry in healthy volunteers and thus asymmetry may be used to differentiate healthy from pathological wrists. Application of the method to the acquired bilateral volunteer data will be needed to estimate normal left-right asymmetry. Further application to the acquired patient data is needed to prove the value of the parameter in the diagnosis of ulnar impaction. The created distance maps may be used to gain further insight into the location of impaction. After the inclusion of the first ten patients it may be fruitful to use these maps to analyse the change in kinematics during movement and see if this can be used to develop new parameters.

Chapter 7: DRUJ stability" proposes an automatic workflow which for the first time enables 3D continuous analysis of DRUJ stability during continuous wrist motion. The workflow was developed and tested on healthy RUD and FE data. Since these movements actually take place in the radiocarpal joint distal to the DRUJ, performing the workflow on the acquired bilateral PS data is needed for a better evaluation of the method. In Chapter 8: A it has been shown that the workflow is applicable to PS movement and patient data. In the future, before clinical use can be considered, the currently used method for anatomical landmark mapping needs to be compared to manual mapping of these landmarks, to estimate the actual clinical effect of inaccuracies in the SSM mapping method. Depending on these results adaptations need to be made to the mapping method. Results indicating potential of the of the presented parameters for analysis of laxity in the wrist is demonstrated in chapter 8.

Chapter 8: "Automatic analysis of an instable wrist" applies the workflow as presented in chapter 7 to a wrist diagnosed with DRUJ instability during PS motion and compares this to the contralateral wrist and a wrist of a healthy volunteer. A clear differentiation can be made between the wrist of the healthy volunteer and the wrists of the patient. However, the findings between the two wrists of the patient

differ from the findings of the radiologist. This indicates potential of 4DCT in quantifying laxity but warrants further investigation in it's ability to diagnose DRUJ instability.

This thesis provides a prototype workflow for fully automatic analyse of the ulnar sided wrist. This is a first step in the diagnosis of ulnar sided wrist problems. There are however still several steps and improvements needed before this workflow can find its way to clinical use. During the project the lack of pathological data proved to make distinguishing between which inaccuracies are clinically relevant and which are not difficult.

Due to this (and the expected limited human resources available for this study in the near future) it is advised to first evaluate the currently proposed parameters and set up a baseline from where to improve before actually attempting to improve the presented variables. After segmentation of the PS data, normal values can be estimated for the whole range of motion of the wrist and normal left-right asymmetry can be estimated for the PS movement. After 10 patients are included a first comparison can be made between the healthy and pathological wrists. Comparison of both the estimated normal values and the measured pathological parameter values as well as the observed visual differences will be a good indicator to which extent the different parameters will be able to differentiate healthy from pathological wrists. Using this data improvements to the parameters can be made where needed while the rest of the patient data is acquired. While dependent on the aforementioned tests it is expected that most gains (both in precision as well as speed) can be achieved by using a robust mapping method allowing for more accurately defining the different POI's described in this thesis in a singular operation. With the potential to increase precision in both LCS definition as well as all parameters except for ulnar proximity.

In conclusion, this thesis provides a first stepping stone for the development of automatic 4DCT analysis to assess the DRUJ and TFCC. Five new or adapted 3D parameters have been proposed and evaluated on 4DCT data of 31 healthy volunteers. All parameters were evaluated for the RUD and FE motion and both 3D ulnar variance and ulnar proximity parameters were also evaluated for the CF motion. Since this is only the first step in a big project, not every method has been performed on PS motion, which is clinically the most important movement for evaluating the DRUJ and TFCC, and only one patient has been analysed. However, a large volunteer dataset including the PS motion was acquired, and a patient study has been set-up. Applying the developed methods to this data will further evolve our knowledge of the DRUJ kinematics and may improve the diagnosis of DRUJ instability and ulnar impaction, thereby facilitating and improving early treatment and preventing progression. Up till that point this thesis gives a new insight into the ulnar sided wrist kinematics and validates and enables continuation of research on the use of 4DCT for DRUJ and TFCC assessment.
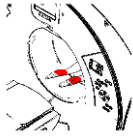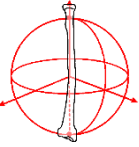
| | | |
|---|---|---|
| **Chapter 2:**<br>**Acquisition of 4DCT data** |  | **Results**: A cadaver study was performed gaining insight into the effect of movement speed and OSM on acquisition and aiding in further research on reconstruction algorithms. A volunteer study was performed acquiring data for PS, AbAd and OR motion. |
| | | **Future outlook**: A study was set-up and METC approved to analyse 30 patients with DRUJ instability or impaction during FE, RUD and PS movement and analyse the test-retest reliability on 20 patients. |
| **Chapter 3:**<br>**Local coordinate system of the ulna** |  | **Results**: A method for automatic LCS calculation was proposed that performs visually robust. |
| | | **Future outlook**: The current method can and has been used for the calculation of ulnar parameters. |
| **Chapter 4:**<br>**Registration of the ulna** |  | **Results**: Several registration methods were tested from which CPD provided the best registration. The found registration error using this method is relatively small to the voxel size. |
| | | **Future outlook**: Registration performs acceptably good but may be further improved by using a similar resolution and reconstruction algorithm for the static and dynamic CT. |
| **Chapter 5:**<br>**Ulnar variance** |  | **Results**: A 3D adaptation of the conventional ulnar variance measurement was developed and applied to continuous 4DCT RUD, FE, and CF motion data. |
| | | **Future outlook**: Application of the developed method to the acquired bilateral PS volunteer data and future patient data may further improve insight in ulnar kinematics and dynamic ulnar variance. |
| **Chapter 6:**<br>**Ulnar proximity** |  | **Results**: A workflow was proposed for automatic ulnar proximity assessment and reference values during RUD, FE and CF were established. |
| | | **Future outlook**: Application of the developed method to the acquired bilateral PS volunteer data and future patient data may further improve insight in ulnar kinematics and ulnar proximity. |
| **Chapter 7:**<br>**DRUJ stability** |  | **Results**: Two parameters were developed, the 3DmRU and the 3DEpi. The method was applied to RUD and FE data. |
| | | **Future outlook**: While the current method has been developed on RUD and FE data, the PS movement is clinically the most important. Applying the developed parameters to the data that will be acquired in the volunteer and patient study will truly show the potential of these parameters. |

*Figure 43: Summary of the thesis*

# Chapter 10:     References

[1]   C. Spies, "Distal radioulnar joint instability: current concepts of treatment," *Archives of Orthopaedic and Trauma Surgery volume,* vol. 140, p. 639–650, 2020.

[2]   A. R. Mirghasemi, "Distal Radioulnar Joint Instability," *Geriatr Orthop Surg Rehabil.,* vol. 6, no. 3, pp. 225-229, 2015.

[3]   T. Saito, "Chronological and geographic trends of TFCC Repair," *Hand Clin.,* vol. 33, no. 4, pp. 593-605, 2017.

[4]   M. Park, "The rate of triangular fibrocartilage injuries requiring surgical intervention," *Orthopedics.,* vol. 22, no. 11, p. 806, 2010.

[5]   M. D. Treiser, "TFCC Injuries: Meta-Analysis and Comparison of Diagnostic Imaging Modalities," *Journal of wrist surgery,* vol. 3, no. 7, pp. 267-272, 2018.

[6]   A. Jawed, "TFCC injuries: How we treat?," *Journal of clinical orthopeadics and trauma,* vol. 4, no. 11, pp. 570-579, 2020.

[7]   T. Smioth, "The diagnostic accuracy of X-ray arthrography for triangular fibrocartilaginous complex injury: a systematic review and meta-analysis," *Journal of hand surgery,* vol. 37, no. 9, 2011.

[8]   K. Casadei, Triangular Fibrocartilage Complex, Treasure Island: StatPearls publishing, 2022.

[9]   D. Shakoor, "Kinematic Analysis of the Distal Radioulnar Joint in Asymptomatic Wrists Using 4-Dimensional Computed Tomography–Motion Pattern and Interreader Reliability," *J Comput Assist Tomogr,* vol. 3, no. 43, pp. 392-398, 2019.

[10] G. I. Bain, "New advances in wrist arthroscopy," *Arthroscopy,* vol. 24, no. 3, pp. 355-367, 2008.

[11] A. Palmer, "Triangular fibrocartilage complex lesions: A classification," *J Hand Surg Am,* vol. 3, no. 13, pp. 391-394, 1989.

[12] A. Raunch, "Four-dimensional CT analysis of wrist kinematics during radioulnar deviation," *Radiology,* vol. 3, no. 298, pp. 750-758, 2018.

[13] E. Teule, "Automatic analysis of wrist kinematics using 4DCT," *Master thesis,* 2022.

[14] Y. R. Chen, "In vivo gliding and contact characteristics of the sigmoid notch and the ulna in forearm rotation," *The journal of hand surgery,* vol. 8, no. 38, pp. 1513-1519, 2013.

[15] R. Szabo, "Distal radioulnar joint instability," *The journal of bone & joint surgery,* vol. 4, no. 88, pp. 884-894, 2006.

[16] M. Wijffels, "Computed tomography for the detection of distal radioulnar joint instability: normal variation and reliability of four CT scoring systems in 46 patients," *Skeletal Radiology,* no. 45, pp. 1487-1493, 2016.

[17] E. C. Rodríguez-Merchán, "Distal Radioulnar Joint Instability: Diagnosis and Treatment," *The archives of bone and joint surgery,* vol. 1, no. 10, pp. 3-16, 2022.

[18] D. J. Bell, "Ulnar variance," Radiopeadia, 14 10 2022. [Online]. Available: https://radiopaedia.org/articles/ulnar-variance. [Accessed 27 01 2023].

[19] J. M. Jung, "Changes in ulnar variance in relation to forearm rotation and grip," *The Journal of Bone and Joint Surgery,* vol. 83, no. 7, pp. 244-251, 2001.

[20] C. T. McNamara, "A Systematic Review and Analysis of Palmer Type I Triangular Fibrocartilage Complex Injuries: Outcomes of Treatment," *Journal of hand an microsurgery,* vol. 2, no. 12, pp. 116-122, 2020.

[21] J. Dobbe, "Evaluation of a Quantitative Method for Carpal Motion Analysis Using Clinical 3-D and 4-D CT Protocols," *IEEE TRANSACTIONS ON MEDICAL IMAGING,* vol. 38, no. 4, pp. 1048-1057, 2019.

[22] E. Teule, "Automatic analysis of wrist kinematics using 4DCT," *Master thesis - Technical Medicine - University of twente,* 2022.

[23] M. G. A. d. Roo, "Accuracy of manual and automatic placement of an anatomical coordinate system for the full or partial radius in 3D space," *Sci Rep,* vol. 10, no. 8114, 2020.

[24] G. E. Marai, "Estimating Joint Contact Areas and Ligament Lengths From Bone Kinematics and Surfaces," *IEEE TRANSACTIONS ON BIOMEDICAL ENGINEERING, ,* vol. 51, no. 5, pp. 790-799, 2004.

[25] I. F, "nnU-Net: a self-configuring method for deep learning-based biomedical image segmentation," *Nat Methods,* vol. 18, no. 2, pp. 203-211, 2021.

[26] M. Haenen, "4DCT for diagnosing dynamic wrist injuries: the influence of inter-subject anatomical shap variations on kinematic parameter extraction".

[27] M. Heyndrickx, "Improving image quality in fast, time-resolved micro-CT by weighted back projection," *Scientific reports,* vol. 10, p. 18029, 2020.

[28] D. T. L. Wong, "Dennis T. L. Wong,corresponding author1 Siang Y. Soh,1,* Brian S. H. Ko,1,* James D. Camer," *Cardiovasc Diagn Ther,* vol. 4, no. 4, pp. 299-305, 2014.

[29] C. Jiang, "High quality reconstruction of dynamic objects using 2D-3D camera fusion," *IEEE International conference on Image processing ,* pp. 2209-2213, 2017.

[30] Kappe, "Four Dimensional Computed Tomography for the Quantitative Assessment of Carpal Bone Kinematics for the Diagnosis of Wrist Injuries with Inconclusive Radiographs," *Master thesis - Technical medicine - University of Twente,* 2020.

[31] A. Myronenko, "Point set registration: Coherent point drift," *IEEE transactions on pattern analysis and machine intelligence,* vol. 32, no. 12, p. 2262–2275, 2010.

[32] B. Paul, "A method for registration," *IEEE Transactions on Pattern Analysis and Machine Intelligence,* vol. 14, no. 2, p. 239–256, 1992.
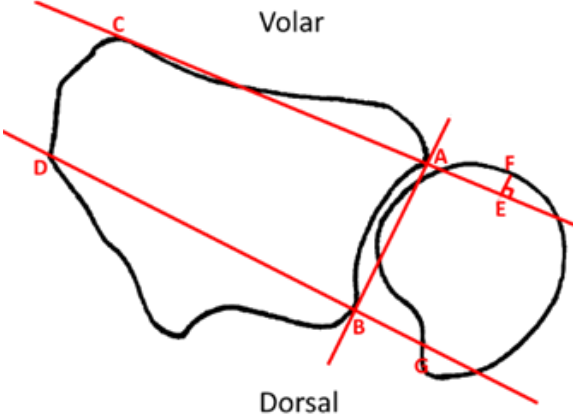
[33] M. Hedjazi, "Point based rigid-body registration using an unscented kalman filter," *IEEE transactions on medical imaging,* vol. 26, no. 12, pp. 1708-1728, 2007.

[34] D. Christie, "Comparative Evaluation on Sparse Point Cloud Registration for Human Bone 3D Pose Estimation," *Not published yet.*

[35] J. G. M. Oonk, "Quantification of the methodological error in kinematic evaluation of the DRUJ using dynamic CT," *Sci rep.,* vol. 13, no. 3159 , 2023.

[36] L. D. Smet, "Ulnar variance: facts and fiction review article," *Acta Orthop Belg,* vol. 60, pp. 1-9, 1994.

[37] O. Hulten, "Uber anatomische variationen der handgelenkknochen," *Acta Radiologica,* vol. 9, pp. 155-168, 1928.

[38] T. Saito, "A Systematic review of Outcomes after Arthroscopic Debridement for Triangular Fibrocartilage Complex Tear," *Plast Reconstr Surg.,* vol. 140, no. 5, pp. 697-708, 2017.

[39] A. Palmer, "Biomechanics of the distal radioulnar joint," *Clin Orthop Relat Res,* vol. 187, pp. 26-35, 1984.

[40] R. Gunta, "Ulnar variance and subchondral bone mineralization patterns in the distal articular surface of the radius," *The journal of handsurgery,* vol. 29, no. 5, pp. 835-840, 2004.

[41] E. Pang, "Ulnar-sided wrist pain in the athlete (TFCC/DRUJ/ECU)," *Curr Rev Musculoskelet Med.,* vol. 10, no. 1, pp. 53-61, 2017.

[42] S. Roner, "Three-Dimensional Automated Assessment of the Distal Radioulnar Joint Morphology According to Sigmoid Notch Surface Orientation," *J Hand Surg Am,* vol. 45, no. 11, pp. 1083-1094, 2020.

[43] R. m. o. t. n. d. r. r. o. c.-a. C. v. p. r. interpretation, "Nora Suojärvi," *Journal of hand surgery (European Volume),* vol. 46, no. 2, 2020.

[44] R. Medoff, "Essential radiographic evaluation for distal radius fractures," *Hand clinics,* vol. 21, pp. 279-288, 2005.

[45] D. Freedman, "Right Versus Left Symmetry of Ulnar Variance: A Radiographic Assessment," *Clinical Orthopaedics and Related Research,* vol. 354, pp. 153-158, 1998.

[46] C. Goldfarb, "Defining Ulnar Variance in the Adolescent Wrist: Measurement Technique and Interobserver Reliability," *The Journal of Hand Surgery,* vol. 36, no. 2, pp. 272-277, 2011.

[47] A. Schuurman, "Assessment of ulnar variance: a radiological investigation in a Dutch population," *Skeletal Radiol ,* vol. 30, pp. 633-638, 2001.

[48] J. Jung, "Changes in ulnar variance in relation to forearm rotation and grip," *The journal of bone & joint surgery,* vol. 83, pp. 1029-1033, 2001.

[49] T. Saito, "A Systematic review of Outcomes after Arthroscopic Debridement for Triangular Fibrocartilage Complex Tear," *Plast Reconstr Surg,* vol. 140, no. 5, pp. 697-708, 2017.

[50] S. Friedman, "The change in ulnar variance with grip," *J Hand Surg Am,* vol. 18, no. 4, pp. 713-716, 1993 .

[51] M. M. Tomaino, "Ulnar Impaction Syndrome," *Hand clin.,* vol. 21, pp. 567-575, 2021.

[52] T. Imaeda, "Ulnar impaction syndrome: MR imaging findings.," *Radiology. ,* vol. 2, no. 495-500, p. 201, 1996.

[53] M. Infanger, "Meniscus and discus lesions of triangular fibrocartilage complex (TFCC): treatment by laser-assisted wrist arthroscopy," *Journal of Plastic, Reconstructive & Aesthetic Surgery,* vol. 62, no. 4, pp. 466-471, 2009.

[54] D. Jain, "Ulnar-Side Wrist Pain Management Guidelines: All That Hurts is Not the TFCC!," *Indian Journal of Orthopaedics,* vol. 55, p. 310–317, 2021.

[55] R. Carr, "Four-Dimensional Computed Tomography Scanning for Dynamic Wrist Disorders: Prospective Analysis and Recommendations for Clinical Utility," *Journal of wrist surgery,* vol. 8, no. 2, pp. 161-167, 2019.

[56] M. Park, "Reliability and normal values of various computed tomography methods for quantifying distal radioulnar joint translation," *J Bone Joint Surg Am,* vol. 90, no. 1, pp. 145-153, 2008.

[57] C. Pan, "Displacement of the distal radioulnar joint of clinically symptom-free patients," *Clin Orthop Relat Res,* vol. 415, pp. 148-156, 2003.

[58] B. Swartman, "Normal values of distal radioulnar translation assessed by three-dimensional C-arm scans: a cadaveric study," *J Hand Surg Eur Vol,* vol. 44, no. 5, pp. 503-509, 2019.

[59] R. Dunkan, "Isolated Volar Dislocation of the Distal Radioulnar Joint: A Case Report," *J Orthop Case Rep.,* vol. 10, no. 2, p. 97–100, 2020.

[60] M. J. Park, "Reliability and normal values of various computed tomography methods for quantifying distal radioulnar joint translation," *The journal of bone and joint surgery,* vol. 1, no. 90, pp. 145-153, 2008.

[61] C.-c. Pan, "Displacement of the Distal Radioulnar Joint of Clinically Symptom-Free Patients," *Clinical orthopeadics and related research,* vol. 2, no. 415, pp. 148-156, 2003.

[62] I. Lo, "The radioulnar ratio: A new method of quantifying distal radioulnar joint subluxation," *The journal of hand surgery,* vol. 26, no. 2, pp. 236-243, 2001.

[63] K. Zhao, "A Technique for Quantifying Wrist Motion Using Four-Dimensional Computed Tomography: Approach and Validation," *J Biomech Eng,* vol. 137, no. 7, p. 0745011–0745015., 2015.

[64] D. Freedman, "Right versus left symmetry of ulnar variance: a radiographic assessment," *Clin Orthop Relat Res,* vol. 354, pp. 153-158, 1998.

[65] L. H. Poppler, "Acute Distal Radioulnar Joint Instability: Evaluation and Treatment," *Hand clin.,* vol. 36, no. 4, pp. 429-441, 2020.

# Chapter 11:     Appendix

## 11.1  CT parameters for evaluating DRUJ stability

There are six different methods of assessing DRUJ instability in conventional CT which will be explored. The parameters are measured at the axial slice showing the widest sigmoid notch. The methods are as follows: the radioulnar line method or Mino method; the modified radioulnar line method; the subluxation ratio; the epicentre method; the radioulnar method and the congruent method [17] [60] [61].

| **Name:** Radioulnar line method / Mino method (/Modified radioulnar line method) |
|---|
|  *Figure 44: Radioulnar line method* |
| **Description:** Ulnar subluxation is quantified as the amount of ulnar head that is located outside of the volar radioulnar line and the dorsal radioulnar line |
| **Extracted data:** <br> Volar radioulnar line: <br> • Volar corner of the sigmoid notch of the radius (A) <br> • Volar radial border of radius (C) <br> Dorsal radioulnar line: <br> • Dorsal corner of the sigmoid notch of the radius (B) <br> • Dorsal radial border of radius (D) <br> Distance that the ulnar wall is outside of the ulnar lines (E-F) |
| **Calculations:** <br> Radioulnar line score = EF / AB <br> Alternative scoring: Radioulnar line score = EF / EG |
| **Comments:** <br> • In literature Radioulnar line method and modified radioulnar line method are used interchangeably |

| **Name:** Modified radioulnar line method | **Name:** Subluxation ratio |
|---|---|



Volar

Dorsal

*Figure 45: Modified radioulnar line method*

**Description:** Ulnar subluxation is quantified as the amount of ulnar head that is located outside of the volar radioulnar line and the line connecting the dorsal margin of the sigmoid notch and Lister's tubercle

**Extracted data:**

Volar radioulnar line:
- Volar ulnar border of the radius (A)
- Volar radial border of radius (C)

Dorsal radioulnar line:
- Dorsal ulnar border of the radius (B)
- Lister's tubercle (H)

Distance that the ulnar wall is outside of the ulnar lines (I - J)

**Calculations:**

Modified radioulnar line score = IJ / AB

Alternative scoring: Modified radioulnar line score = IJ / IK

---



Volar

Dorsal

*Figure 46: Subluxation ratio*

**Description:** Ulnar subluxation is quantified as the amount of ulnar head that is located outside of two lines perpendicular (angle of 90 degrees) to the line connecting the volar and dorsal margins of the sigmoid notch.

**Extracted data:**

Volar margin of the sigmoid notch (A)

Dorsal margin of the sigmoid notch (B)

Distance that the ulnar wall is outside of the perpendicular line (R-L)

**Calculations:**

Subluxation ratio score = RL / AB

77

| **Name:** Epicentre method | **Name:** Radioulnar ratio [62] |
|---|---|
| Volar  Dorsal | Volar  Dorsal |
| Figure 47: Epicentre method | Figure 48: Radioulnar ratio |
| **Description:** Ulnar subluxation is quantified as the distance between the middle of the sigmoid notch and the intersection point of the perpendicular line to the line connecting the volar and dorsal margins of the sigmoid notch which intersects the centre of rotation of the DRUJ. | **Description:** Ulnar subluxation is quantified as the ratio between the distance between the dorsal and volar margin of the sigmoid notch and the line perpendicular to this line that crosses the centre of the ulnar head |
| **Extracted data:** Intersection point (O) of: <br> • The line perpendicular to the line connecting: <br> o Volar margin of the sigmoid notch (A) <br> o Dorsal margin of the sigmoid notch (B) <br> • And crossing the centre of rotation of the DRUJ defined as the midpoint between <br> o Centre of the ulnar styloid (N) <br> o Centre of the ulnar head (M) <br> Middle of the sigmoid notch (P) which is the midpoint between: <br> • Volar margin of the sigmoid notch (A) <br> Dorsal margin of the sigmoid notch (B) | **Extracted data:** Volar margin of the sigmoid notch (A) <br> Dorsal margin of the sigmoid notch (B) <br> The intersection (Q) between this line and the perpendicular line that crosses the centre of the ulnar head (M) |
| **Calculations:** Epicentre method score = OP / AB | **Calculations:** Radioulnar ratio score = AQ / AB |

# Protocol metingen kadaver arm

## Samenvatting

| 1. Statisch protocol | Standaard positie | 5 x 1 frame |
|---|---|---|
| 2. Dynamisch protocol | Standaard positie | 2 x 1 sec |
| 3. Statisch protocol | Midden scanner | 1 x 1 frame |
| 4. Dynamisch protocol | Pronatie-supinatie | 2 x 10 sec |
| 5. Dynamisch protocol | Pronatie | 2 x 7 sec |
| 6. Dynamisch protocol | Pronatie | 2 x 10 sec |
| 7. Statisch met plaat | Standaard positie | 2 x 1 frame |
| 8. Dynamisch met plaat | Pronatie | 2 x 10 sec |

Extra: van alle data moet ruwe data worden opgeslagen

## Inhoud

## Benodigdheden

| Wat | Wie kan dit regelen |
| --- | --- |
| 1 kadaver arm | Richard |
| Access koelcel voor arm (orthopedisch lab) | Richard |
| Osteosynthese plaat | Brigitte |
| Access CT 1 | Koen |
| Access segmentatie methode arm | Axti |

## Algemene planning

| Wat | Wie | Wanneer |
| --- | --- | --- |
| Aanvragen kadaver arm | Jesse en Richard | 1,5 maand voor scan moment |
| Plannen avond gebruik CT 1 (voor 2 uur) | Jesse en Koen | 1,5 maand voor scan moment |
| Vervoer arm van anatomie naar orthopedisch lab | Jesse en Richard | 1 dag voor scan moment |
| Voorboren gaten plaat en opnieuw inpakken arm | Jesse, Richard | Dag van scan moment |
| Vervoer arm van orthopedisch lab naar CT | Jesse en Richard | Dag van scan moment |
| Scan serie 1-6 | Jesse en Koen | Dag van scan moment |
| Vastschroeven plaat en opnieuw inpakken arm | Jesse | Dag van scan moment |
| Scan serie 7 en 8 | Jesse en Koen | Dag van scan moment |
| Los schroeven plaat en opnieuw inpakken arm | Jesse | Dag van scan moment |
| Vervoer arm terug naar orthopedisch lab | Jesse | Dag van scan moment |
| Beoordeling pronatie-supinatie beelden | 4DCT team plastisch en Ruud | Binnen week na scan moment |
| Segmentatie scans | Wie daar tzt over gaat | Binnen maand na scan moment, behalve de pronatie-supinatie beelden, deze wanneer mogelijk |
| Analyse segmentaties | 4DCT team plastisch | Binnen twee maand na scan moment, behalve de pronatie-supinatie beelden, deze wanneer mogelijk |
| Analyse reconstructie methodes | Maranda en axti | Whenever ze willen |

# Overzicht beeldvorming

*belangrijk: van alle scans moet ook de ruwe data worden opgeslagen*

| Serie | Scan protocol | Positie | Field of view (proximaal distaal) | Field of view (dicom grid) | Benodigde scan tijd (seconden) | Benodigde voorbereidingstijd (seconden) |
|---|---|---|---|---|---|---|
| **1.A**: Statisch protocol standaard | 1 frame statisch protocol | Midden van de gantry | Gehele arm | Theoretische locaties beide armen | 5 | 600 |
| **2.A**: Dynamisch protocol standaard | 5 sec versie dynamisch protocol | Bovenstaande positie (niet verplaatsen) | 12 cm (incl. carpale botten en radius en ulna kop) | Theoretische locaties beide armen | 1 | 10 |
| **1.B**: Statisch protocol standaard | 1 frame statisch protocol | Standaard positie rechter arm (in houder) | Gehele arm | Theoretische locaties beide armen | 5 | 120 |
| **2.B**: Dynamisch protocol standaard | 5 sec versie dynamisch protocol | Bovenstaande positie (niet verplaatsen) | 12 cm (incl. carpale botten en radius en ulna kop) | Theoretische locaties beide armen | 1 | 10 |
| **1.C**: Statisch protocol standaard | 1 frame statisch protocol | Standaard positie linker arm (in houder) | Gehele arm | Theoretische locaties beide armen | 5 | 120 |
| **2.C**: Dynamisch protocol standaard | 5 sec versie dynamisch protocol | Bovenstaande positie (niet verplaatsen) | 12 cm (incl. carpale botten en radius en ulna kop) | Theoretische locaties beide armen | 1 | 10 |
| **1.D**: Statisch protocol standaard | 1 frame statisch protocol | Standaard positie rechter arm (in houder) | Gehele arm | Theoretische locaties beide armen | 5 | 120 |
| **1.E**: Statisch protocol standaard | 1 frame statisch protocol | Standaard positie linker arm (in houder) | Gehele arm | Theoretische locaties beide armen | 5 | 120 |

| | | | | | | |
|---|---|---|---|---|---|---|
| **3.A**: Statisch protocol standaard | 1 frame statisch protocol | Standaard positie rechter arm (in houder) | Gehele arm | Gehele arm | 5 | 120 |
| **4.A**: Pronatie-supinatie in 10 sec | 10 sec versie dynamisch protocol | Standaard positie rechter arm (in houder) | 12 cm | Theoretische locaties beide armen | 10 | 300 |
| **4.B**: Pronatie-supinatie in 10 sec | 10 sec versie dynamisch protocol | Standaard positie linker arm (in houder) | 12 cm | Theoretische locaties beide armen | 10 | 120 |
| **4.extra:** Pronatie-supinatie 16 CM FOV | 10 sec versie dynamisch protocol | Standaard positie linker arm (in houder) | 16 cm | Theoretische locaties beide armen | 10 | 120 |
| **5.A**: Pronatie in 7 sec | 7 sec versie dynamisch protocol | Standaard positie rechter arm (in houder) | 12 cm | Theoretische locaties beide armen | 10 | 120 |
| **5.B**: Pronatie in 7 sec | 7 sec versie dynamisch protocol | Standaard positie linker arm (in houder) | 12 cm | Theoretische locaties beide armen | 10 | 120 |
| **6.A**: Pronatie in 10 sec | 10 sec versie dynamisch protocol | Standaard positie rechter arm (in houder) | 12 cm | Theoretische locaties beide armen | 10 | 120 |
| **6.B**: Pronatie in 10 sec | 10 sec versie dynamisch protocol | Standaard positie linker arm (in houder) | 12 cm | Theoretische locaties beide armen | 10 | 120 |
| **7.A**: Statische scan met plaat | 1 frame statisch protocol | Standaard positie rechter arm (in houder) | Gehele arm | Theoretische locaties beide armen | 5 | 1200 |
| **8.A**: Pronatie in 10 sec met plaat | 10 sec versie dynamisch protocol | Standaard positie rechter arm (in houder) | Gehele arm | Theoretische locaties beide armen | 10 | 300 |
| | | | | **Totaal:** | 107 (3 min) | 3620 (60 min) |

## Beschrijving experimenten

| Experiment 1: | Verschil tussen dynamische en statische scan |
|---|---|
| **Beschrijving:** | Momenteel zien we een registratiefout in het registreren van de statische scan naar de dynamische scan. Dit zou kunnen komen door intrinsieke verschillen tussen de scans (bijvoorbeeld een partial volume effect) of door een verschil van protocol tussen de scans (bijvoorbeeld bewegingen tijdens de scans). Met dit experiment proberen we de intrinsieke verschillen los van de protocol verschillen te bekijken. Doordat de hand niet beweegt zal het enige verschil tussen beide scans het intrinsieke verschil tussen de scans zijn |
| **Hypothese:** | Door de lagere resolutie heeft de dynamische scan een groter partial volume effect dan de statische scan. Ongeveer enkele milimeters. |
| **Benodigde beelden:** | 1.A(-E) en 2.A(-E) |
| **Verwerking data:** | Alle beelden zullen volgens de standaard procedure gesegmenteerd worden. Vervolgens zullen ze digitaal over elkaar heen gelegd worden. Als het goed is kan dit precies aan de hand van de CT coördinaten. Vervolgens wordt de point to surface afstand tussen beide segmentaties bepaald. |
| **Opmerkingen:** | Kan waarschijnlijk ook gesimuleerd worden door verschillende reconstructie methodes |

| Experiment 2: | Effect locatie in scanner op beeldkwaliteit en segmentatie |
|---|---|
| **Beschrijving:** | Het is bekend dat er een relatief betere signal to noise ratio (SNR) is in het midden van de rotatie van de CT. Momenteel maken we de trade-off van twee handen tegelijkertijd in de scanner tegen een lagere beeldkwaliteit. Het exacte effect hiervan is niet bekend. |
| **Hypothese:** | De beeldkwaliteit is in het midden van het scan volume beter dan aan de buitenranden van het scan volume, dit verschil is echter waarschijnlijk minimaal en de vraag is of het te merken is in de segmentaties. |
| **Benodigde beelden:** | 1.A&B(-E) en 3.A&B |
| **Verwerking data:** | Alle beelden zullen volgens de standaard procedure gesegmenteerd worden. Vervolgens zullen ze op elkaar geregistreerd worden via de gebruikelijke methode. |
| **Opmerkingen:** | |

| Experiment 5: | Test-retest betrouwbaarheid |
|---|---|
| **Beschrijving:** | Tijdens het meet moment zullen we elke scan minstens twee maal maken zodat we de kans minimaliseren dat we door een foutieve scan data missen. Echter kunnen we hier ook test-retest metingen mee doen. Hierdoor kunnen we verklaren of een gemeten verschil in de eerdere testen verklaard kan worden door de onafhankelijke variabelen of door de workflow zelf. |
| **Hypothese:** | De test-retest variatie is zeer minimaal, de scan kwaliteit is consistent en de workflow robuust. |
| **Benodigde beelden:** | Alle waarbij de A versie vergeleken wordt met de B(-E) versie |
| **Verwerking data:** | We kunnen de segmentaties in elke scan vergelijken, ik denk wel dat we dit qua efficiëntie wel uitstellen tot na dat we verschillen merken in één van de eerdere experimenten. |
| **Opmerkingen:** | |


| Experiment 6: | Het effect van verschillende reconstructie methodes op de dynamische CT data |
|---|---|
| **Beschrijving:** | Vanuit de axti kwamen er suggesties dat we door de ruwe CT data op een andere manier te reconstrueren de kwaliteit van de scans mogelijk verbeterd kan worden. Met de huidig gebruikte scanner kan door het opslaan van de ruwe data retrospectief het aantal gebruikte rotaties per frame, de field of view (FOV) en het reconstructie algoritme aangepast worden. |
| **Hypothese:** | Door het gebruik van een kleinere fractie rotaties per frame zullen de bewegingsartefacten verminderd worden maar zal het beamhardening effect toenemen. Door het DICOM format is de resolutie van de scan direct gekoppeld aan de FOV, een kleinere FOV betekent dus ook een hogere resolutie. Mogelijk kunnen we hierdoor het partial volume effect wegnemen. |
| **Benodigde beelden:** | Alle opgenomen beelden kunnen hiervoor gebruikt worden maar waarschijnlijk: 1A-E |
| **Verwerking data:** | Waarschijnlijk aan Maranda en de axti |
| **Opmerkingen:** | Hiervoor is het belangrijk dat de ruwe data wordt opgeslagen. |

**Experiment 3:**      De pronatie-supinatie beweging en bewegingsartefacten

| | |
|---|---|
| **Beschrijving:** | Momenteel zijn we vrij grote bewegingsartefacten tijdens de pronatie-supinatie beweging. De vraag is of dit een probleem op gaat leveren tijdens de segmentatie fase. De beeldkwaliteit kan mogelijk verbeterd worden door een langzamere beweging. Het distaal radiaal ulnair (DRU) gewricht subluxeert waarschijnlijk tijdens sterke pronatie. Daarom willen we proberen om te focussen op deze pronatie beweging en die in verschillende tijdsstappen van 7 en 10 langzamer te laten verlopen. Hierbij hopen we onder de 10 seconden een snelheid te vinden die leidt tot een acceptabele kwaliteit. |
| **Hypothese:** | Een verlaagde rotatie snelheid leidt waarschijnlijk tot minder bewegingsartefacten. |
| **Benodigde beelden:** | 4.A(&B); 5.A(&B); 6.A(&B) |
| **Verwerking data:** | Alle beelden zullen in de week na de scan geanalyseerd waarna een keuze kan worden gemaakt voor de pronatie(-supinatie) acquisitie lengte in patiënten. Vervolgens zullend de beelden ook gesegmenteerd worden waarna het effect van de snelheid op de segmentatie bepaald kan worden. Hiervoor moet echter wel eerst het segmentatie algoritme verbeterd worden. |
| **Opmerkingen:** | |

**Experiment 4:**      Het effect van een plaat op de automatische segmentatie van CT data

| | |
|---|---|
| **Beschrijving:** | Uiteindelijk willen we onze methode ook gaan gebruiken om het effect van een chirurgische ingreep op de kinematica van de pols te bepalen. Direct na een chirurgische ingreep bevind er veelal osteosynthese materiaal in de pols. Hiervan is bekend dat het zorgt voor beam hardening artefacten die een groot effect hebben op de beeldkwaliteit. Met dit experiment proberen we te bepalen wat het effect is van deze effecten op het segmentatie algoritme. Indien de segmentaties van onvoldoende kwaliteit zijn kunnen we met behulp van reconstructie methoden of andere technieken proberen deze segmentaties te verbeteren tot dat ze wel volstaan. |
| **Hypothese:** | Het beam hardening effect zal waarschijnlijk grote effecten hebben op het segmentatie algoritme dat hier niet op getraind is. |
| **Benodigde beelden:** | 7.A(&B) & 8.A(&B) |
| **Verwerking data:** | We zullen eerst een van de beelden via de normale workflow converteren naar een segmentatie waarna we kunnen kijken naar het effect van de plaat op de segmentatie. Vervolgens kunnen we daarna de beeldkwaliteit proberen te verbeteren waarna de scan opnieuw gesegmenteerd kan worden als we verbetering van de resultaten verwachten. |
| **Opmerkingen:** | |

## 11.3 Protocol volunteer and patient study

# RESEARCH PROTOCOL

Diagnostic performance of dynamic four-dimensional computed tomography (4DCT) compared to

arthroscopy for analysing distal radioulnar joint instability

Project proposal for research collaboration

between plastic surgery and radiology department.

(28-08-2023)

1

**PROTOCOL TITLE** 'Diagnostic performance of dynamic four-dimensional computed tomography (4DCT) compared to arthroscopy for analysing distal radioulnar joint instability'

| | |
|---|---|
| **Protocol ID** | 4D Dynamic CT scan;<br><br>- Evaluation of visibility wrist joints<br>- Evaluation of sensibility and specificity to analyse distal radioulnar joint instability |
| **Short title** | 4DCT wrist low dose and DRUJ |
| **EudraCT number** | Not applicable |
| **Version** | 3.0 |
| **Date** | 28-08-2023 |
| **Coordinating investigator/project leader** | Dr E.P.A. vd Heijden, plastic surgeon<br><br>Plastic Surgery department Radboudmc<br><br>Brigitte.vanderheijden@radboudmc.nl |
| **Principal investigator(s) (in Dutch: hoofdonderzoeker/ uitvoerder)** | Dr E.P.A. vd Heijden, plastic surgeon<br>Plastic Surgery department Radboudmc<br>Brigitte.vanderheijden@radboudmc.nl<br>Dr. R Becks, radiologist<br>Radiology department Radboudmc<br>Ruud.Becks@radboudmc.nl<br>Dr. S. Hummelink, technical physician<br>Plastic Surgery department Radboudmc<br>Stefan.Hummelink@radboudmc.nl |
| **Sponsor (in Dutch: verrichter/opdrachtgever)** | Prof. Dr. D. Ulrich, plastic surgeon<br><br>Plastic Surgery department Radboudmc<br><br>Dietmar.Ulrich@Radboudmc.nl<br><br>Prof. Dr. W.M Prokop, radiologist<br><br>Department of radiology and nuclear medicine<br><br>Radboudmc |

2

| | Mathia.Prokop@Radboudumc.nl |
|---|---|
| **Subsidising party** | |
| **Independent expert (s)** | Dr THJ Nijhuis, plastic surgeon |
| | Plastic Surgery department Radboudumc |
| | Tim.Nijhuis@Radboudumc.nl |
| **Laboratory sites *<if applicable>*** | Not applicable |
| **Pharmacy *<if applicable>*** | Not applicable |

3

**PROTOCOL SIGNATURE SHEET**

| Name | Signature | Date |
|---|---|---|
| **Sponsor or legal representative:** <br><br> *<please include name and function>* <br><br><br> *<For non-commercial research,>* <br> **Head of Department:** <br> *<include name and function>* | Prof. Dr. D. Ulrich, plastic surgeon <br> Head of plastic surgery department <br> Radboudumc | 11/5/2023 |
| **[Coordinating Investigator/Project leader/Principal Investigator]:** <br> *<please include name and function>* | Dr E.P.A. vd Heijden, plastic surgeon <br> plastic surgery department <br> Radboudumc | 10/05/2023 |

4

**TABLE OF CONTENTS**

5

6

**LIST OF ABBREVIATIONS AND RELEVANT DEFINITIONS**

| | |
|---|---|
| 4DCT | Four dimensional computed tomography |
| ABR | General Assessment and Registration form (ABR form), the application form that is required for submission to the accredited Ethics Committee; in Dutch: Algemeen Beoordelings- en Registratieformulier (ABR-formulier) |
| AE | Adverse Event |
| AR | Adverse Reaction |
| CA | Competent Authority |
| CCMO | Central Committee on Research Involving Human Subjects; in Dutch: Centrale Commissie Mensgebonden Onderzoek |
| CMC-1 | Carpal metacarpal 1 |
| DRUJ | Distal radioulnar joint |
| DSMB | Data Safety Monitoring Board |
| EU | European Union |
| EudraCT | European drug regulatory affairs Clinical Trials |
| GCP | Good Clinical Practice |
| GDPR | General Data Protection Regulation; in Dutch: Algemene Verordening Gegevensbescherming (AVG) |
| IB | Investigator's Brochure |
| IC | Informed Consent |
| IMP | Investigational Medicinal Product |
| IMPD | Investigational Medicinal Product Dossier |
| MCP-1 | Metacarpal phalangeal 1 |
| METC | Medical research ethics committee (MREC); in Dutch: medisch-ethische toetsingscommissie (METC) |
| (S)AE | (Serious) Adverse Event |
| SPC | Summary of Product Characteristics; in Dutch: officiële productinformatie IB1-tekst |
| Sponsor | The sponsor is the party that commissions the organisation or performance of the research, for example a pharmaceutical company, academic hospital, scientific organisation or investigator. A party that provides funding for a study but does not commission it is not regarded as the sponsor, but referred to as a subsidising party. |
| SUSAR | Suspected Unexpected Serious Adverse Reaction |

93

**TFCC**    Triangular fibrocartilage complex

**UAVG**    Dutch Act on Implementation of the General Data Protection Regulation; in Dutch:

Uitvoeringswet AVG

**WMO**    Medical Research Involving Human Subjects Act; in Dutch: Wet Medisch-

wetenschappelijk Onderzoek met Mensen

94

**SUMMARY**

**Rationale:** The wrist is a complex array of joints. It involves articulation of eight small carpal bones, two forearm bones and five hand bones, with intricate inter- and intra-osseous kinematics. The wrist facilitates multidirectional movement in a synergistic manner that allow for the unique range of mobility of the hand and forearm. Intrinsic (interosseous) and extrinsic (capsular) ligaments are the primary passive stabilizers of the wrist. The muscles of the hand and forearm are secondary, dynamic stabilizers.

Of all the injuries, hand and wrist injuries have the highest social and economic impact; annual health costs and loss of labor productivity of approximately 540 million Euros [1]. Part of the wrist injuries concerns ligament lesions which, untreated, will progress to carpal instability and finally osteoarthritis [2] [3] [4]. Out of the annual 25.000 wrist injuries [5], approximately 7-10% will lead to instability [6],for which reconstruction and salvage operations are needed, costing each €3.700 including physiotherapy; a total of 9.25M€. After surgery, patients get 3-6 months revalidation and are unable to work, costing €405 per day [7]; a total of €55.350 per person or 138M€ in total. If patients are diagnosed earlier, less surgeries will be necessary, drastically decreasing the societal costs and patient discomfort.

Real-time fluoroscopy is currently the only imaging modality that can be used to detect dynamic abnormalities in these patients [8]. However, fluoroscopy suffers from several drawbacks: images are limited to 2-dimensions, bone superimposition is constantly present, and the sensitivity of the examination is highly operator dependant. This makes it impossible to reproducibly and objectively quantify any abnormalities, if present.

Because of its high sensitivity and specificity, wrist arthroscopy is still the gold standard for diagnosing intra-articular pathology and ligament tears of the wrist [9]. Arthroscopy however, is an invasive and relatively expensive procedure with a complication rate of 2%. Another drawback of arthroscopy is the fact that the function of the ligaments can still not be dynamically assessed for three reasons: 1) the wrist and soft tissue are distended during the procedure to open the wrist joints for introduction of the scope and instruments preventing movement and 2) the patient is unable to move the wrist because of the anaesthesia and 3) movements of the wrist is not possible because of the rigidity of the scope that has been inserted into the wrist.

A promising imaging method that could contribute to this field is 4DCT scanning. Using recently developed, continuous acquisition of 3D CT images during movement, it might be able to assess

patients with suspected instability with higher diagnostic performance by facilitating kinematic assessment of wrist motions. The wrist is composed of several small joints. The flexion-extension and ulnar-radial deviation motion mainly happens in the radiocarpal and midcarpal joint. In a previous study (both volunteer and clinical study), we have focused on imaging the scapholunate joint (SL-joint), which is part of the midcarpal joint and is stabilized by the scapho-lunate ligament (SLIL) (ABR number NL72518.091.19). The radiocarpal and midcarpal (including the SL joint) both move during flexion and extension and during radial and ulnar deviation movements of the wrist. To fully investigate the diagnostic performance of 4DCT for the whole wrist, we also want to study pronation-supination, abduction-adduction and opposition-reposition motion which takes place in the so-called distal radio-ulnar joint (DRUJ) and in the scapho-trapezium-trapezoid joint (STT) and  the carpometacarpal-1 (CMC-1) joint respectively. The DRUJ is stabilized by the Triangular Fibrocartilage Complex (TFCC ligament). The STT and CMC joint by at least 16 ligaments.  With a mechanism similar to the scapholunate joint these joints can also become unstable causing progressive pain and damage to the structures in the wrist. In these cases arthroscopy is also often used causing the range of difficulties mentioned above. Because of these promising first results with the scapholunate joint, we expect a diagnostic application of 4DCT also for the other types of wrist instability. Due to the rotating gantry movement different movements may cause different motion artifacts. Therefore, 4DCT imaging of other wrist joints during clinically relevant wrist motions are required. This will make it possible to set-up a method for fully automatic instability diagnosis in the wrist based on 4DCT.

The superior 3-dimensional spatial resolution of 4DCT compared to fluoroscopy allows this technique to accurately detect even slight positional changes of the bones, in contrast to 2D fluoroscopy [10]. While conventional static 3D imaging methods can provide valuable information about carpal bone anatomy and alignment, dynamic imaging has the advantage of assessing the carpus, distal radius and ulna, and joint spaces throughout the range of movements and capturing their complex interplay. This will provide a way to better understanding of normal wrist kinematics and improve diagnosis of subtle instabilities and decrease the need for arthroscopy. Moreover, if surgical intervention is deemed appropriate, the source of the instability might be more precisely identified. Detailed knowledge of the nature of instability will allow clinicians to offer more specific and appropriate surgery for each patient. Following from this, the effect of surgical interventions on wrist kinematics can be more thoroughly investigated, helping to guide and shape further clinical treatment.

An important drawback of 4DCT scan is the radiation exposure, like in fluoroscopy. However, in our previous study on the scapholunate ligament (ABR number NL72518.091.19) we have established a

useful and robust workflow for processing low-dose, noisy 4DCT data.  Using this workflow it is possible to get accurate 4D images of the moving wrist with a mean effective radiation dose of 0.02 mSv, which compares favourably with a normal background radiation for any individual (2 mSv per year). In accordance with this protocol, we want to investigate the feasibility of imaging of the other movements and wrist joints not yet studied.

The distal radioulnar joint (DRUJ) is an inherently unstable joint located between the radius and ulna and is stabilized by a ligament complex called the triangular fibrocartilage complex (TFCC), which is composed of different ligaments. The dorsal and palmar radioulnar ligament are the most important stabilizing ligaments of the TFCC [11]. TFCC injuries, causing DRUJ instability, may occur after trauma as an isolated lesion or in conjunction with a distal radial fractures, which occurs in up to 43% of cases. TFCC lesions might also occur nontraumatically but caused by chronic compression of the ulnar head against the lunate which is called ulnar impaction syndrome [12] [13]. This abnormal loading leads to degenerative injury of the TFCC. If left untreated, TFCC injuries can lead to progressive pain worsening, functional compromise and ultimately secondary osteoarthritis [14]. Surgical treatment of the TFCC injury is indicated with instability of the DRUJ [15].

Due to the progressive nature of the injury patients with an early diagnosis of a TFCC injury may benefit from less-invasive treatment options, have a better prognosis, and experience less residual disability [15]. However, current imaging of the TFCC remains difficult, dynamic instabilities demonstrate abnormalities only during motion. Computed tomographic arthrography and magnetic resonance arthrography are currently the two most viable imaging techniques, but the sensitivity and specificity of these static imaging techniques are relatively low compared to arthroscopy, with a sensitivity of respectively 0.89 and 0.78 and a specificity of respectively 0.89 and 0.85 [16]. Normal MRI is also used but has a sensitivity of 0.76 and a specificity of 0.82.

Due to the novelty, only a few studies have been published on wrist kinematics using 4DCT scans. These studies have demonstrated its potential for the evaluation of DRUJ instability, particularly in cases of inconclusive initial clinical assessment [17] [18]. Hardly any study has been performed to analyse the movement of the DRUJ [14] [19] [20]. No diagnostic studies of patients with suspect TFCC injury have been performed in which the findings of the 4DCT have been compared to that of gold standard, i.e. arthroscopy.

**Objective**: The study will consist of 4 parts performed sequentially. First we want to perform a volunteer study with healthy participants to investigate the viability of 4DCT scanning of the wrist for evaluating wrist bones configurations and movements (translations and rotations) during a new set of wrist motions that

have not been evaluated in our previous study (NL72518.091.19). We want to investigate the pronation and supination motion of the DRUJ and we want to investigate the abduction-adduction and opposition-reposition of the CMC and STT joint. By performing an extra volunteer study we will obtain reference values for all motions of the different joints of the wrist. The second part will be a left right study on this same group of volunteers. The final goal of this study is to design a workflow capable of diagnosing patients suspect of TFCC injury based on bone kinematics and the left right difference of these bone kinematics. To obtain normal marges for left right differences and be able to differentiate pathological left-right differences from normal left right differences, the left right difference will be studied in this healthy volunteer group when the imaging and segmentation quality is deemed appropriate. We will analyse the data connected to the DRUJ directly, the data connected to the CMC and STT will be saved till for later use when a new researcher is attracted.

If a good left right difference is obtained we will perform an explorativeclinical study on patients with chronic wrist pain, suspect for DRUJ instability. The objective of the clinical study is to determine the ability  of the 4DCT scan (during a series of movements in which DRUJ instability is predicted to be best visible) in the diagnosis of DRUJ instability in comparison with arthroscopic findings (gold standard). If the 4DCT shows to have an ability to diagnose TFCC lesions comparable to that of wrist arthroscopy, it is the aim to further this technique with the ultimate goal to introduce 4DCT as first choice imaging modality for diagnosing wrists suspected for DRUJ instability. Lastly in a reliability study, we want to investigate the intra-patient test-retest reliability to show the robustness of our acquisition protocol.

**Study design:** explorative pilot volunteer study and explorative clinical study

**Study population:** The healthy participants, in the age group of 20-50 year, have no history of trauma of wrists and have no complaints of the wrists. With the knowledge and experience of our previous study focused on the scapholunate ligament (NL72518.091.19), we estimate that 30 healthy participants (bilateral scans so 60 wrists) will be needed for the volunteer study to determine the visibility of the wrist joints (DRUJ, CMC-1 and MCP-1); acquire normal values and investigate the left right differences between the wrists. Based on a previous study by Brinkhorst et al. [21], who investigated reliability of the 4DCT protocol for wrist joints during a different set of motions.

For the clinical study the kinematics of 30 patients with chronic unilateral wrist pain, in this study suspect for DRUJ instability, will be studied to evaluate the effect of TFCC injury on the wrist kinematics and evaluate the use of 4DCT for the diagnosis of TFCC injury. Both wrists (30 DRUJ instability wrists and 30 asymptomatic wrists) are studied. The asymptomatic wrist of the DRUJ instability patient will serve as a healthy control data. Within two-three weeks, a wrist arthroscopy will be performed of the injured wrist to evaluate the TFCC.We estimate that 20 of the patients (20

wrists) that underwent a 4DCT scan for the clinical study will be needed to undergo a second unilateral scan to investigate the intra-patient test-retest reliability of the protocol.

99

In summary, we expect to include 30 participants for the volunteer (reference) study, .and 30 patients with suspected DRUJ instability for the clinical study of which 20 will be scanned a second time for the reliability study,

**Intervention (if applicable)**: In the volunteer study healthy participants will undergo a bilateral 3D CT scan in neutral wrist position and a bilateral dynamic 4DCT scan while moving the wrist according to the reference protocol as described below.

For patients suspect of DRUJ instability a plain bilateral wrist radiograph, a static bilateral CT scan, a bilateral 4DCT scan and a unilateral arthroscopy the symptomatic wrist will be performed. Both the plain radiographs and the arthroscopy concerns normal diagnostic work-up of patients suspect for DRUJ instability. In the reliability study 20 of the patients included in the clinical study will undergo a second unilateral dynamic 4DCT scan while moving according to the DRUJ protocol.

*Scanning protocol:* During 4DCT scanning, the participants will be positioned standing or sitting to the side of the scanner table, with the arms fixed in a neutral position and the radiocarpal joints centred in the scan volume. The healthy participants will actively move their wrists continuously and homogeneously in a pronation-supination cycle; an abduction-adduction cycle and an opposition-reposition cycle according to the reference protocol as described below. The patients suspected of DRUJ instability will actively move the wrist continuously and homogeneously in a pronation-supination cycle; a radio-ulnar deviation cycle and a clenched fist cycle according to the DRUJ protocol described below. Both the radio-ulnar deviation cycle and the clenched fist cycle have already been studied in healthy participants, these are clinically relevant wrist movements in the assessment of DRUJ instability.

The reference protocol is as follows: For the pronation movement, patients have to move their wrist from a neutral position to maximal pronation in 10 seconds. For the abduction-adduction cycle, the thumb must be moved from maximal abduction, to maximal adduction and to maximal abduction in 4 seconds.

For the opposition-reposition cycle, the thumb must be moved from maximal opposition, to maximal reposition and to maximal opposition in 7 seconds. One cycle of pronation-supination; one cycle of abduction-adduction and one cycle of opposition-reposition each last 21 seconds per hand. Total exposure to radiation will be 21 seconds and examination time in the CT room, including patient positioning and instruction, will be roughly 15 minutes. The healthy participants in the reliability

100

study group will undergo a second unilateral scanning of all three movements 15 minutes after finishing the first scan.

The DRUJ protocol is as follows: For the pronation movement, patients have to move the wrist from neutral to maximal pronation, in 10 seconds. For the radio-ulnar deviation cycle, patients have to move the wrists from neutral to maximal radial deviation, back to neutral and then to maximal ulnar deviation and return to the starting point (neutral position) in 7 seconds. For the clenched fist cycle the patient actively squeezes their wrists and keeps exerting force for a few seconds after  which they relax again in 4 seconds. One cycle of pronation-supination; one cycle of radio-ulnar deviation and one cycle of squeezing each last 18 seconds per hand. Total exposure to radiation will be 18 seconds and examination time in the CT room, including patient positioning and instruction, will be roughly 15 minutes.

**Main study parameters/endpoints:** The first endpoint is to define if it is possible to make low-dose, high-quality 4DCT  images of the radius, ulna and carpal bones and their movements (translations and rotations related to each other) while moving the wrist and thumb according to the previously described imaging protocols, obtain normal values of the kinematic parameters and investigate the left right wrist difference. The second endpoint is to evaluate the test-retest reliability of 4DCT dynamic scanning of the radius, ulna and carpal bones). The third endpoint is the determination of the ability of the 4DCT to analyse DRUJ instability in comparison with arthroscopy (gold standard).

**Nature and extent of the burden and risks associated with participation, benefit and group relatedness:**

All 30 healthy participants will get a bilateral static 3DCT scan and a bilateral 4DCT scan.
The 4DCT is associated with a dose of 0.02 mSv whereas the bilateral static 3DCT scan is associated with 0.005 mSv. The group who undergoes the 2 4DCT scans will receive a total effective dose of 0.05 mSv which compares favourably with the with a normal background radiation for any individual (2 mSv per year).
In the clinical study, DRUJ instability patients will get a plain bilateral wrist radiograph, a static bilateral CT scan, a bilateral 4DCT scan and a unilateral arthroscopy of the symptomatic wrist. Both the plain radiographs and the arthroscopy concerns normal diagnostic work-up of patients suspect

for DRUJ, so this concerns no extra burden or risk. Prior to the arthroscopy, patients will
complementary undergo a static 3D and a dynamic 4DCT of both wrists which is at a much lower
dose, estimated below 0.015 mSv. This burden is a manageable risk compared to the natural
background radiation in the Netherlands (2mSv).

Within this group, 20 participants will get another unilateral 4DCT scan at least 15 minutes after the first
scanning session.

102

### 1.  INTRODUCTION AND RATIONALE

The wrist is a complex joint. It involves articulation of eight small carpal bones, five finger bones and two forearm bones with intricate inter- and intra-osseous kinematics. They demonstrate multidirectional movements and synergy that allow for the uniquely range of motion of the hand. Intrinsic and extrinsic ligaments in and about the wrist are the primary, static stabilizers of the wrist. The muscles of the forearm are the secondary, dynamic stabilizers. Instabilities based on ligament tears or insufficiencies are a relatively common pathology which leads to pain and eventually to osteoarthritis of the wrist when untreated [14]. Due to the importance of the wrist and hand in daily life and in most modern workplaces, this imposes a substantial morbidity on patients and a considerable societal cost. Patients with an early diagnosis of ligament tears may benefit from less-invasive treatment options, have a better prognosis, and experience less residual disability [15]. Dynamic or pre-dynamic instabilities of the wrist only demonstrate abnormalities during motion. This would explain the frequent lack of observable pathologies in static radiographic in patients with clinically significant wrist pain. Currently, real-time fluoroscopy is the only imaging modality that can be used to detect dynamic abnormalities in these patients [8]. However, fluoroscopy suffers from several drawbacks: images limited to 2-dimensions, bone superimposition and the inability to objectively quantify any abnormalities if present. Its correct execution and interpretation is also extremely operator dependent, and requires an experienced clinical MSK radiologist working closely together with an experienced hand-surgeon.

In cases of inconclusive radiographic evaluation, MRI or CT arthrography can be used to assess ligament structural integrity but not true ligament function, which can be particularly problematic in patients with partial ligament tears or pathological ligamentous laxity without a tear [9]. Wrist arthroscopy still is the gold standard for diagnosing ligament tears of the wrist. The advantage of arthroscopy is real live image of the ligament tears and in the presence of subtle ligament tears, there is the possibility to intervene simultaneously. The disadvantage is that arthroscopy is an invasive and expensive technique with operational risks like infection, bleeding and unintended damage of articular structures. Another drawback of arthroscopy is the fact that the function of the ligaments cannot be assessed during the procedure for three reasons: 1) the wrist and soft tissue are distended to open the wrist joints for introduction of the scope and instruments and 2) the patient is unable to move the wrist because of the anaesthesia and 3) the rigidity of the scope does not permit wrist movements.

Technology advances and the new scanning technique of 3D CT over time (four-dimensional; 4DCT) has made it possible to assess the kinematic while the wrist moves, depicting slight positional bone changes with high temporal and spatial resolution. This technique has shown potential for the evaluation of carpal instability, particularly in cases of inconclusive initial assessment. Previous studies by Tay et al. [22] and Neo et al. [23] have shown the feasibility of using CT imaging to achieve dynamic real-time or 4-dimensional computed tomographic (4DCT) imaging of the moving wrist joint. Ranota et al. [24] have measured  distal radial-ulnar and radio-carpal joint congruency following distal radius fractures using 4DCT.

103

Radiation exposure is a drawback in 4DCT, like in fluoroscopy. Our prior research has demonstrated the feasibility for use in imaging concerning the scapholunate joint and determined the optimal dose for wrist scanning. In collaboration with the orthopaedic research lab of the Radboud University Medical Center we have established a useful and robust workflow for processing even low-dose, noisy imaging data. Making it possible to keep the total effective dose to a maximum of 0.045 mSv for the group receiving most radiation.

The 4DCT images will provide a way to better understanding of normal wrist kinematics, improve diagnosis and treatment of wrist instabilities, and decrease the need for arthroscopy. To demonstrate this, we want to perform a volunteer (reference) study in which we demonstrate the use of 4DCT for a new range of clinically relevant wrist motions and obtain insight in normal movement of the wrist. Furthermore, we want to perform an explorativeclinical study in which we want to determine the ability of the 4DCT to analyse lesions of the TFCC and the degree of DRUJ instability in comparison with arthroscopy (gold standard).

The distal radioulnar joint (DRUJ) is an inherently unstable joint located between the radius and ulna stabilized by the triangular fibrocartilage complex (TFCC) [11]. TFCC injuries, causing DRUJ instability, may occur after distal radial fractures in up to 43% of cases, or due to chronic degenerative injury caused by ulnar impaction syndrome [12] [13]. If left untreated TFCC injuries can lead to progressive pain worsening, functional compromise and ultimately secondary osteoarthritis [14]. Current imaging of the TFCC remains difficult. Computed tomographic arthrography and magnetic resonance arthrography are currently the two most viable imaging techniques with a sensitivity of respectively 0.89 and 0.78 and a specificity of respectively 0.89 and 0.85 [16] but need invasive injection of contrast fluid. MRI without contrast is also used but has an even lower sensitivity of 0.76 and a specificity of 0.82. The current golden standard is arthroscopy, which is however an invasive technique and therefore not employed in the acute setting.

With the explorative 18linical study, we want to evaluate the movements of the wrist bones of patient with TFCC injury and compare these with those of asymptomatic wrists. By quantifying the deviations in the injured wrists, the 4DCT scan can become an important diagnostic tool in future for early diagnosis of TFCC injury and thus decrease the need for arthroscopy and increase the viability for early diagnosis resulting in less-invasive treatment options, a better prognosis, and less residual disability [15].

## 2. OBJECTIVES

The goal of the volunteer study is to investigate the use of 4DCT scanning of the wrist for the evaluation of wrist bone movements (translation and rotation) during a new series of clinical relevant movements and evaluate wrist kinematic of healthy participants; obtain normal values of the kinematic parameters and evaluate the difference in wrist kinematics between the dominant and non-dominant hand. The reliability study will be performed to evaluate the test-retest reliability of the proposed protocol. The explorative clinical study will be performed to analyse the wrist bone movements of wrists suspect DRUJ instability and compare them with the uninjured wrist.

**Primary Objective:**

*Volunteer study:* 1: Investigate the visibility of wrist joint movements that have not been explored in our previous study (NL72518.091.19). Clinically relevant wrist motions for DRUJ instability (radius and ulna), carpometacarpal joint 1 (CMC-1) instability (distal trapezium and metacarpal 1) and metacarpophalangeal joint 1 (MCP-1) instability (metacarpal 1 and proximal phalanx 1) will be analysed. 2: determine normal values of the kinematic parameters for clinical relevant movement of the wrist joints. 3: Investigate the similarity between the dominant and non-dominant wrist. Creating insights in what left right difference can be present without pathologies being present.

The following radiographic signs will be evaluated: radioulnar angle; sigmoid notch to ulnar head joint distance; radioulnar ratio; radioulnar line distance; subluxation ratio; epicentre distance; radioulnar joint volume; ulnar variance and ulnar head to carpal bones joint distance [25] [26] [27] [28] [29] all these parameters are further described in *3. STUDY DESIGN.*

*Reliability study:* Investigate the test-retest reliability of the protocol used in the volunteer study. To investigate the robustness of the workflow

*Clinical study:* determine the diagnostic performance of the 4DCT scan in the diagnosis of DRUJ instability in comparison with arthroscopic findings (gold standard). For this purpose, values of 4DCT parameters of DRUJ wrists (arthroscopy proven TFCC injury), will be compared with non-DRUJ instability wrists (arthroscopy proven no TFCC injury, although clinically suspected).

**Secondary Objective(s):**

*Clinical study*: assess the association between 4DCT parameters and arthroscopic grades of TFCC injury (the Palmer classification).

105

### 3. STUDY DESIGN

Single institution, a explorative volunteer study with participants followed by an explorativeclinical study in the Radboud University Medical Center.
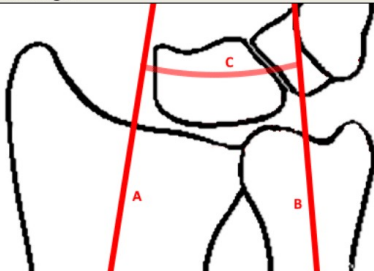
We will include 30 healthy participants with no medical history of wrist trauma, surgery or wrist complaints and in age range of 20-50 and; and 30 patients with chronic unilateral wrist pain suspect for DRUJ instability.

For the volunteer study all 30 healthy participants first undergo a bilateral 3D CT scan in neutral wrist position for usage of reference. The field of view of this scan includes all carpal bones and the two forearm bones. The scan technique is a Toshiba  delivered application and CE certified. Subsequently, the forearms are placed in a supporting frame which minimizes lower-arm motion during 4DCT image acquisition. Prior to image acquisition, participants will undergo a training session on how to move their wrist according to the imaging protocol. A bilateral dynamic 4DCT scan is made while actively moving the wrists according to a protocoled cycle of movements. To reduce radiation exposure, the z-axis coverage is reduced to 12 cm in the 4DCT scan. Videos of the wrist movements are shown to the participant during image acquisition, which will help the participants to perform the movements at a constant pace. This will provide images with highest quality and will provide the source data considering carpal bone movements and function of ligaments during active wrist motions.
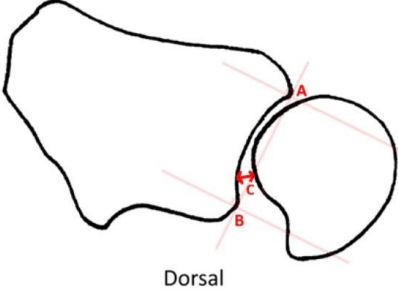
For this DRUJ instability study, a static 3D CT scan and a dynamic 4DCT scan of the both wrists of the patient suspect for DRUJ instability will be done after the X ray which is performed during standard clinical practice. The protocol is the same as described above in the volunteer study but the patients follow the DRUJ movement protocol with movements that are clinically relevant for DRUJ instability diagnosis. For the reliability study 20 of the patients included in the volunteer study will additively undergo an extra unilateral 4DCT scan at least 15 minutes after the bilateral 4DCT scan. Which wrist is scanned is decided by random selection. Except for the scanning being performed unilateral instead of bilateral the protocol is exactly the same as the 4DCT protocol as described above.

The following radiographic signs will be evaluated: radioulnar angle; sigmoid notch to ulnar head joint distance; radioulnar ratio; radioulnar line distance; subluxation ratio; epicentre distance; radioulnar joint volume; ulnar variance and ulnar head to carpal bones joint distance [25] [26] [27] [30] [31]. All radiographic signs will be described below:

**Radioulnar angle:**

| |
|---|
| **Name:** Radiounlnar angle |
|   *Figure 1: radioulnar angle* |
| **Description:**<br>The angle between the axis of the radius and the angle of the ulna |
| **Extracted data:**<br>Axis of the radius (A)<br>Axis of the ulna (B) |
| **Calculations:**<br>Angle between axis of the radius and axis of the ulna © |

107
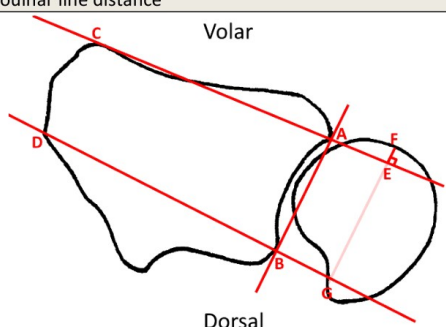
**Sigmoid notch to ulnar head distance:**

| **Name:** Sigmoid notch to ulnar head distance |
|---|
|  Figure 2: Sigmoid notch to ulnar head distance |
| **Description:**<br>To calculate the sigmoid notch to ulnar head distance, first the sigmoid notch is defined as the concave area between the volar to dorsals margins of the sigmoid notch. For all vertices within this area the minimam distance to the ulnar head is calculated |
| **Extracted data:**<br>Volar margin of the sigmoid notch (A)<br>Dorsal margin of the sigmoid notch (B)<br>Area sigmoid notch |
| **Calculations:**<br>Minimum distance sigmoid notch to ulnar head (C) |

108

**Radioulnar ratio:**

| **Name:** Radioulnar ratio [23] |
|---|
| Volar<br><br><br><br>Dorsal |
| Figure 3: Radioulnar ratio |
| **Description:** Ulnar subluxation is quantified as the ratio between the distance between the dorsal and volar margin of the sigmoid notch and the line perpendicular to this line that crosses the centre of the ulnar head |
| **Extracted data:**<br>Volar margin of the sigmoid notch (A)<br>Dorsal margin of the sigmoid notch (B)<br>The intersection (Q) between this line and the perpendicular line that crosses the centre of the ulnar head (M) |
| **Calculations:**<br>Radioulnar ratio score = AQ / AB |

109

**Radioulnar line distance:**

| **Name:** Radioulnar line distance |
|---|
|  *Figure 4: Radioulnar line method* |
| **Description:** Ulnar subluxation is quantified as the amount of ulnar head that is located outside of the volar radioulnar line and the dorsal radioulnar line |
| **Extracted data:**<br>Volar radioulnar line:<br>   • Volar ulnar border of the radius (A)<br>   • Volar radial border of radius (C)<br>Dorsal radioulnar line:<br>   • Dorsal ulnar border of the radius (B)<br>   • Dorsal radial border of radius (D)<br>Distance that the ulnar wall is outside of the ulnar lines (E-F) |
| **Calculations:**<br>Radioulnar line score = EF / AB<br>Alternative scoring: Radioulnar line score = EF / EG |
| **Comments:**<br>   • In literature Radioulnar line method and modified radioulnar line method are used interchangeably |

110

**Subluxation ratio:**

| **Name:** Subluxation ratio |
|---|



*Figure 5: Subluxation ratio*

| |
|---|
| **Description:** Ulnar subluxation is quantified as the amount of ulnar head that is located outside of two lines perpendicular (angle of 90 degrees) to the line connecting the volar and dorsal margins of the sigmoid notch.. |
| **Extracted data:** |
| Volar margin of the sigmoid notch (A) |
| Dorsal margin of the sigmoid notch (B) |
| Distance that the ulnar wall is outside of the perpendicular line (R-L) |
| **Calculations:** |
| Subluxation ratio score = RL / AB |

111
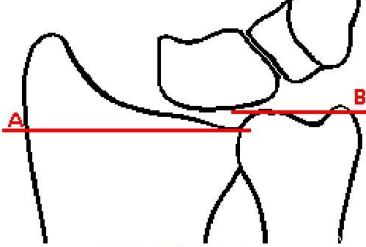
**Epicentre distance:**

| **Name:** Epicentre method |
|---|
| Volar<br><br>Dorsal |
| Figure 6: Epicentre method |
| **Description:** Ulnar subluxation is quantified as the distance between the middle of the sigmoid notch and the intersection point of the perpendicular line to the line connecting the volar and dorsal margins of the sigmoid notch which intersects the centre of rotation of the DRUJ. |
| **Extracted data:**<br>Intersection point (O) of:<br><ul><li>The line perpendicular to the line connecting:<ul><li>Volar margin of the sigmoid notch (A)</li><li>Dorsal margin of the sigmoid notch (B)</li></ul></li><li>And crossing the centre of rotation of the DRUJ defined as the midpoint between<ul><li>Centre of the ulnar styloid (N)</li><li>Centre of the ulnar head (M)</li></ul></li></ul>Middle of the sigmoid notch (P) which is the midpoint between:<br><ul><li>Volar margin of the sigmoid notch (A)</li></ul>Dorsal margin of the sigmoid notch (B) |
| **Calculations:**<br>Epicentre method score = OP / AB |

112

**Radioulnar joint volume:**

| **Name:** Radioulnar joint volume |
| --- |

Volar



*Figure 7: Joint volume analysis*

Dorsal

| |
| --- |
| **Description:** Joint volume analysis quantifies ulnar subluxation as the volume of ulna taking part in the DRUJ. The volume of the DRUJ is defined as a specific distance from the radius inside of two lines perpendicular to the line connecting the volar and dorsal margins of the sigmoid notch (see subluxation ratio). |
| **Extracted data:** Volar margin of the sigmoid notch (A) Dorsal margin of the sigmoid notch (B) Edge sigmoid notch |
| **Calculations:** Ulnar volume inside region of interest (light red) |
| **Comments:** Using absolute volume might give big normal ranges due to the differing size of the ulnar head. Having relative values to the total volume of the ulnar head may improve results |

113

**Ulnar variance:**

| **Name:** Ulnar variance |
| --- |
| <br>*Figure 8: Ulnar variance* |
| **Description:** Ulnar variance measures the amount the ulna protrudes the radius. It is defined as the distance proximal to distal between the articular surface of the radius and the distal articular surface of the ulna. If the distal articular surface of the ulna is located more than 2.5mm distal of the articular surface of the radius this is diagnosed as positive ulnar variance |
| **Extracted data:**<br>Articular surface of the radius as defined by the top of the sigmoid notch (A)<br>Distal articular surface of the ulna (B) |
| **Calculations:**<br>Ulnar variance = A-B (over the axis of the radius) |

114

**Ulnar head to carpal bones joint distance:**

| |
|---|
| **Name:** joint distance analysis |
| *Figure 9: Joint distance analysis* |
| **Description:** Ulnar impaction is the ulnar head impacting upon the ulnar-sided carpal bones [29]. Having full 3D CT data of the complete motion of the wrist allows to directly measure the distance between the ulnar head and the carpal bones. This distance may be used to estimate if the ulnar head impacts on the carpal bones. |
| **Extracted data:** <br> Distal surface of the ulnar head <br> Proximal surfaces of the lunate and triquetrum |
| **Calculations:** <br> Minimum distance between the surface of the ulnar head and the surfaces of the lunate and triquetrum |

115

Setting: Collaboration between Radiology department, Plastic Surgery department and Orthopedic research lab of the Radboud University Medical Center.

Expected duration: volunteer study 6 months, explorative clinical study two years.

## 4. STUDY POPULATION

### 4.1 Population (base)

For the volunteer study, healthy volunteers between 18-50 years of age are included. For the clinical study, patients with unilateral chronic wrist pain suspected for DRUJ instability are included. Clinically suspect of DRUJ instability is based on the presence of a combination of the following: pain at the ulnar side of the wrist, context of wrist trauma or chronic overload; a positive piano key test and/or a positive DRUJ stress test and/or positive ballottement test.

Participants with major joint stiffness or medical history of wrist surgery or fracture (radius, ulna or one of carpal bones) will not be included.

### 4.2 Inclusion criteria

In order to be eligible to participate in this study, the participant must meet all of the following criteria:

- Between 18-50 years (healthy volunteer only)
- A 3D CT scan is required.
- Informed consent from both the healthy volunteer and patient.
- An arthroscopy is required: this is decided on by clinical signs such as pain in the lower wrist during ulnar deviation or pronation and supination, clicking and visible subluxation in the DRUJ area; physical examination such as a positive TFCC compression test or a non-stable TFCC and imaging such as damage or signs of previous damage to the adherence points of the TFCC or arthrosis on places subject for TFCC injury.
A patient

### 4.3 Exclusion criteria

A participant who meets any of the following criteria will be excluded from participation in the volunteer study:
- &lt; 18 year and &gt; 50 years
- medical history of wrist: trauma, pain and/or surgery
- persons with limited wrist movements
- wrists with arthritis on plain radiograph or 3D CT scan
- pregnancy

A patient with suspicion of DRUJ instability who meets any of the following criteria will be excluded from participation in the clinical study:
- medical history of wrist fracture, known ligament lesion other than the TFCC and/or wrist surgery
- inability to undergo diagnostic arthroscopy
- wrists with arthritis on plain radiograph or 3D CT scan
- pregnancy

### 4.4 Sample size calculation

Based on our previous explorative study on movement parameters in the SL joint (NL72518.091.19) we expect 30 volunteers and 30 patients to give a good insight into the ability of 4DCT to detect

117

pathologies in wrist movement.  Based on a previous study by Brinkhorst et al. [21], who investigated reliability of the 4DCT protocol for wrist joints during adifferent set of motions, we estimate that 20 of the healthy participants (20 wrists) that underwent a 4DCT scan for the volunteer study will be needed to undergo a second unilateral scan to investigate the intra-patient test-retest reliability of the protocol.

118

## 5.  TREATMENT OF SUBJECTS

Not applicable

119

## 6.  INVESTIGATIONAL PRODUCT

Not applicable

## 7. NON-INVESTIGATIONAL PRODUCT

Not applicable

121

## 8.   METHODS

### 8.1   Study parameters/endpoints

#### 8.1.1  Main study parameter/endpoint

Main endpoint of the *volunteer study:* investigate the visibility of the partaking bones of the DRUJ; the CMC-1 joint and the  STT joint and their movement. Investigate the left right similarity and determine normal values. 4DCT parameters to be measured will be: radioulnar angle; sigmoid notch to ulnar head joint distance; radioulnar ratio; radioulnar line distance; subluxation ratio; epicentre distance; radioulnar joint volume; ulnar variance and ulnar head to carpal bones joint distance [25] [26] [27] [28] [29].

Main endpoint of the *reliability study*: investigate the reliability of the workflow used for the volunteer study

Main endpoint for the *clinical study*: determine the diagnostic performance (of the 4DCT scan in the diagnosis of TFCC lesion and DRUJ instability in comparison with arthroscopic findings (gold standard). For this purpose, values of 4DCT parameters of DRUJ instability (with respectively arthroscopy proven  TFCC lesion), will be compared with respectively non-DRUJ instability (arthroscopy proven no TFCC although clinically suspect).

#### 8.1.2  Secondary study parameters/endpoints (if applicable)

*Clinical study*: assess the association between 4DCT parameters and arthroscopic grades of TFCC lesion (Palmer classification)

*Table 1: Palmer classification of TFCC injuries [32]*

| Type 1 | Traumatic (occurs secondary to trauma, i.e. fractures of the distal radius) |
|---|---|
| 1A | Central perforation |
| 1B | Ulnar avulsion |
| 1C | Distal avulsion |
| 1D | Radial TFCC disruption |

| Type 2 | Degenerative (Due to ulnar impaction) |
|---|---|
| 2A | TFCC wear |
| 2B | TFCC wear + Lunate and/or ulnar chondromalacia |
| 2C | TFCC perforation + Lunate and/or ulnar chondromalacia |
| 2D | TFCC perforation + Lunate and/or ulnar chondromalacia + Lunotriquetral Ligament perforation |
| 2E | TFCC perforation + Lunate and/or ulnar chondromalacia + Lunotriquetral Ligament perforation + Ulnocarpal arthritis |

### 8.1.3  Other study parameters (if applicable)

Population information: Patient age, sex, study/profession/hobby, hand dominance, trauma.

### 8.2    Randomisation, blinding and treatment allocation

*Volunteer study*: randomisation will be used to decide which wrist will be scanned first
*Reliability study*: randomisation will be used to decide which wrist will be scanned unilaterally
Clinical study:  The surgeon who is performing the arthroscopy is blind for the 4DCT scan observations. The 4DCT data are only documented in the EPD after performance  and documentation of the arthroscopy. The hand surgeon who is performing the arthroscopy is not the same as the one who is investigating the 4DCT.

### 8.3    Study procedures

The scanning protocol includes one 3D standard CT scan and one dynamic 4DCT scans. The movement series of the 4DCT scans for the volunteers consists of three active cycles (pronation-supination of the wrist, abduction-adduction and opposition-reposition of the thumb). The movements series of the 4DCT scans of the patients suspect for TFCC lesion and DRUJ instability consists of pronation-supination, radioulnar deviation and a clenched fist movement.

The participant will be positioned standing or sitting to the side of the scanner table, with the arm placed upon the CT table in a neutral position. First, a static CT including both wrists and forearms will be acquired. Then, the participant will place the wrists in a supporting frame which minimizes lower-arm motion. After a brief instruction the participant will actively move both

123

wrists according to the movements described above while a continuous, low-dose CT is acquired. Both participant and investigator will wear lead aprons and thyroid protectors will be deployed to further reduce radiation exposure.

Settings are 80 kV tube voltage, 0.275 second gantry rotation time, 40 mA current, and continuous scanning mode, using 10 cm detector length. The total scan time for all movements is included in the protocol above.

Obtained images will be reconstructed at a 10 Hertz sampling rate with 0.5 mm resolution in the z-axis using both bone and soft tissue kernels.

Parameters to be measured on the static CT and on each frame of the 4DCT scan are: radioulnar angle; sigmoid notch to ulnar head joint distance; radioulnar ratio; radioulnar line distance; subluxation ratio; epicentre distance; radioulnar joint volume; ulnar variance and ulnar head to carpal bones joint distance [25] [26] [27] [28] [29].

### 8.4   Withdrawal of individual subjects

Subjects can leave the study at any time for any reason if they wish to do so without any consequences. The investigator can decide to withdraw a subject from the study for urgent medical reasons.

#### 8.4.1  Specific criteria for withdrawal (if applicable)

Participants with a scan with unexpected wrist pathology will be withdrawn

### 8.5   Replacement of individual subjects after withdrawal

As long as participants have not received (extra-regulatory) CT or 4DCT scans participants will be replaced by another healthy participant and withdrawn patients will be replaced with another patient with suspicion of DRUJ instability. Patients and or participants who have already underwent an (extra-regulatory) CT or 4DCT scan will not be replaced.

### 8.6   Follow-up of subjects withdrawn from treatment

Not applicable

### 8.7 Premature termination of the study

Not applicable. Dynamic CT scan is used in different ways all over the world. The technique itself is not new. So, we expect no reason to stop the study premature.

## 9. SAFETY REPORTING

### 9.1 Temporary halt for reasons of subject safety

In accordance to section 10, subsection 4, of the WMO, the sponsor will suspend the study if there is sufficient ground that continuation of the study will jeopardise subject health or safety. The sponsor will notify the accredited METC without undue delay of a temporary halt including the reason for such an action. The study will be suspended pending a further positive decision by the accredited METC. The investigator will take care that all subjects are kept informed.

### 9.2 AEs, SAEs and SUSARs

#### 9.2.1 Adverse events (AEs)

Adverse events are defined as any undesirable experience occurring to a subject during the study, whether or not considered related to [the investigational product / trial procedure/ the experimental intervention]. All adverse events reported spontaneously by the subject or observed by the investigator or his staff will be recorded.

#### 9.2.2 Serious adverse events (SAEs)

A serious adverse event is any untoward medical occurrence or effect that

- results in death;
- is life threatening (at the time of the event);
- requires hospitalisation or prolongation of existing inpatients' hospitalisation;
- results in persistent or significant disability or incapacity;
- is a congenital anomaly or birth defect; or
- any other important medical event that did not result in any of the outcomes listed above due to medical or surgical intervention but could have been based upon appropriate judgement by the investigator.

An elective hospital admission will not be considered as a serious adverse event.

The investigator will report all SAEs to the sponsor without undue delay after obtaining knowledge of the events.

The sponsor will report the SAEs through the web portal *ToetsingOnline* to the accredited METC that approved the protocol, within 7 days of first knowledge for SAEs that result in death or are life threatening followed by a period of maximum of 8 days to complete the initial preliminary report. All other SAEs will be reported within a period of maximum 15 days after the sponsor has first knowledge of the serious adverse events.

125

### 9.2.3  Suspected unexpected serious adverse reactions (SUSARs)

Not applicable

### 9.3    Annual safety report
Not applicable

### 9.4    Follow-up of adverse events

All AEs will be followed until they have abated, or until a stable situation has been reached. Depending on the event, follow up may require additional tests or medical procedures as indicated, and/or referral to the general physician or a medical specialist.

SAEs need to be reported till end of study within the Netherlands, as defined in the protocol

### 9.5    [Data Safety Monitoring Board (DSMB) / Safety Committee]

The dynamic 4D CT scan of the wrist has an estimated radiation dose of up to 0.02 mSv in total. The largest effective dose received by a single particioner is estimated to be 0.05 mSv. This will burden a justifiable risk compared to the natural background radiation in the Netherlands (2mSv). Therefore, this is a low risk study according to the NFU risk classification. No DSMB need to be implemented.

**10. STATISTICAL ANALYSIS**

In general, quantitative variables will be described by using mean standard deviation, and categorical variables by using frequency and/or percentage.

### 10.1 Primary study parameter(s)

Primary study parameter Volunteer study:

60 wrists of 30 healthy participants will be scanned and quantitative (e.g. in millimetres or degrees) automatic measurements of the 4DCT parameters mentioned in paragraphs 8.1.1 will be performed. Intraclass correlation coefficient (ICC) of the quantitative measurements will be calculated to assess the intra- and interobserver variability and left right similarity. The kinematic values of normal wrists will be used as reference for analyzing the unstable wrists.

Primary study parameter Reliability study:

40 wrists of 20 participants will be used (of which 20 wrists have been scanned during the Volunteer study and 20 are rescanned during the reliability study) and quantitative (e.g. in millimeters or degrees) measurements of the 4DCT parameters mentioned in paragraphs 8.1.1 will be performed automatically. Test-retest reliability will be calculated with the coefficient of multiple correlation evaluating the similarity between the two motion patterns. The total waveform reliability present between test and retest will be evaluated using the root mean square deviation.

Primary study parameter explorative Clinical study:

4DCT parameter measurements will be compared to arthroscopically proven TFCC injuries (based on Palmar classification using unpaired student T-tests or Wilcoxon's tests, depending on the distribution. We will construct an univariate logistical regression model with as outcome a TFCC injury at arthroscopy or not, and as independent variables each one of the continuous 4DCT parameters separately, corrected for the same 4DCT parameter values of the asymptomatic contralateral wrist (and demographic parameters if proven to have a significant effect). From this, we can abstract ROC curves for different 4DCT parameters to estimate the distinctiveness to differentiate pathological and non-pathological cases of these parameters. All point estimates will be reported along with relevant variability estimates. The goodness of fit of models was verified by the deviance and Pearson $\chi2$ and the Hosmer-Lemeshow goodness-of-fit test. The threshold for statistical significance will be set to P

<0.05. Statistical analysis will be performed with R software.

127

**10.2  Secondary study parameter(s)**

Secondary study parameter volunteer study: A multivariate linear regression analysis will be performed to analyze the effect of demographic variables (age and sex) on the 4DCT parameters measured.

Explorative clinical study: To investigate different grades of TFCC-injury on 4DCT we plan to construct a multinomial logistic regression model with the outcome variables being the different Palmer grades of TFCC injury and the independent variables the 4DCT parameters.

**10.3  Other study parameters**

Patient age, sex, weight, length, study/profession/hobby and number of scans with inferior quality will be presented in a table.

**10.4  Interim analysis (if applicable)**

Not applicable

## 11. ETHICAL CONSIDERATIONS

### 11.1 Regulation statement

The study will be conducted according to the principles of the Declaration of Helsinki (64th WMA General Assembly, Fortaleza, Brazil, October 2013) and in accordance with the Medical Research Involving Human Subjects Act (WMO) and UMC Governance code published by the NFU.

### 11.2 Recruitment and consent

Healthy participants will be recruited by advertisements in the Radboud University and Hospital. Participants who apply will receive the participant information letter. Within one week they will be called and ask if they are willing to participate in the study. If yes, they will be invited at the policlinic of Plastic Surgery and informed about the study by the principal investigator Dr. EPA van der Heijden, plastic surgeon. Any questions the participant has will be answered. If the participant is willing, he/she will sign the informed consent form and be enrolled.

Patients with suspicion of DRUJ instability will be included by the principal investigator Dr. EPA van der Heijden, plastic surgeon. As routine clinical care, plain radiographs of both wrists will be performed for diagnosis purpose. Hereafter the 4DCT scan will be planned and performed. After 4DCT scanning, patients will get an arthroscopy (gold standard) to evaluate the TFCC based on Palmar classification.

### 11.3 Objection by minors or incapacitated subjects (if applicable)

Not applicable

### 11.4 Benefits and risks assessment, group relatedness

On top of the effective radiation dose of a normal static CT scan (0.005 mSv) the dynamic 4DCT scan of the wrist has for the healthy participants an estimated total effective radiation dose of approximately 0.02m s V . The reliability group also has to wait for 15 minutes in between scans. In the clinical study, patients will complementary to the standard clinical pro undergo a dynamic 4DCT of the wrists which attributes to an added estimated total effective radiation dose of approximately 0.01 msV, for the reference protocol this is doubled This will burden a trivial risk compared to the natural background radiation in the Netherlands (2mSv). The idea is that the results of these study will benefit future patients with wrist sprains. In the future 4DCT scanning may provide the surgeon

129

with information where to aim for during surgery possibly decreasing the possibility for complications The comparison of the left and right wrist will provide an understanding on the validity of comparing the injured wrist with the uninjured wrists in clinical practice. The test-retest reliability will help to provide normal ranges which will help to correctly diagnose patients and help to prevent false-positive or false-negative indication for surgical treatment.

### 11.5  Compensation for injury

The sponsor/investigator has a liability insurance which is in accordance with article 7 of the WMO.

The sponsor (also) has an insurance which is in accordance with the legal requirements in the Netherlands (Article 7 WMO). This insurance provides cover for damage to research subjects through injury or death caused by the study.
The insurance applies to the damage that becomes apparent during the study or within 4 years after the end of the study.

### 11.6  Incentives (if applicable)

Participants may choose to receive a 3D printed version of their wrist or a 20-euro's gift voucher.
Patients of the clinical study will be fully reimbursed for their parking and travelling costs.

130

## 12. ADMINISTRATIVE ASPECTS, MONITORING AND PUBLICATION

### 12.1  Handling and storage of data and documents

For the participants, data will be anonymized after evaluation of the 3D CT has been evaluated and no abnormalities are found. Raw 4DCT data is stored on the research storage servers of dept. of Radiology and anonymized data is stored on the research storage servers of dept. of Plastic Surgery. The Digital Research Environment (DRE) is used to store other documents and files. If the standard 3D CT scan of the healthy volunteer shows obvious abnormalities, the volunteer will be informed and excluded and scan data will be deleted.

### 12.2  Monitoring and Quality Assurance

Since this is a volunteer study and a small clinical study with a negligible risk according to the NFU risk classification, monitoring will be performed by a BROK certified member of the department of radiology and nuclear medicine. The monitoring will be executed once as the duration of the study is expected to be less than one year.

### 12.3  Amendments

Amendments are changes made to the research after a favourable opinion by the accredited METC has been given. All amendments will be notified to the METC that gave a favourable opinion.

### 12.4  Annual progress report

The sponsor/investigator will submit a summary of the progress of the trial to the accredited METC once a year. Information will be provided on the date of inclusion of the first subject, numbers of subjects included and numbers of subjects that have completed the trial, serious adverse events/ serious adverse reactions, other problems, and amendments.

### 12.5  Temporary halt and (prematurely) end of study report

The investigator/sponsor will notify the accredited METC of the end of the study within a period of 8 weeks. The end of the study is defined as the last patient's last visit.

The sponsor will notify the METC immediately of a temporary halt of the study, including the reason of such an action.

In case the study is ended prematurely, the sponsor will notify the accredited METC within 15 days, including the reasons for the premature termination.

131

Within one year after the end of the study, the investigator/sponsor will submit a final study report with the results of the study, including any publications/abstracts of the study, to the accredited METC.

**12.6 Public disclosure and publication policy**

The investigators will be author of submitted manuscripts in case they fulfill criteria for authorship according to regulations of scientific journals.

132

### 13. STRUCTURED RISK ANALYSIS
*Not applicable*

133

## 14. REFERENCES

[1]  C. dePutter, R. Selles en S. Polinder, „Economic impact of hand and wrist injuries: health-care costs and productivity costs in a population-based study," *J Bone Joint Surg Am. 2012,* vol. 94, nr. 9, p. 56, 2012.

[2]  M. Garcia-Elias en M. Folgar, „The management of wrist injuries: An international perspective," *Injury,* vol. 37, nr. 11, pp. 1049-1056, 2006.

[3]  H. Gully, „Injuries Initially Misdiagnosed as Sprained Wrist (Beware the Sprained Wrist)," *Emerg. Med. J.,* vol. 19, nr. 1, pp. 41-42, 2002.

[4]  R. Lindscheid en J. Dobyns, „Carpal instability," *Orthopade,* vol. 22, nr. 1, p. 72, 1993.

[5]  A. M. v. d. Molen, „Proefschrift: Carpale letsels, onderzoek naar de verzuimaspecten ten gevolge van carpale letsels in Nederland," 1997.

[6]  T. Bentley en N. Hope, „Continuing Education Activity," in *Wrist Dislocation*, Treasure Island, StatPearls, 2022.

[7]  R. Klees, „Wat kost een zieke werknemer? Bereken je kosten," MKB, 24 March 2021. [Online]. Available: https://www.mkbservicedesk.nl/personeel/verzuim-reintegratie/wat-kost-ziekteverzuim-per-medewerker-bereken-je-kosten. [Geopend 23 February 2023].

[8]  A. E. Naga, „Reliability of the Dorsal Tangential View in Assessment of Distal Radioulnar Joint Reduction in the Neutral, Pronated, and Supinated Positions in a Cadaver Model," *J Hand Surg Am,* vol. 45, nr. 4, p. 359, 2020.

[9]  S. Ochman, B. Wieskötter en M. Langer, „High-resolution MRI (3T-MRI) in diagnosis of wrist pain: is diagnostic arthroscopy still necessary?," *Arch Orthop Trauma Surg,* vol. 137, nr. 10, pp. 1443-1450, 2017.

[10] A. Rauch, F. Dap en G. Dautel, „Four-dimensional CT Analysis of Wrist Kinematics during Radioulnar Deviation," *Radiology,* nr. 750-758, p. 289, 2018.

[11] R. Szabo, „Distal radioulnar joint instability," *The journal of hand & bone surgery,* vol. 4, nr. 88, pp. 884-894, 2006.

[12] T. Smith, „The diagnostic accuracy of X-ray arthrography for triangular fibrocartilaginous complex injury: a systematic review and meta-analysis," *Journal of hand surgery,* vol. 37, nr. 9, 2011.

[13] K. Casadei, Triangular Fibrocartilage Complex, StatPearls publishing, 2022.

[14] D. Shakoor, „Kinematic Analysis of the Distal Radioulnar Joint in Asymptomatic Wrists Using 4-Dimensional Computed Tomography–Motion Pattern and Interreader Reliability," *J Comput Assist Tomogr.,* vol. 43, nr. 3, pp. 392-398, 2019.

[15] A. Jawed, „TFCC injuries: How we treat?," *J Clin Orthop Trauma.,* vol. 11, nr. 4, p. 570–579, 2020.

[16] M. Treiser, „TFCC Injuries: Meta-Analysis and Comparison of Diagnostic Imaging Modalities," *Journal of wrist surgery,* vol. 7, nr. 3, pp. 267-272, 2018.

134

[17] R. Carr, „Four-Dimensional Computed Tomography Scanning for Dynamic Wrist Disorders: Prospective Analysis and Recommendations for Clinical Utility," *Journal of wrist surgery,* vol. 8, nr. 2, pp. 161-167, 2019.

[18] J. White, „The use of 4D-CT in assessing wrist kinematics and pathology: a narrative view," *The bone & joint journal,* vol. 101, nr. 11, pp. 1325-1330, 2019.

[19] S. Robinson, „Evaluation of Four-Dimensional Computed Tomography as a Technique for Quantifying Carpal Motion," *Journal of biomechanical engineering,* vol. 143, nr. 6, 2021.

[20] B. Swartman, „Normal values of distal radioulnar translation assessed by three-dimensional C-arm scans: a cadaveric study," *Journal of hand surgery,* vol. 44, nr. 5, pp. 503-509, 2019.

[21] M. Brinkhorst, „Quantifying in vivo scaphoid, lunate, and capitate kinematics using four-dimensional computed tomography," *Skeletal radiology,* 2020.

[22] S. Tay en N. Jais, „Kinematic analysis of the scaphoid using gated four-dimensional CT," *Clinical Radiology,* vol. 72, pp. 794-799, 2017.

[23] P. Neo en N. Jais, „Dynamic imaging with dual-source gated Computed Tomography (CT): Implications of motion parameters on image quality for wrist imaging," *Medical Engineering and physics,* vol. 35, pp. 1837-1842, 2013.

[24] P. Ranota, „Four-Dimensional Computed Tomography to measure distal radial-ulnar and radio-carpal joint congruency following distal radius fractures," *Journal of orthopeadics,* vol. 26, nr. 10, pp. 31-39, 2021.

[25] E. C. Rodríguez-Merchán, „Distal Radioulnar Joint Instability: Diagnosis and Treatment," *The archives of bone and joint surgery,* vol. 1, nr. 10, pp. 3-16, 2022.

[26] C.-c. Pan, „Displacement of the Distal Radioulnar Joint of Clinically Symptom-Free Patients," *Clinical orthopeadics and related research,* vol. 2, nr. 415, pp. 148-156, 2003.

[27] M. J. Park, „Reliability and normal values of various computed tomography methods for quantifying distal radioulnar joint translation," *The journal of bone and joint surgery,* vol. 1, nr. 90, pp. 145-153, 2008.

[28] L. Cerezal, F. d. Pinal en F. Abascal, „Imaging findings in ulnar-sided wrist impaction," *RadioGraphics,* vol. 22, nr. 1, p. 281–299, 2004.

[29] T. Imaeda, R. Nakamura en K. Shionoya, „Ulnar impaction syndrome: MR imaging findings," *Radiology,* vol. 201, nr. 2, pp. 495-500, 1996.

[30] D. J. Bell, „Ulnar variance," Radiopeadia, 14 10 2022. [Online]. Available: https://radiopaedia.org/articles/ulnar-variance. [Geopend 27 01 2023].

[31] Y. Weerakkody, „Ulnar impaction syndrome," Radiopeadia, 11 12 2022. [Online]. Available: https://radiopaedia.org/articles/ulnar-impaction-syndrome. [Geopend 27 01 2023].

[32] A. Palmer, „Triangular fibrocartilage complex lesions: A classification," *J Hand Surg Am,* vol. 3, nr. 13, pp. 391-394, 1989.

135

136

## 11.4 Description of scripts used

| INPUT | Static bone meshes |
| --- | --- |
| | Statistical shape model radius |
| | Motion tags |
| | Static to dynamic transformation data |

| STATIC ANALYSIS | Calculate_axis_radius.m |
| --- | --- |
| | Calculate_axis_capitate.m |
| | 1. Calculate_axis_ulna.m |
| | 2. Calculate_ulnar_variance_stat.m |
| | 3. SSM_Pnt_Mapping.m |

| TRANSFORMATION | Static to dynamic transformation |
| --- | --- |
| | GCS to LCS radius transformation |

| DYNAMIC ANALYSIS | 4. Calculate_motion_angle.m |
| --- | --- |
| | 5. Calculate ulnar carpal proximity |
| | 6. Calculate_3DEpi.m |
| | 7. Calculate_3DmRu.m |

| INTERPOLATION | 8. Interpolate_wrist_position_Incl_PS.m |
| --- | --- |

| OUTPUT | Ulnar variance |
| --- | --- |
| | Ulnar carpal proximity |
| | 3DEpi |
| | 3DmRu |

*Figure 49: Flowchart depicting the main DRUJ script used for calculation of the DRUJ parameters*

137

| Calculation | |
|---|---|
| **1. Calculate the local coordinate system of the ulna** | |
| Calculate_LCS_Ulna.m | **Description**: As described in Chapter 3: Local coordinate system of the ulna this function calculates the local coordinate system and the global coordinate system to local coordinate system transformation matrix. Both for the whole ulna as well as different fractions of the distal ulna. |
| | **Input**: Ulna and lunate mesh |
| | **Output**: Local coordinate system ulna and global coordinate system to ulnar local coordinate system transformation matrix |
| **2. Calculate static ulnar variance POI's** | |
| Calculate_ulnar_variance_stat.m | **Description**: Calculates the static ulnar variance and the parameters needed for dynamic ulnar variance calculation (articular surface radius and articular surface ulna) as described in Chapter 5: Ulnar variance as well as the styloid length used in Chapter 6: Ulnocarpal proximity and the center of mass of the ulnarstyloid used for PS angle estimation (used in Chapter 8: A) |
| | **Input**: Ulna and Radius mesh and global coordinate system to ulnar local coordinate system transformation matrix |
| | **Output**: Static ulnar variance, radial articular surface, ulnar articular surface, styloid length and center of mass ulnar styloid |
| **3. Automatic point mapping using an SSM** | |
| SSM_Pnt_Mapping.m | **Description**: Automatic mapping of the radial POI used for 3DmRU and the 3DEpi calculation (Chapter 7: DRUJ stability) using manually selected points on a radial SSM meanshape and a radial SSM |
| | **Input**: Statistical shape model of the radius and a predefined SSM of the radius with 31 shape modes |
| | **Output**: Indexes of the automatically mapped volar radial border, dorsal radial border, listers tubercule, dorsal margin sigmoid notch and volar margin sigmoid notch |
| **4. Calculate angle of the wrist (motion)** | |
| Calculate_motion_angle.m | **Description**: Measuring the angle of the wrist as an indicator for the angle of movement during FE, RUD and PS. Expressed in the capitate radius angle for the PS and the FE movement and the angle between the x axis of the radial LCS and the vector from the origin of the ulna to the center of mass of the ulnar styloid |
| | **Input**: LCS of the capitate, radius and ulna and the center of mass of the ulnar styloid |
| | **Output**: Angle of the wrist expressed in three directions |
| **5. Calculate dynamic ulnar proximity** | |
| Calculate_ulnar_proximity.m | **Description**: Automatic calculation of the distance from the lunate and triquetrum to the ulna (Chapter 6: Ulnocarpal proximity) as well as the indexes corresponding to these measurements used for closest point mapping |
| | **Input**: Meshes of the ulna, lunate and triquetrum as well as the global coordinate system to ulnar local coordinate system |

| | |
|---|---|
| | transformation matrix and a cut-off distance to search for the minimal distance |
| | **Output**: the distance from the lunate and triquetrum to the ulna as well as the indexes corresponding to these measurements |

| **6. Calculate dynamic 3DEpi** | |
|---|---|
| calculate_3DEpi.m | **Description**: Automatic calculation of the 3DEpi (Chapter 7: DRUJ stability) using the previously acquired indices of the volar and dorsal margin of the sigmoid notch and the local coordinate system of both the ulna and the radius |
| | **Input**: Indices of the volar and dorsal margin of the sigmoid notch, the local coordinate system of the radius and the ulna and the static mesh of the radius and the ulna |
| | **Output**: 3DEpi score and information needed for visualisation 3DEpi |

| **7. Calculate dynamic 3DmRu** | |
|---|---|
| Calculate_3DmRu.m | **Description**: Automatic calculation of the 3DmRu (Chapter 7: DRUJ stability) using the previously acquired indices of the volar and dorsal margin of the sigmoid notch and the volar and dorsal radial border as well as the ulnar mesh |
| | **Input**: Indices of the volar and dorsal margin of the sigmoid notch and the volar and dorsal radial border; the local coordinate system of the radius and the ulna and the static mesh of the radius and the ulna. |
| | **Output**: 3DmRu score and information needed for visualisation 3DmRu |

| **8. Interpolate data** | |
|---|---|
| Interpolate_wrist_position_ Incl_PS.m | **Description**: Adapted version of the script developed by Erin Teule to interpolated the data based on wrist position adapted to work with (and without) PS motion |
| | **Input**: Parameter values; corresponding angles per motion angle and a struct containing which frame numbers belong to which motions |
| | **Output**: Interpolated parameter values per motion angle |

## Visualisation

| **9. Visualise ulnar variance and ulnar proximity dynamically** | |
|---|---|
| Visualisation_dyn_UV_UP.m | **Description**: Script creating a gif visualising the ulnar variance and ulnar proximity during motion (see Figure 42.A) per motion |
| | **Input**: Interpolated ulnar variance and ulnar proximity data |
| | **Output**: GIF dynamically visualising the motion of the wrist together with the calculated ulnar variance and ulnar proximity |

| **10. Visualise 3DEpi and 3DmRu dynamically** | |
|---|---|
| Visualisation_dyn_3DEpi_3DmRu.m | **Description**: Script creating a gif visualising the 3DEpi and 3DmRu during motion (see Figure 42.A) per motion |
| | **Input**: Interpolated 3DEpi and 3DmRu data |
| | **Output**: GIF dynamically visualising the motion of the wrist together with the calculated 3DEpi and 3DmRu |